STABILITY AND MOLECULAR FEATURES OF AQUEOUS FILMS

by

Vu Nguyen Thuy Truong

A dissertation submitted to the faculty of
The University of Utah
in partial fulfillment of the requirements for the degree of

Doctor of Philosophy

Department of Metallurgical Engineering

The University of Utah

May 2018

Copyright © Vu Nguyen Thuy Truong 2018

All Rights Reserved

The University of Utah Graduate School

STATEMENT OF DISSERTATION APPROVAL

The dissertation of **Vu Nguyen Thuy Truong**

has been approved by the following supervisory committee members:

Jan D. Miller	, Chair	**11/02/2017** Date Approved
Anh V. Nguyen	, Member	**11/03/2017** Date Approved
Xuming Wang	, Member	**11/02/2017** Date Approved
Michael L. Free	, Member	**11/02/2017** Date Approved
Vladimir Hlady	, Member	**11/02/2017** Date Approved
Liem X. Dang	, Member	**11/09/2017** Date Approved

and by **Manoranjan Misra** , Chair/Dean of

the Department/College/School of **Metallurgical Engineering**

and by David B. Kieda, Dean of The Graduate School.

ABSTRACT

The behavior of foam films is significant in many areas such as mineral flotation, food processing, and oil recovery. The film stability between two bubbles in foams has been motivated by different research interests. This dissertation contributes to the understanding of the film stability based on several methods of evaluation.

First, the structure of thin water films during the rupture process was investigated by a new approach, which combines molecular dynamics simulation (MDS) with image processing analysis. The procedure was developed to convert the MDS trajectories to readable 3D images. The films were studied at different thicknesses by MDS to determine the critical thickness at which film ruptures. The potential energy of each thickness during simulation time was analyzed. A new procedure involving the calculation of molecular porosity was developed. Results indicate a critical molecular porosity value of 49% for film rupture.

Second, disjoining pressure (DP) in thin films was examined by using Matlab. The surface charge regulation approach was applied to develop a new model for computing of DP. The case of sodium dodecyl sulfate (SDS) adsorption from NaCl solution was studied. A model of film drainage rate was developed accordingly which showed a good agreement with experimental data from the literature.

Finally, features of interfacial water at air-water interfaces of anionic SDS and

cationic dodecyl amine hydrochloride (DDA) solutions were examined by combining sum frequency generation (SFG) vibrational spectroscopy measurements and MDS. The SFG spectra and MDS results revealed that interfacial waters for SDS solutions was highly-ordered compared with those for DDA solutions. SFG results revealed that interfacial waters at pH 9 in both SDS and DDA solutions showed less-ordered than at pH 7. Experiments on foam stability and foam weight were conducted under the same conditions. Results revealed that for SDS solutions, foams were more stable at pH 7 than at pH 9. The opposite was observed for DDA solutions, in which case stability decreased when pH increased. Results were explained based on the extent of surfactant hydration at interfaces which is thought to account for film stability as revealed from results on foam stability.

TABLE OF CONTENTS

LIST OF TABLES

Tables

LIST OF FIGURES

Figures

ACKNOWLEDGEMENTS

I would like to start off by expressing my sincerest appreciation to my supervisor, Professor Jan D. Miller, for his guidance, motivation, and encouragement throughout my PhD study and research. He is a role model in hard work with extraordinary passion and dedication to scientific research. Without his patience, valuable advice, and great inspiration this would have been a more strenuous journey. Professor Miller's consistent enthusiasm on research has deeply impressed and motivated me to further pursue research studies. For all of these I will always be thankful.

I would also like to acknowledge Professor Anh V. Nguyen at the University of Queensland, Brisbane, Australia for providing me a once-in-a-lifetime opportunity to work abroad. A part of this dissertation was completed under his supervision and I much appreciate all of his guidance, valuable suggestions, knowledge and time. I enjoyed discussions with him about the research on colloid and interfaces.

Thanks are extended to Dr. Michael Free, Dr. Vladimir Hlady, Dr. Liem X. Dang, and Dr. Xuming Wang for being members of my supervisory committee and their valuable advice and comments on my dissertation research. Particularly, I want to thank Dr. Xuming Wang for all his help, guidance, and supportive suggestions during my entire PhD journey.

I also want to take the time to acknowledge Dr. Chen-Luh Lin for helping me in the study of film structure, suggestions and comments in this dissertation. A whole-hearted

thanks to Dr. Liem X. Dang, a great “uncle”, for his support, care, and encouragement throughout my PhD journey. Also, I would like to thank Dr. Tuan H.A. Nguyen at the University of Queensland for his advice, discussion and suggestions for my dissertation research.

Thanks to my fellow research colleagues and friends for their help and support during my study and dissertation research. Special thanks to my best friend, Phuong Nguyen, for her support, open-ears and encouragement during my entire PhD journey.

Finally, I want to thank the Department of Metallurgical Engineering at the University of Utah for providing a pleasant and friendly environment that helped me through all the hard work. Thanks to Ms. Sara Wilson for helping me with academic concerns and questions. A special thanks is given to Ms. Dorrie Spurlock for her help, sharing and support for my entire PhD program.

Last, but not least, I would like to dedicate my PhD dissertation to my parents, sisters and brothers for their unconditional love and encouragement during my pursuit in this study. Without their love and care, it would have been impossible for me to complete this journey all these years.

CHAPTER 1

INTRODUCTION

The stability of an aqueous film between two bubbles, known as a foam film, is of crucial importance in many industrial fields such as in the food industry, during oil recovery, waste-water treatment, and especially in mineral flotation. The froth flotation process is considered to be one of the most significant technological developments in the twentieth century. As a result of this technology, access to the world's natural mineral resources increased exponentially as billions of tons of mineral resources could be treated economically (Parekh and Miller, 1999). In the froth flotation process, hydrophobic particles attach on the surfaces of air bubbles and rise from the pulp phase to the froth phase. The overall performance of this flotation process relies on the collection of desired particles at the froth phase. Frothers and collectors, generally known as surfactants, are added during froth flotation to cause desired particles to become hydrophobic, as well as to reduce bubble size and to prevent bubble coalescence. Of critical importance to achieving a high recovery of mineral particles is the stability of bubbles in both the pulp phase and the froth phase. Accordingly, the study of the stability of a thin aqueous film between two bubbles becomes critical to understanding the physicochemical behavior of film stability which is of special interest to support the froth flotation process. In this

regard, the overall significant consideration throughout this the dissertation is to investigate film stability in some specific aspects.

1.1 Film Stability: New Insights

1.1.1 Classification of Aqueous Films

Research studies on the stability of thin aqueous films have been challenging for decades due to the thermodynamic instability of foams and foams films. The stability of foam and foam films is controlled primarily by the thinning and rupture of aqueous films between two bubbles. In the early stage of film thinning, the continuous aqueous phase drains out mostly due to the gravitational force. When the thickness of aqueous films decreases to a few hundred nanometers, the gravity effect can be negligible, and the stability of aqueous films is driven by physicochemical factors such as surfactant adsorption, film structure, intermolecular interactions (so-called disjoining pressure), and/or surface elasticity. On the basis of a film's thickness, h, and its characteristic properties, aqueous films can be classified into the three following types(Exerowa et al., 1981):

(1). Thick films ($h > 100$ nm);

(2). Common black film (10 nm $< h < 100$ nm);

(3). Newton black film ($h < 5$nm);

Much research on intermolecular interactions has been performed, including study of dispersion, electrostatic, and steric/hydration forces. The classical Derjaguin-Landau-Verwey-Overbeek (DLVO) theory which includes attractive van der Waals and repulsive electrostatic interactions has been applied to explain the stability of common black films.

It has been explained that common black films are stabilized mainly by repulsive electrostatic interaction (Cosima and Regine, 2003). The behavior of Newton black films, which maintain stability at ultrathin thickness, cannot be attributed to the classical DLVO theory due to the short-range repulsive interaction observed. Hence, steric interaction was introduced to explain this behavior, which arises when adsorbed layers overlap (Israelachvili and Wennerstroem, 1992).

1.1.2 Application of Molecular Dynamics Simulation to the Study of Film Stability

Molecular dynamics simulations (MDS) were developed with the aim of understanding the structural and dynamic properties of atoms and molecules as well as the interactions between them. Computational simulation can act as a bridge between microscopic length and time scales and the macroscopic world of the laboratory, providing information about interactions between molecules. Computational simulation has become a significant tool in scientific research when actual experiments are impossible, expensive or even dangerous to conduct. Many popular molecular dynamics software programs have been developed to encourage computational research studies such as Charmm, Gromacs, Amber, Lammps and so on. In these simulation software programs, generally a potential energy function is required to model the basic interactions between atoms and molecules in the system being studied. For instance, in the Amber program, the potential energy consists of the electrostatic, van der Waals and bonded interactions. The bonded interaction is actually the summation of the energy function of the bond stretch, angle bend, dihedral and improper torsions. The other significant parameters in MDS programs are force fields,

which describe the force acting on each atom of the molecules. Many researchers have examined and developed force field databases for increasing the capability of MDS study in the research community. For instance, various kinds of molecular water models have been developed with the appropriate force field packages. The rigid SPC/E water model incorporates the closest average configurational energy to the experimental value (-41.5 KJ/mol) (Mahoney and Jorgensen, 2000), and has been applied to all the simulation studies in this dissertation. In addition, Amber software developers have built a force field database for organic molecules, GAFF, providing an appropriate parameter set for the study of surfactant molecules (Wang et al., 2004).

Due to the remarkable development of computational capabilities in the twentieth century, MDS has been used widely for research studies in many areas including theoretical chemistry, surface chemistry, biology, materials science, and so on. With regard to the study of aqueous film stability, MDS has been applied to the study of Newton black film in recent decades. Although the stability of ultrathin Newton black films was believed to be controlled by short-range steric repulsive interaction, no generally accepted theory of steric force has been proposed. Understanding of the stability of Newton black films still remains unclear in the experimental realm. On this basis, the nature of the short-range repulsive interaction is expected to be dependent on the structure of a Newton black film. Hence, it is necessary to gain a better understanding of the structure of a Newton black film, which possibly can be accomplished by MDS study. Gamba et al. stimulated a Newton black film with the same composition as the film reported in the literature (Bélorgey and Benattar, 1991; Gamba et al., 1992). Bélorgey and Benattar used X-ray reflectivity experiments on sodium dodecyl sulfate (SDS) films to shed light on the

complex structure of Newton black films. Unfortunately, quantitative discrepancies between the simulation results and experimental data were noted. Bresme and Faraudo investigated the structural properties of aqueous films stabilized by SDS monolayers. The simulation results indicated that the surfactant headgroups exhibited a high degree of in-plane ordering, and water molecules existed in the bilayer structure in the form of solvation water (Bresme and Faraudo, 2004). Yang et al. used MDS to study film stability on the basis of critical film thickness as the function of film size and simulation duration (Yang et al., 2009). Goddard examined the structures and properties of Newton black films in the presence of three different types of surfactants by MDS. Also, the disjoining pressure isotherms were calculated and it was found that the change in disjoining pressure was strongly coupled to the change in the inner structure of the Newton black films such as the density profile and the solvation of ions (Jang and Goddard, 2006). Research studies on the computation of disjoining pressure from MD simulations were investigated by several research groups (Bhatt et al., 2003; Peng et al., 2015). However, this perspective is still under debate and requires further consideration.

1.1.3 New Insights

Research studies on film stability using MDS tools have revealed new findings regarding the structural and dynamic properties of thin aqueous films. However, reported results are still very disconnected and no outlook conclusions have been found in this research aspect. Of special interest with regard to the MDS study of film stability is the fundamental knowledge of how the surfactant molecules can stabilize a Newton black film until it reaches the ultrathin thickness of about less than 5 nm, and how the film rupture

occurs at the molecular level of understanding. A promising outlook in this dissertation is to investigate the stability and instability of aqueous films with new research approach. By using MDS, the preliminary results of surfactant-free water films visually revealed that there was an existence of low-density and high-density areas during the trajectories of water molecules. These results lead to the hypothesis that the molecular network of water molecules in thin aqueous films possibly plays a crucial role in the film stability or instability. In this dissertation, the new insight has been considered and investigated in the first step of the study of surfactant-free water films.

1.2 Disjoining Pressure in Thin Liquid Films

The term "disjoining pressure" was first introduced to the science of thin liquid films by Derjaguin in the late 1930s, and has been considered as one of the milestones in the theoretical explanation of foam films. The disjoining pressure, Π, at mechanical equilibrium was determined by Derjaguin and Churaev to be the difference between the pressure within a film between two surfaces, P, and the pressure in the bulk phase, P_0, (Derjaguin and Churaev, 1978).

$$\prod = P - P_0 \tag{1-1}$$

In other words, in order for the two bubbles shown in Figure 1.1 to be stable, a thin film between them is required to carry an internal pressure for "disjoining" two interfaces and counter-balancing the external pressure, which is possibly the capillary pressure in this situation. In terms of thermodynamic variables, the disjoining pressure was defined by a variation in the Gibbs free energy of the system, G, with a film thickness, h, at constant chemical potential, μ, temperature, T, and surface area, A (Derjaguin, 1989).

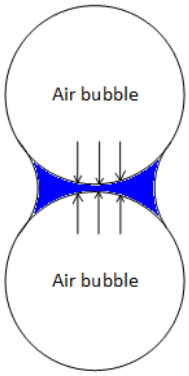

Figure 1.1 Water film between two air bubbles.

$$\Pi(h) = -\left(\frac{dG}{dh}\right)_{\mu,T,A} \tag{1-2}$$

1.2.1 Experimental Measurement of Disjoining Pressure Isotherm

Experimentally the disjoining pressure isotherm, which is actually the disjoining pressure as a function of the film thickness, can be measured with a thin-film balance approach based on the original design of Mysels and Jones (1966). A schematic diagram of the thin film balance is provided in Figure 1.2.

Basically, a single thin film is formed in a hole drilled through a fritted glass disc, onto which a glass capillary tube is fused. Within the cell, a precisely controlled capillary pressure is pressed on the film, which is balanced by the disjoining pressure at equilibrium. A syringe pump coupled to a pressure controller is used to regulate the gas pressure. The disjoining pressure then can be calculated by

$$\Pi = P_g - P_l + \frac{2\sigma}{r} - \Delta\rho g h_c \tag{1-3}$$

where P_g and P_r are the gas and external reference pressures (for example, atmospheric pressure), respectively; σ is the surface tension of the surfactant solution; r is the radius of

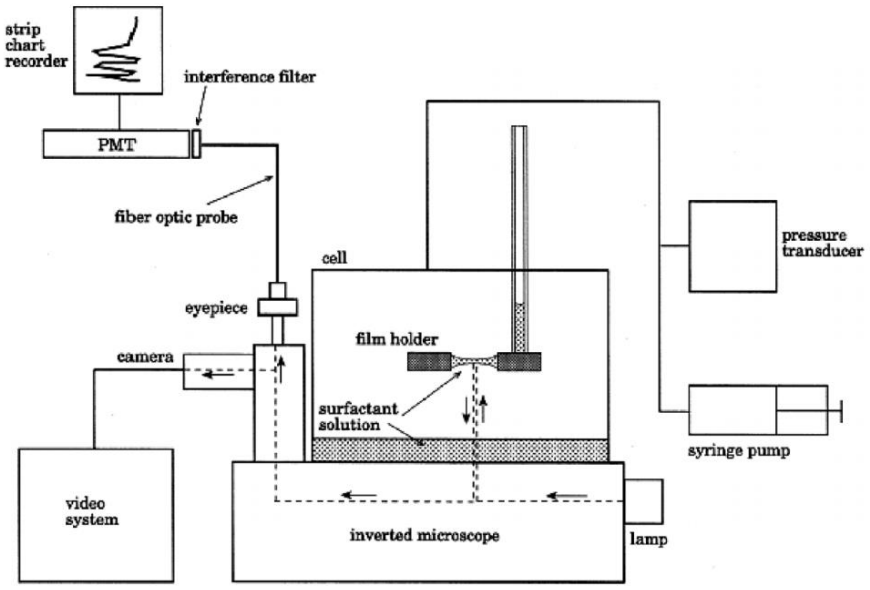

Figure 1.2 A schematic diagram of the thin film balance technique (Manev and Nguyen, 2005).

the capillary tube; $\Delta\rho$ is the density difference between the aqueous solution and the gas; g = 9.81 ms^{-2}; h_c is the height of solution in the capillary tube above the film. Each parameter is measured independently, so disjoining pressure can be determined.

The thickness of the film is determined interferometrically using the Scheludko microinterferometric technique together with the video recorder (Sheludko, 1967). The microscopic film is illuminated by a monochromatic light with a wavelength of 546 nm. As a result of the interference of the light reflected by the film surfaces, the Newton fringes are observed and recorded in the computer using the high-speed video camera system. The film thickness is calculated from the standard Scheludko interferometric equation.

$$h = \frac{\lambda}{2\pi n_0}[l\pi \pm arc\sin\sqrt{\frac{\Delta(1+\tilde{r}^2)}{(1-\tilde{r}^2)+4\tilde{r}^2\Delta}}] \tag{1-4}$$

where $\Delta = (I - I_{\min})/(I_{\max} - I_{\min})$, I is the instantaneous intensity of the photocurrent, I_{min}

and I_{max} are its minimal and maximal values, λ is the light wavelength, $\tilde{r} = (n_0 - 1)^2 / (n_0 + 1)^2$ is the Fresnel reflection coefficient for the air-solution interface, $l = 0, 1, 2, ...$ is the order of the interference.

1.2.2 Disjoining Pressure Components

A number of research studies on the disjoining pressure in a thin aqueous film have been reported in recent decades. Changes in the interfacial region, which generate the disjoining pressure in a thin aqueous film, originate from intermolecular forces. Initially, the disjoining pressure was considered to be a fundamental element in the classical Derjaguin-Landau-Verwey-Overbeek (DLVO) theory of stability of lyophobic colloids (Derjaguin, 1941; Overbeek and Verwey, 1948). It consists of the van der Waals (molecular) interactions and electric diffuse double layer (electrostatic) interactions. Later on, discrepancy between the DLVO theory and experimental results was found so non-DLVO interactions were proposed accordingly (Kralchevsky et al., 2011; Tchaliovska et al., 1994; Tsekov and Schulze, 1997; Wang and Yoon, 2004). The components of disjoining pressure basically can be defined as,

$$\prod(h) = \prod_{DLVO} + \prod_{non-DLVO} = \prod_{vdW} + \prod_{edl} + \prod_{non-DLVO} \quad (1\text{-}5)$$

1.2.2.1 Van der Waals Disjoining Pressure

The van der Waals interaction between surfaces is well-defined in many published books and articles (Derjaguin, 1989; Mahanty and Ninham, 1977; Nguyen, 2000; Nguyen and Schulze, 2003). The interaction originates from the electromagnetic fields between two dipoles, and it can be calculated by using either the microscopic Hamaker approach or the

macroscopic Lifshitz approach. Applying in a thin aqueous film, the van der Waals disjoining pressure as a function of film thickness, *h*, can be determined by a combination approach (Nguyen, 2000) as,

$$\Pi_{vdW} = -\frac{d}{dh}\{-\frac{A(h,\kappa)}{12\pi h^2}\} = \frac{A(h,\kappa)}{6\pi h^3} + \frac{1}{12\pi h^2}\frac{dA(h,\kappa)}{dh} \tag{1-6}$$

where *A(h,κ)* is the Hamaker - Lifshitz function and *h* is the film thickness. For symmetric foam films, the van der Waals interaction is always attractive and destabilizes foam films. Hence, repulsive interactions are required to possibly balance this attractive force and stabilize foam films.

1.2.2.2 Electrical Double Layer Disjoining Pressure

The electrical double layer disjoining pressure results from the overlapping of the diffuse electric layers on two film surfaces at small separation distances. This interaction becomes evident when the surfaces are charged in the presence of ionic surfactants. The existence of a repulsive interaction between two charged interfaces stabilizes foam films. The electrostatic interaction is more clearly observed when the film thickness reaches twice the characteristic Debye length of the diffuse ionic layers. The Debye length can be defined as

$$\lambda = 1/\kappa = \sqrt{\frac{\varepsilon\varepsilon_0 k_B T}{e^2 \sum z_i^2 n_i(\infty)}} \tag{1-7}$$

where κ is the Debye constant, k_B is Boltzmann's constant, T is the absolute temperature (in Kelvin), $n_i(\infty)$ is the number per unit volume of ions of type i with valence z_i in the bulk solution far from the interface.

Generally, the electrical double layer disjoining pressure can be calculated as in the

equation below, after solving the Poisson-Boltzmann equation under a variety of different boundary conditions to obtain the potential, ψ_m, at the mid-plane position of the aqueous films.

$$\Pi_{el} = k_B T \sum n_{i\infty} [\exp(-\frac{ez_i \psi_m}{k_B T}) - 1] \tag{1-8}$$

The boundary conditions are dependent on the surface properties such as the surface potential and/or surface charge. At some specific position, such as the mid-plane position of a symmetric film, the first derivative potential is zero, and is usually used as one of the boundary conditions for solving the Poisson-Boltzmann equation. Further, the electrostatic interaction also depends on the charging mechanism at the interface, and is often described by one of the three following conditions: the surface potential remains constant; the surface charge remains constant; and the surface charge and potential change by a charge regulation (Nguyen and Schulze, 2003). Besides, a number of approximate solutions to the Poisson-Boltzmann equation together with Derjaguin approximation can be used to predict the electrostatic interaction such as the Debye-Huckel approximation and the superposition approximation. The constant surface potential condition is often applied when low potential exists at the interface, or the film thickness is an average value. If the system cannot regulate its charge during the interaction, the constant surface charge condition can be considered. Many research studies have been conducted to validate the theoretical modeling of these conditions for the prediction of electrical double layer disjoining pressure. Chan et al. developed two theoretical models of electrostatic repulsion based on both the constant surface potential and constant surface charge (Chan et al., 1980). Further, Exerowa et al. measured the disjoining pressure of aqueous films in SDS and NaCl solutions, and compared the experimental data to that predicted by Chan's models

(Exerowa et al., 1987). It was reported that discrepancies occurred between the values, so the theory of electrostatic repulsion has not been well-understood. Another similar observation was reported by Mishra et al., in which the disjoining pressure isotherm was measured for aqueous films of SDS and NaCl solutions (Mishra et al., 2005). Deviations between the measured disjoining pressure and theoretical values of the DLVO theory (with constant surface charge conditions for the prediction of electrostatic repulsion) developed by Chan et al. were observed. Eventually, it has been recognized that the charge regulation condition is the most accurate one because the surface potential and surface charge are regulated together during the interaction. However, due to the complexity of the charge regulation condition, theoretical study quantifying the effect of the electrical double layer disjoining pressure on this aspect still remains limited. Part of this dissertation will attempt to explain the interaction. Furthermore, it is well-established that the adsorption of ions modifies the surface charge and the surface potential, and these parameters regulate the electrical properties of the interfaces as well as the aqueous films. Hence, it is expected that the adsorption of surfactant ions somehow can affect the electrostatic interaction of foam films.

1.2.2.3 Non-DLVO Disjoining Pressure Components

In addition to the DLVO disjoining pressure components, non-DLVO disjoining pressure components such as steric interaction, hydration interaction, and hydrophobic interaction are proposed and proven to be important in determining the stability of aqueous films.

$$\Pi_{non-DLVO} = \Pi_{steric} + \Pi_{hydration} + \Pi_{hydrophobic} + ... \tag{1-9}$$

Steric interaction is introduced to take into account the stability observed in Newton black soap films (with the film thickness less than 5 nm). This steric repulsion is considered to occur when the adsorbed layers overlap. The other interaction also involved in ultrathin Newton black films is the hydration interaction, which originates from molecular ordering at the interfaces. When two interfaces approach, this order is disturbed and the force of either attraction or repulsion is created. It was reported that these short-range interactions can be very complex and depend on how molecules structure at the interfaces (Vance, 1999). In contrast, hydrophobic interaction is considered as a long-range attractive force, which is reported to be much stronger than the attractive van der Waals interactions in aqueous films. However, currently no generally accepted theory has been developed for these forces. In this dissertation, the non-DLVO disjoining pressure components are excluded from the scope of research.

1.2.3 Effect of Disjoining Pressure on Film Drainage Kinetics

Film drainage kinetics have been of great importance in determining overall foam behavior in recent decades. Scheludko was the first pioneer who applied the Stefan-Reynolds equation to describe film drainage. A general Stefan-Reynolds equation is shown in the below equation.

$$V_{\mathrm{Re}} = -\frac{dh}{dt} = \frac{2h^3}{3\mu R^2}\Delta P = \frac{2h^3}{3\mu R^2}(P_\sigma - \Pi) \tag{1-10}$$

where ΔP is the driving pressure, h is the film thickness, t is the lifetime of film thinning, μ is the viscosity of the aqueous film, and R is the film radius. If, at an appropriate film thickness, the disjoining pressure Π is equal to the capillary pressure P_σ, the driving pressure is equal to zero, leading to the formation of an equilibrium film. It is noted that

the application of the Stefan-Reynolds equation to the film thinning theory requires several assumptions, such as

(1). The viscosity in the film is equal to that of the bulk phase.

(2). The rate of film thinning through evaporation is neglected.

(3). The liquid flow is between plane parallel surfaces.

(4). There is no radial component of the velocity at the surface, which means the surfaces are considered as tangentially immobile surfaces.

Two independent research directions regarding film drainage kinetics have been followed by many research groups, including either the role of surface rheology, or the effect of intermolecular forces. With regard to surface rheology, Radoev and co-workers dedicated their research studies to the effect of surface diffusion as well as surface shear viscosity in the consideration of mobile film surfaces (Radoev et al., 1974; Manev et al., 1997a). Later on, several other research groups contributed to the studies on this research (Karakashev et al., 2010; Manev et al., 1997a; Manev and Nguyen, 2005; Tsekov and Evstatieva, 2004). In this dissertation, the effect of intermolecular forces is considered. As introduced in the previous Section 1.2, research on intermolecular interactions has been investigated including the DLVO classical theory and non-DLVO interactions. Accordingly, the theory of film drainage kinetics was developed based on the theory of disjoining pressure components. Karakashev et al. applied the constant surface potential and constant surface charge conditions of electrostatic interactions to develop the theoretical model of film drainage kinetics for aqueous films of ionic and nonionic surfactants (Karakashev and Ivanova, 2010; Karakashev et al., 2008; Karakashev and Nguyen, 2007). The results revealed a variation between the theoretical values and the

experimental data, which requires further consideration. Yoon and Wang examined the film thinning of surfactant solutions and investigated the effect of hydrophobic forces in film thinning (Wang and Yoon, 2005, 2008). However, the fundamental quantitative theory of hydrophobic attractive forces is still under debate. In this dissertation, the effect of intermolecular forces on film drainage kinetics will be investigated, together with the study of disjoining pressure components in aqueous films.

1.3 Interfacial Water Structure

Certainly, water is the most important chemical substance on earth and has been widely studied throughout many decades due to the demand for water in our daily lives as well as in industrial processes such as the froth flotation process. The physical and chemical properties of water have been investigated since the very beginning of scientific development (Frank, 1972; Rao, 1972; Walrafen, 1972). However, questions regarding interfacial properties of water at the air-water interface, which are considerably different from water in the bulk phase, have been unsolved until recent decades. Of special interest are the properties of interfacial water in charged surfactant solutions because of the common applications of surfactant solutions in many industrial fields. In the froth flotation process, it is well-known that the selective separation of valuable mineral particles is achieved by the addition of specific surfactants including collectors and/or frothers, which basically stabilize the froth phase and improve grade and recovery yields (Fuerstenau et al., 2007). In other words, the flotation behavior of mineral components is dependent on the nature and structure of the surfaces and/or interfaces. Many research studies have been conducted on the behavior of surfactants at surfaces. However, very little attention has been

paid to characterizing the features of interfacial water. Fundamentally understanding on how interfacial waters interacts with the surfactants and/or what is the orientation of interfacial waters can help describing more clearly the nature of surfactant adsorption at the air-water interface. Due to the development of advanced experimental techniques and computational resources in recent years, significant progress has been achieved in exploring the microscopic properties of aqueous surfaces at the molecular level. Two research approaches of fundamental importance for the study of interfacial water features are presented.

1.3.1 Sum Frequency Generation (SFG) Vibrational Spectroscopy

Sum frequency generation (SFG) vibrational spectroscopy was first introduced in 1987 by Shen's research group to study the identification of surfactants and the interaction between surfactants and interfaces. Since then, SFG spectroscopy has become a powerful tool for detection of molecules at surfaces, including solid/liquid, solid/air and liquid/air interfaces (Bain, 1995; Chen et al., 2010; Johnson and Tyrode, 2005; Nguyen et al., 2015; Nickolov et al., 2004; Yeh et al., 2001). SFG is actually a second-order nonlinear optical process, which can be used to study the vibrational modes and orientations of molecules at interfaces. The advantages of SFG spectroscopy include its simple experimental set-up; its application to all interfaces accessible by light; its nondestructive and high feature; and its sensitivity with good spatial, temporal, and spectral resolution (Shen, 1989).

In a measurement from the SFG spectroscopy, the SFG signal is generated at a frequency which is the sum of the frequencies of two incident laser beams, including a tunable infrared (IR) beam (ω_{IR}) and a visible beam (ω_{Vis}), as shown in Figure 1.3. When

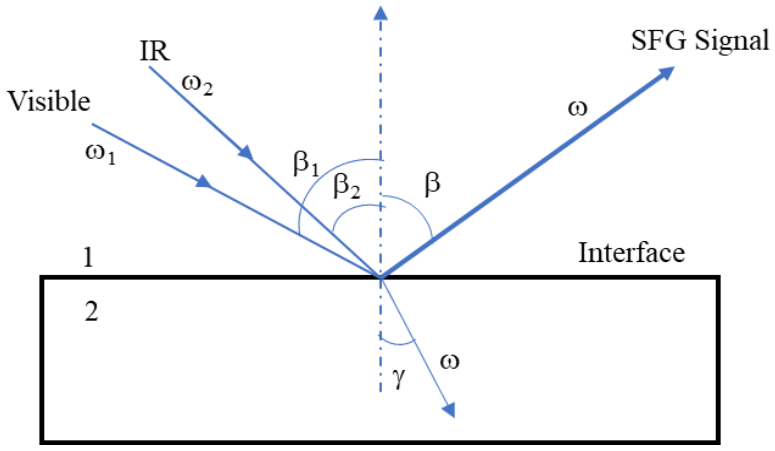

Figure 1.3 Schematic plot of reflection SFG set-up.

the IR beam is tuned through the spectral region of interest and the photon energy coincides with the energy of the molecular vibrational mode, the SFG intensity I_{SFG} is enhanced resonantly, which is quantified by

$$I_{SFG} = \frac{8\pi^3\omega^2 \sec^2\beta}{c^3 n_1(\omega_1) n_1(\omega_2)} \left|\chi_{eff}^{(2)}\right|^2 I_{Vis} I_{IR} \tag{1-11}$$

where ω, ω_1, ω_2 are the frequencies of the SFG signal, visible and IR laser beams, respectively; β is the reflection angle of the sum frequency field; $n_i(\omega_i)$ is the refractive index of medium i at frequency ω; I_{Vis} and I_{IR} are the intensity of a visible beam and an IR beam, respectively; $\chi_{eff}^{(2)}$ is the effective second-order nonlinear susceptibility tensor of the surfaces, which is related to the second-order nonlinear susceptibility in the lab coordinate system. Of particular interest in this dissertation study is the ssp experimental polarization combination, which includes the s polarized SFG, s polarized visible and p polarized infrared polarization combination. It is noted here that the xy plane in the laboratory coordination system is the plane of the interface with the z axis as the surface normal. In this case, p polarization denotes the optical field in the xz plane, and s represents

polarization perpendicular to the xz plane (Wang et al., 2001; Zhuang et al., 1999). The quantity $\chi^{(2)}_{eff,ssp}$, therefore, can be determined by

$$\chi^{(2)}_{eff,ssp} = L_{yy}(\omega)L_{yy}(\omega_1)L_{zz}(\omega_2)\sin\beta_2\chi^{(2)}_{yyz} \tag{1-12}$$

where χ_{yyz} is the component of $\chi^{(2)}_{eff,ssp}$ with laboratory coordinates; $L_{jj}(\omega_i)$ *(j = x, y, z)* are the Fresnel coefficients at frequency ω_i.

For the neat water at the pure air-water interface, Shen and coworkers first reported three distinct peaks in the OH stretching region as observed in Figure 1.4. A narrow peak at about 3,690 cm^{-1} was associated with the free OH bond, which H terminal was not bonded with any neighboring molecules. The other two peaks were assigned to OH with hydrogen bonded with neighboring molecules. The 3,200-cm^{-1} peak represented the "ice-like" structure as a similar peak was observed in the ice spectrum, whereas the 3,450-cm^{-1} peak was associated with the disordered local network. The observation of the ice-like peak suggests that the structure of the water surface is more ordered than the bulk phase.

Later on, study of the interfacial water structure in the surfactant solution was continued to facilitate improved understanding. Many research studies have sought to answer the questions of how surfactants alter the hydrogen bonding of water at the interfaces. In other words, the OH stretching region of interfacial water molecules was examined in the presence of surfactant molecules. The research studies were conducted at the air-water, oil-water and solid-water interfaces (Ye et al., 2001);(Bain, 1995; Fan et al., 2009; Gragson et al., 1997b; Knock et al., 2003). With respect to the air-water interfaces, Gragson et al. examined the structure of interfacial waters at air-water interface in non-ionic and ionic surfactant solutions (Gragson et al., 1996, 1997b). It was reported that in the presence of charged surfactants, the interfacial water molecules were highly oriented

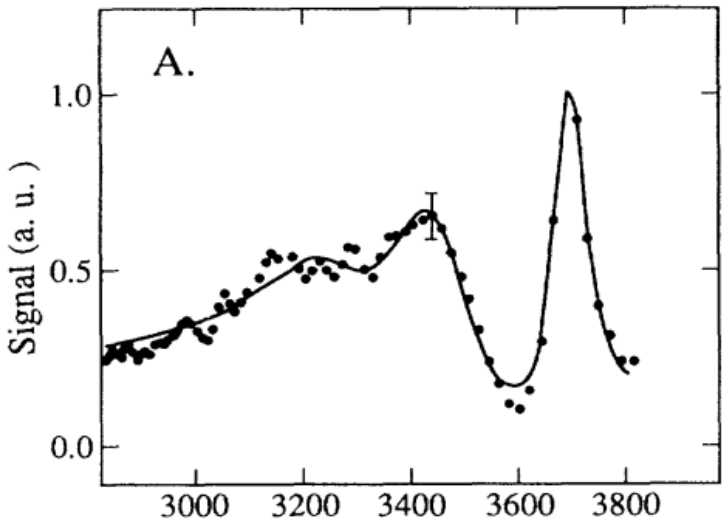

Figure 1.4 SFG spectrum for the pure air-water interface (ssp polarization combination). Reprinted from (Du et al., 1993).

depending on the anionic or cationic nature of the surfactant headgroup. As for the non-ionic surfactant solutions, the ordering of interfacial water molecules showed minimal interaction with the surfactant molecules. The strongly-aligned water molecules in the charged solutions were explained by the development of an electrostatic field, which was formed by the adsorption of surfactant molecules at the interfaces. Later on, Nguyen et al. investigated the interfacial water structure at the adsorption layer of cetyltrimethylammonium bromide (CTAB) from low concentrations to its critical micelle concentration (Nguyen et al., 2015). It was revealed that interfacial water layers achieved the most orderly arrangement at a surfactant concentration of around 0.1 mM, at which the surfactant surface coverage had not yet reached saturation. In another study, Nihonyanagi et al. examined the counterion effect on interfacial water at positively and negatively charged surfactant interfaces to consider the origin of the Hofmeister series (Nihonyanagi et al., 2014). Recently, Li et al. used SFG spectroscopy to investigate the anion effects on

the adsorption and packing of octadecylamine hydrochloride molecules at the air-water interface (Li et al., 2017). SFG spectroscopy has been proven to be a very powerful experimental approach to study not only the adsorption behavior of surfactant molecules but also the structure and orientation of interfacial water molecules at surfaces and interfaces at the molecular level.

1.3.2 Molecular Dynamics Simulation

In recent decades, Molecular Dynamics Simulation (MDS) has been proven to be an efficient research approach for the fundamental understanding of structural and dynamic properties of interfacial waters at surfaces and interfaces at the atomic level. Many research studies have explored properties of the interfacial water at air-solid, air-liquid and oil-liquid interfaces.

Striolo and co-workers have devoted particular attention to the computational study of interfacial water structure and the interaction of interfacial water with mineral interfaces including silica, alumina and oxide surfaces (Argyris et al., 2009; Argyris et al., 2011; Striolo, 2011). The studies revealed that the structural properties and dynamic behavior of interfacial water molecules were strongly altered by interaction with the solid substrates. In other words, the water molecules at the surfaces played a decisive role in the hydrophobic/ hydrophilic characterization of the solid substrates. Previous studies in our research group have also addressed the great importance of the interfacial water to the interfacial phenomena of surfaces such as talc crystals, layer silicate surfaces, alkali chloride salt crystals, and selected sulfide surfaces (Du and Miller, 2007; Wang et al., 2014); (Jin et al., 2014).

With regard to the study of air-water interfaces, many atomistic computational simulations have focused on the adsorption behavior of surfactant molecules, instead of the interfacial water features at the interfaces. Tarek et al. investigated the monolayers of C_{14}TAB at the air-water interface, and found that the hydrocarbon chains were highly disordered with an average of two to three gauche defects per chain (Tarek et al., 1995). Bandyopadhyay and Chanda examined the properties of a monolayer of nonionic surfactant, diethylene glycol monododecyl ether ($C_{12}E_2$), adsorbed at the air-water interface. The study revealed a strong tendency for water molecules to form hydrogen-bonded bridged structures with the adjacent oxygen atoms of the oxyethylene groups (Bandyopadhyay and Chanda, 2003). The adsorption of sodium dodecyl sulfate at the air-water interface was simulated by Scheweighofer et al. at low surface coverage. The results showed that the surfactant chain is strongly bent and tilted, and the sulfate head group and a portion of the carbon chain were immersed in water. Also, the water molecules surrounding the head group were orientated in response to the charge of the head group (Schweighofer et al., 1997). The findings clearly provided a molecular picture of surfactant and interfacial water molecules at the air-water interface. However, not much attention has been paid to the structural properties and dynamic behavior of interfacial water molecules at air-water interfaces in the literature. In this dissertation research, the following characteristics of the interfacial water molecules are being investigated to gain more fundamental understanding of air-water interfaces. Basically, the analysis programs extract information about interfacial water molecules from the trajectory files of MD simulations. All the programs were coded in Fortran 90 language.

1.3.2.1 Atomic Number Density Profile

The relative number density profile of interfacial water molecules in the aqueous phase provides a quantitative analysis of their distribution. The simulation periodic box is divided into 0.5 Å bins parallel to the selected surface, making it possible to count the number of water molecules. In this dissertation, the position of a water molecule is defined as the position of the center of mass for the water molecule. The number of water molecules in each bin is normalized with the number of water molecules in the bulk phase. Further the normalized fraction of water molecules as a function of the bin's distance from the interface is plotted, making the relative number density profile.

1.3.2.2 Hydrogen Bonding Network

In this dissertation, the SPC/E water model was used for all studies of interfacial water features at the air-water interfaces. Two water molecules are defined as hydrogen bonded if the distance between two oxygen atoms is less than 3.5 Å and the O…O-H angle is simultaneously less than 30^{o} (Luzar and Chandler, 1996). Then the number of hydrogen bonds per water molecule was calculated by dividing the hydrogen bonding number in each water layer by its corresponding water number. Further, the number of hydrogen bonds per water molecule as a function of distance from the interfaces was plotted.

1.3.2.3 Water Dipole Orientation

In this dissertation, the water dipole orientation was defined by the angle, alpha α, between the water dipole moment (oriented from negative to positive) and the surface normal. The angle α is determined by the cosine function, which was computed from the

coordination of the water molecules. Further, the relative density distribution of water dipoles was plotted as a 3-dimensional surface with the x axis as the degree of angle α, the y axis as distance from the interface, and the z axis as the relative number density.

1.3.2.4 Water Residence Time

Besides the structural properties of interfacial water molecules, the dynamic properties, such as water residence time, also can be analyzed by using MD simulation results. The water residence time is described as the time that a water molecule spends in each water layer along the surface. The average residence time of water molecules in each layer is calculated and plotted versus its distance from the interfaces.

1.4 Research Objectives

The research objectives of this dissertation consist of the following major goals.

(1). Investigate the rupture process of surfactant-free water films by developing a new procedure in which a combination of MD simulations and image processing techniques are analyzed. Such a procedure has not been reported in the literature.

(2). Develop a new theoretical model to predict the electrical double layer component of disjoining pressure in aqueous films based on the effect of surfactant adsorption, the so-called charge regulation condition. Accordingly, develop a model of film drainage kinetics for aqueous films. Validate theoretical values by experimental data from the literature for aqueous films of SDS and NaCl solutions.

(3). Examine the features of interfacial water at air-water interfaces of SDS and DDA solutions by SFG measurements and MD simulations at neutral and high pH values.

Analyze MDS results with different parameters of interfacial water properties and compare with the results from SFG spectroscopy. Conduct foam weight and foam stability experiments to confirm the hypothesis that interfacial water features strongly contribute to the stability of aqueous films, thereby enhancing foam stability.

1.5 Dissertation Organization

After the Introduction presented in Chapter 1, an investigation of film structure during the rupture process is presented in Chapter 2. First, MD simulations were employed for 10 nm x 10 nm water films at different thicknesses to determine the critical film thickness at which film rupture occurs. Further, the potential energies of water films are revealed. Finally, a new analysis approach is reported by using image processing technique to examine the trajectories of water molecules from MDS results during the simulation time. Percolation analysis following MD simulation was investigated to examine the connectivity of the molecular pores in the water films. Accordingly, molecular porosity during simulation time of the water films at different thicknesses was calculated. Finally, the critical molecular porosity is determined.

Chapter 3 theoretically discusses the effect of SDS adsorption in thin aqueous films and film drainage kinetics. A theoretical modelling approach using a Matlab computational tool to predict the electrical double layer component of disjoining pressure as a function of film thickness is presented. The theoretical results were validated by the appropriate experimental data of disjoining pressure isotherms from the literature. Subsequently, a theoretical model of the film drainage rate was developed based on the new model of the electrical double layer disjoining pressure. Theoretical values of film drainage rate are

compared with the experimental data from the literature.

Chapter 4 examines the features of interfacial water at the air-water interfaces of SDS and DDA solutions at neutral and high pH values, which are revealed by SFG spectroscopy and MD simulations. The structures of interfacial waters were investigated by SFG measurements at the air-water interfaces of SDS and DDA solutions at different concentrations and two pH values of 7 and 9. MD simulations of interfacial water molecules at the air-water interfaces of both SDS and DDA solutions at neutral and high pH values were examined. The structures of interfacial waters were analyzed from MDS results including the relative number density profile, the hydrogen bonding, the water dipole orientation and the residence time. Analysis results of interfacial water molecules from MD simulations were in good agreement with SFG experimental results. Finally, foam weight and foam stability experiments, using the same conditions as those from which SFG measurements were obtained, were examined. The results of these tests confirm the hypothesis that the highly-ordered and strongly-oriented interfacial water molecules at air-water interfaces enhance the stability of aqueous films, so foams become more stable.

Chapter 5 summarizes the findings of this dissertation and provides recommendations for future research.

It is expected that the contributions from this dissertation will enhance our fundamental knowledge of the film stability between two bubbles and improve the future development of flotation technology.

CHAPTER 2

FILM STRUCTURE DURING RUPTURE AS REVEALED BY IMAGE PROCESSING OF MD SIMULATIONS

2.1 Introduction

Foam, a colloidal system of a dispersed gas phase and a continuous liquid phase, is widely used in our daily lives and for the industrial fields such as mineral flotation, oil recovery, food processing and so on. The continuous liquid phase generally water forms a thin film between bubbles or drops in the foam. The control of this thin aqueous film has become the decisive effect in the control of foam stability. Hence, the study of thin aqueous film has been of special interest for several decades. Since late 1959, Scheludko et al. and Mysels et al. invented an experimental approach to measure the single film thickness (Scheludko and Exerowa, 1959; Mysels, 1959). Later on, many experimental research studies have been accomplished by different research groups (Bergeron and Radke, 1992; Exerowa et al., 1987; Karakashev et al., 2008; Mishra et al., 2005; Schelero and von Klitzing, 2015; Yoon and Aksoy, 1999). Researchers have attempted to gain a better understanding of the properties of the thin aqueous film. Hence, the critical parameters in the film stability can be determined. One of the major concerns is the disjoining pressure and interaction forces which critically control the film stability. This research topic has

also been considered in many theoretical works (Kralchevsky et al., 2011; Kralchevsky et al., 1999; Radke, 2015; Yaminsky, 1994).

In recent decades, research on the stability of thin aqueous films has been examined by the use of a computational tools to obtain improved fundamental understanding at nanometer scale. By using the Gromacs simulation program, Weng et al. studied the effect of film thickness on the interfacial properties and found that the local surface tension distribution significantly varied with the film thickness, with a small variation in density profiles and surface tension values (Weng et al., 2000). Bhatt et al. for the first time calculated the disjoining pressure isotherm of free thin films from the MD simulation results (Bhatt et al., 2002). Later on, Peng et al. proposed another methodology to compute the disjoining pressure from MD simulation results and also found that the temperature significantly affected the disjoining pressure isotherm (Peng et al., 2015). In another aspect on thin film stability, Yang et al. used MDS to investigate the aqueous film rupture and determined the critical film thickness (Yang et al., 2009). The simulation conditions including the film size and the simulation time were examined. Peng et al. added the critical rupture time to the study of rupture process and also studied the effect of ions on the film rupture process (Peng et al., 2012).

Despite a number of research studies, the fundamental understanding of the thin aqueous film stability is still incomplete, especially in the film rupture process. In this chapter, for the first time, the image processing approach was used in combination with MD simulations to provide a new insight into film stability. Image processing has been widely used in the fields of medicine, astronomy and mineral processing in recent decades. Particularly in mineral processing application, image processing has been used to

investigate the particle size, shape, density, porosity and the pore network structures for multiphase systems (Fuerstenau and Han, 2003; Miller and Lin, 2009). In this study, image processing was applied to analyze the structure of molecular pores, defined as the void space between water molecules in aqueous films. It is expected that the molecular pore network significantly affects to the rupture of a thin water film. This chapter is structured with the following organization. Firstly, the MD simulation results for water films of different thickness are reported and the critical film thickness is defined. The film rupture process is visualized and discussed. Secondly, the potential energy for the water films at different thicknesses during the simulation time are analyzed and studied. Finally, the molecular porosity and percolation theory achieved by applying image processing analysis are discussed to provide an explanation for the film rupture process.

2.2 Computational Approach

2.2.1 Molecular Dynamics Simulation

In this dissertation research, the simulation box was composed of a thin surfactant-free water film sandwiched by two vacuum spaces. To construct the desired size of a thin water film, GROMACS software was used, which provides a packing of water molecules with density of close to 1,000 g/L. Basically, thin films of 10 nm x 10 nm with different thickness were studied to determine the critical film thickness. The number of water molecules for a specific thickness is listed in Table 2.1. It is noted that GROMACS, one of the popular molecular dynamics simulations packages primarily used for biomolecules, provides a special tool to construct a specific size of water films, which Amber simulation software is not able to. However, GROMACS is mainly designed for simulations of

Table 2.1 Number of water molecules assigned for the specific film thickness of (10 nm x 10 nm) films by Gromacs software.

Thickness (nm)	Number of water molecules
1.0	3,214
1.2	3,907
1.3	4,358
1.4	4,607
1.5	5,039
2.0	6,242

proteins, lipids and nucleic acids. Being available at the Center of High Performance Computing (CHPC) at the University of Utah, Amber simulation software was studied and used in this dissertation, which is more friendly and has a built-in force field database for not only water models but also for organic surfactant molecules.

The thin water film was then centered in the simulation box's z direction. The simulation box size was assigned as 10 nm x 10 nm x 10 nm. A periodic boundary condition was applied for the three directions.

The Amber 14 was used for the simulation of water thin films in this study. The total potential energy in the Amber program includes the Coulombic (electrostatics) interactions, the short-range interactions (van der Waals energy), and the bonded interactions as shown in Equation (2-1). It is noted that the bonded terms include the bond stretch and angle bend energy that are represented in the water models as harmonic terms.

$$E_{total} = E_{Coulombic} + E_{vdW} + E_{bond} + E_{angle} \quad (2\text{-}1)$$

Equation (2-2) describes the Coulombic energy, in which the energy of the

interaction is inversely proportional to the distance of separation r_{ij}.

$$E_{Coulombic} = \frac{e^2}{4\pi \in_0} \sum_{i \neq j} \frac{q_i q_j}{r_{ij}} \tag{2-2}$$

where q_i and q_j are partial charges for atom i and atom j, e is the charge of an electron, ϵ_0 is the dielectric permittivity of a vacuum (8.85419 x 10^{-12} F/m).

The van der Waals energy, represented by the conventional Lennard-Jones (12-6) functions, is shown in Equation (2-3).

$$E_{vdW} = \sum_{i \neq j} \varepsilon_{ij} \left[\left(\frac{r_{m,ij}}{r_{ij}} \right)^{12} - \left(\frac{r_{m,ij}}{r_{ij}} \right)^{6} \right] \tag{2-3}$$

where ε_{ij} is the depth of the potential well, and $r_{m,ij}$ is the distance at which the potential reaches its minimum.

The Particle Mesh Ewald (PME) was used to describe the Coulomb long-range interactions and a cutoff of 9 Å was applied for the Coulombic and van der Waals interactions. The simple extended point-charge (SPC/E) water model, which provides a good representation of the dielectric properties as well as thermodynamic properties at a relatively low computational cost, was used for all the simulations of thin water films.

The thin water films were simulated in the NVT ensemble where the number of particles (N), the simulation box volume (V) and the temperature (T) were kept constant. The temperature was kept at 298.0 K using the Anderson thermostat. The energy of the system was initially minimized and equilibrated for 100 ps before the simulation. Simulations were carried out with a 2-fs time step, and the simulation time was varied up to the time at which film rupture occurred.

2.2.2 Conversion from MDS Results to Readable Image Processing Formats

Basically, MDS results provide the trajectories of water molecules throughout the simulation time. However, image processing software is not able to read the format of Amber output trajectory files. Hence, a procedure to convert Amber output files to image processing readable files was developed as described in Figure 2.1. It is noted that the Amber output file is a movie of trajectories which include a specific number of image frames up to the initial setting configuration. Since it is of interest to investigate the dynamics of water molecules during the simulation time, the trajectory of water molecules for 500 ps of simulation time was analyzed. So, the movie of trajectories is split into a series of coordinate pdb files by using cpptraj tool in Amber. It is noted that the pdb files, files containing the atomic coordinates, were constructed by Amber from the protein data bank (pdb) format which provided a standard representation for macromolecular structure data derived from X-ray diffraction and NMR studies (http://www.wwpdb.org/ /documentation /file-format.php). An example of the pdb file in Amber simulation software is shown in Figure 2.2, which includes the information of x, y and z coordinates of water molecules. A code written in C language was developed to create the digitized 3D image files, which are of readable format for the image processing software. To proceed this code, the input files (called as temporary input files in Figure 2.1) required the information of xyz coordinates and the radius of each atom. The concept is that each hydrogen atom or oxygen atom in water molecules is considered to be a sphere with the van der Waals radius reported in the literature (Bondi, 1964). The x, y, and z coordinates were extracted from the pdb files. An example of the temporary input file is shown in Figure 2.3, in which x, y,

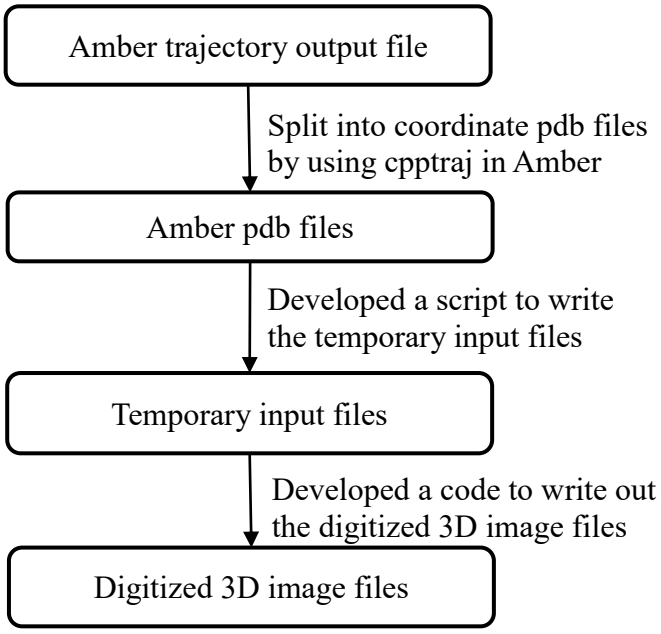

Figure 2.1 Procedure to convert the Amber output trajectory files to the digitized 3D image files for image processing.

```
CRYST1  100.000  100.000  113.000  90.00  90.00  90.00                    1
ATOM      1  O   WAT     1      53.018  50.815  69.675  1.00  0.00           O
ATOM      2  H1  WAT     1      53.964  50.694  69.598  1.00  0.00           H
ATOM      3  H2  WAT     1      52.915  51.723  69.960  1.00  0.00           H
ATOM      4  O   WAT     2      55.229  62.961  69.862  1.00  0.00           O
ATOM      5  H1  WAT     2      55.487  63.365  69.034  1.00  0.00           H
ATOM      6  H2  WAT     2      55.524  63.578  70.532  1.00  0.00           H
ATOM      7  O   WAT     3      67.089  64.662  66.973  1.00  0.00           O
ATOM      8  H1  WAT     3      66.671  64.318  67.762  1.00  0.00           H
ATOM      9  H2  WAT     3      66.552  65.416  66.726  1.00  0.00           H
ATOM     10  O   WAT     4      67.483  56.630  67.076  1.00  0.00           O
ATOM     11  H1  WAT     4      67.261  57.400  66.552  1.00  0.00           H
ATOM     12  H2  WAT     4      68.067  56.963  67.757  1.00  0.00           H
ATOM     13  O   WAT     5      60.824  58.052  65.968  1.00  0.00           O
ATOM     14  H1  WAT     5      60.682  58.816  66.527  1.00  0.00           H
ATOM     15  H2  WAT     5      60.134  57.439  66.221  1.00  0.00           H
ATOM     16  O   WAT     6      67.309  58.304  60.661  1.00  0.00           O
ATOM     17  H1  WAT     6      67.446  59.204  60.366  1.00  0.00           H
ATOM     18  H2  WAT     6      66.358  58.194  60.662  1.00  0.00           H
ATOM     19  O   WAT     7      57.406  60.972  69.696  1.00  0.00           O
ATOM     20  H1  WAT     7      56.745  61.652  69.825  1.00  0.00           H
ATOM     21  H2  WAT     7      57.814  60.869  70.556  1.00  0.00           H
ATOM     22  O   WAT     8      57.202  59.719  66.203  1.00  0.00           O
ATOM     23  H1  WAT     8      57.987  59.761  66.749  1.00  0.00           H
ATOM     24  H2  WAT     8      56.589  60.325  66.619  1.00  0.00           H
ATOM     25  O   WAT     9      65.747  66.802  59.932  1.00  0.00           O
ATOM     26  H1  WAT     9      65.525  67.734  59.936  1.00  0.00           H
ATOM     27  H2  WAT     9      65.150  66.412  60.571  1.00  0.00           H
ATOM     28  O   WAT    10      53.953  53.312  62.811  1.00  0.00           O
ATOM     29  H1  WAT    10      54.659  53.560  62.214  1.00  0.00           H
ATOM     30  H2  WAT    10      53.218  53.100  62.236  1.00  0.00           H
                             x       y       z
```

Figure 2.2 An example of the pdb file.

```
# Geometry_file
RA
E        53.018      50.815      69.675  1.52 1.52 1.52
E        53.964      50.694      69.598  1.20 1.20 1.20
E        52.915      51.723      69.960  1.20 1.20 1.20
E        55.229      62.961      69.862  1.52 1.52 1.52
E        55.487      63.365      69.034  1.20 1.20 1.20
E        55.524      63.578      70.532  1.20 1.20 1.20
E        67.089      64.662      66.973  1.52 1.52 1.52
E        66.671      64.318      67.762  1.20 1.20 1.20
E        66.552      65.416      66.726  1.20 1.20 1.20
E        67.483      56.630      67.076  1.52 1.52 1.52
E        67.261      57.400      66.552  1.20 1.20 1.20
E        68.067      56.963      67.757  1.20 1.20 1.20
E        60.824      58.052      65.968  1.52 1.52 1.52
E        60.682      58.816      66.527  1.20 1.20 1.20
E        60.134      57.439      66.221  1.20 1.20 1.20
E        67.309      58.304      60.661  1.52 1.52 1.52
E        67.446      59.204      60.366  1.20 1.20 1.20
E        66.358      58.194      60.662  1.20 1.20 1.20
E        57.406      60.972      69.696  1.52 1.52 1.52
E        56.745      61.652      69.825  1.20 1.20 1.20
E        57.814      60.869      70.556  1.20 1.20 1.20
E        57.202      59.719      66.203  1.52 1.52 1.52
E        57.987      59.761      66.749  1.20 1.20 1.20
E        56.589      60.325      66.619  1.20 1.20 1.20
E        65.747      66.802      59.932  1.52 1.52 1.52
E        65.525      67.734      59.936  1.20 1.20 1.20
E        65.150      66.412      60.571  1.20 1.20 1.20
E        53.953      53.312      62.811  1.52 1.52 1.52
E        54.659      53.560      62.214  1.20 1.20 1.20
E        53.218      53.100      62.236  1.20 1.20 1.20
                     x           y           z       r(x) r(y) r(z)
```

Figure 2.3 An example of the temporary input file.

z is x coordinate, y coordinate and z coordinate, respectively, for each atom, and r(x), r(y), r(z) are the radius of atoms in x, y and z directions. The van der Waals radius for oxygen and hydrogen atom is 1.52 Å and 1.2 Å, respectively. A script was written to create the temporary input files, and then the digitized 3D image files were finally made by the specific code.

2.2.3 Image Processing

Image processing is a method to convert an image into digital form and proceed with operations for analysis. Usually the input is the image and the output can be an image

or the characteristics of an image. In this research, an image processing software named ImageJ/ Fiji was used to analyze the simulation results. ImageJ is an open source Java written program developed by National Institute of Health (NIH), which is easy to use and is able to enhance image and/or extract useful information such as edge detection, histogram and particle analysis (Abràmoff et al., 2004). Of particular interest in this research is the molecular pores during the rupture of the water film. In this regard, the molecular porosity was determined by using ImageJ/ Fiji. The computation procedure is shown in Figure 2.4. At first, the digitized 3D image in raw file format was obtained from the conversion procedure as mentioned in previous Section 2.2.1, which is an 8-bit image with 100 pixel x 100 pixel x 100 pixel corresponding to 10 nm x 10 nm x 10 nm in dimensions. Further these images need to remove the slices of vacuum layers from the simulation box, so the image analysis further can be processed accurately. The images were inverted so the molecular pores between water molecules were taken into account for analysis. Figure 2.5 shows an illustration of the original raw image and the inverted image. Before proceeding with molecular pore analysis by using the 3D Object Counter, the inverted images were segmented by the Watershed function in ImageJ. It is worth noting that segmentation is the separation process of the image into objects of interest, which is an important part of image analysis.

Basically, the 3D Object Counter function provides the information of molecular pore volume in voxel units. In this way, the molecular pore volume during the simulation time was determined for different water film thicknesses. Further the molecular porosity was computed by the similar concept of porosity in porous media. In other words, the molecular porosity is defined by the void fraction in Equation (2-4). Thus, the molecular

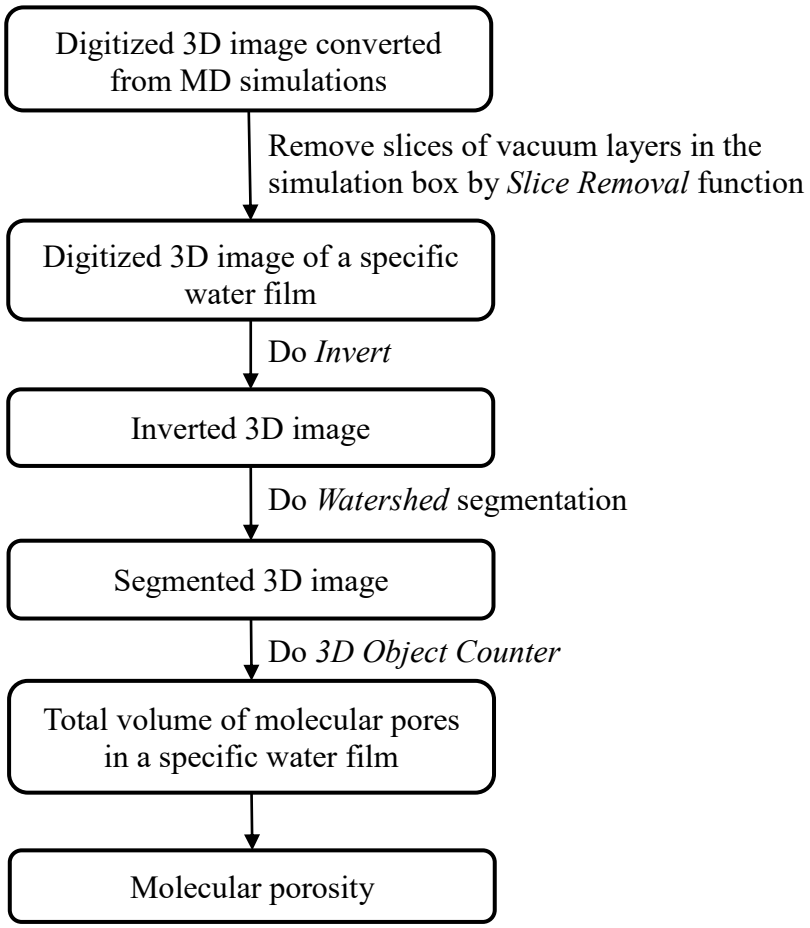

Figure 2.4 Computation procedure of molecular porosity for a digitized 3D image.

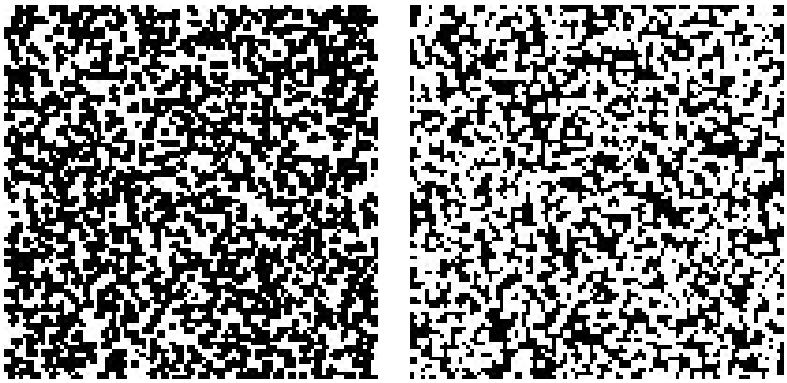

Figure 2.5 Illustration of a slice of the original raw image (left image) and a slice of the inverted image (right image). Black spots in the left image are water molecules and black spots in the right image are molecular pores.

porosity can be found and evaluated at the point of water film rupture.

$$\phi = \frac{V_p}{V_t} \tag{2-4}$$

where V_p is volume of molecular pores in the water film and V_t is total volume of the water film.

Since the MDS results provided the trajectories of water molecules during the simulation time, a movie of water trajectories was achieved. It was split into a series of pdb files in Amber simulation software as discussed above. Each pdb file was converted into a digitized 3D image file, which further was processed by image processing technique to compute the molecular porosity. In other words, a series of pdb files are required to be processed by the same procedure. For instance, a duration of 500 ps simulation time with 2 fs time-step provided a series of 250 pdb files. To proceed this procedure smoothly, a macro script was written in ImageJ/Fiji software to repeat the computation procedure for 250 pdb files. As a result, the molecular porosity as a function of simulation time was obtained.

2.3 Results and Discussion

2.3.1 Critical Water Film Thickness at Nanometer Scale

The critical film thickness is considered as the thickness at which water film rupture occurs. In other words, the connectivity of void space (molecular pores) and rupture is not observed for thicker films and on this basic a critical thickness is defined. In this study, three values of the water film thickness were initially investigated including 1 nm, 1.5 nm and 2 nm. It is noted that the water film thickness is actually the initial thickness before MD simulation. It was observed that at 1 nm of thickness, the water film was broken after

500 ps of simulation time. The water film of 1.5 nm and 2 nm in thickness was continued to run for further 10 ns to confirm the film stability. The film thicknesses in the range between 1 nm and 1.5 nm were later simulated with the increment of 0.1 nm. It was found that starting from 1.4 nm for the water film thickness, the stability of the thin water film was sustained for longer simulation times. In order words, the critical water film thickness was determined as 1.3 nm. Table 2.2 summarizes the selected simulation results of the (10 nm x 10 nm) water films at different thicknesses. These simulation results are very similar with the reported studies of thin water films using different simulation software as shown in Table 2.3 (Jang and Goddard, 2006; Peng et al., 2012; Yang et al., 2009).

Figure 2.6 shows several snapshots from MDS results of the rupture process of the 1.3-nm water film. It was observed that the water trajectories created the low-density areas and high-density areas before a small hole for film rupture formed after about 110 ps of simulation time. This small hole grew to a larger size until the film broke into two separate pieces. Figure 2.7 shows snapshots of water film before breaking into two specific water pieces. More interestingly it was found that after the water film was broken, it was converted to the droplet state as shown in Figure 2.8. It is noted that due to the periodic boundary condition of simulation, the real rupture process of a 1.3-nm water film is illustrated as seen in Figure 2.7 and Figure 2.8. The conversion of the broken film can possibly be explained by the lower potential energy of the droplet state. Due to the minimum surface area of the spherical droplet, the potential energy of the water droplet is reduced, so the thin water films tend to form the water droplet after it is broken.

Table 2.2 Stability results of the (10 nm x 10 nm) water films at different thicknesses.

Thickness (nm)	Status of Film Stability	Simulation Time
1.0	Rupture	1 ns
1.3	Rupture	1 ns
1.5	No rupture	10 ns
2.0	No rupture	10 ns

Table 2.3 Simulation results for critical water film thickness as reported in literature and this study.

Film dimension	Critical Film Thickness	Reference
10 nm x 10 nm x 1.33 nm	1.33 nm	(Peng et al., 2012)
10 nm x 10 nm x 1.32 nm	1.32 nm	(Yang et al., 2009)
10 nm x 10 nm x 1.3 nm	1.3 nm	This study

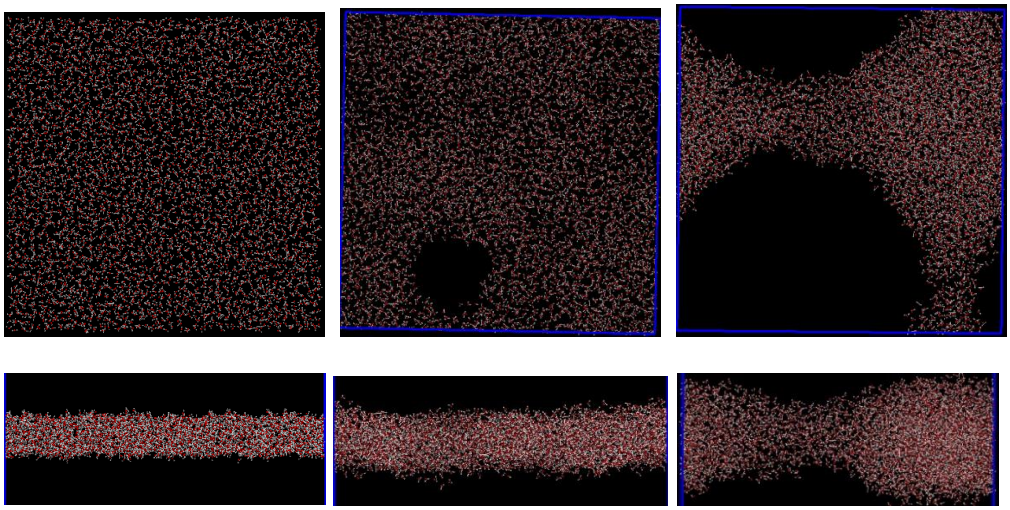

Figure 2.6 The rupture process of 1.3-nm water film. The left snapshots are the beginning state; the center snapshots are after 110 ps of simulation time; and the right snapshots are after 500 ps of simulation time. Top snapshots are the top view and bottom snapshots are the side view.

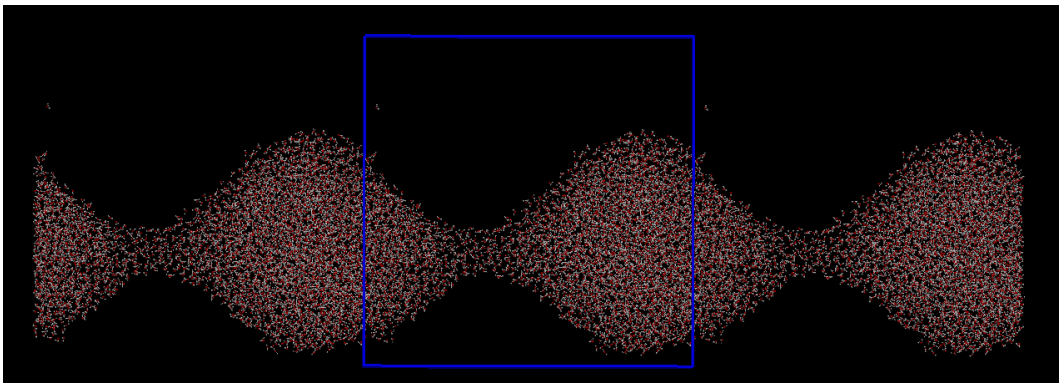

Figure 2.7 Snapshots of water film before breaking into two water pieces (the top view).

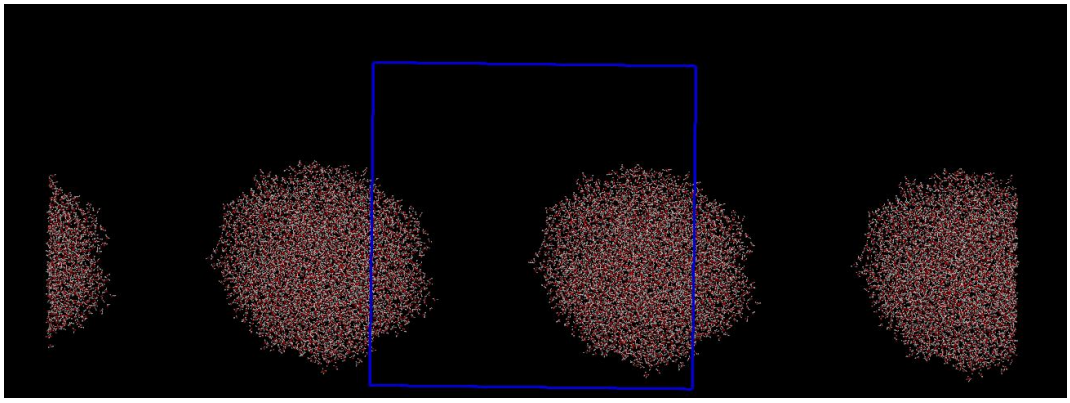

Figure 2.8 Snapshots of droplet state after 1ns of simulation time for 1.3-nm water film (the top view).

2.3.2 Analysis of the Water Film Instability

2.3.2.1. Potential Energy of the Water Film

To obtain better understanding of the water film rupture process, the potential energy of the water film as a function of simulation time was examined and the results are shown in Figure 2.9. It can be seen that as for the stable films, the potential energies remained constant and just fluctuated around the equilibrium values whereas the potential energies of broken films continued to decrease with the increase in simulation time. A slight decrease of potential energy was observed for the 1.3-nm water film and a dramatic decrease was for the 1-nm water film. The decrease of potential energy for these broken films occurred at a similar time when the small hole started to form inside the films as discussed previously in Section 2.3.1. It is noted that the increase of potential energies during the first few picoseconds corresponds to the heating process from 0 K to 298 K in the simulation system.

As introduced in Section 2.2.1, the total potential energy in Amber simulation program consists of the Coulombic (electrostatics) interaction energy, the van der Waals interaction energy and the bonded energies (bond, angle and dihedral terms). Basically, in the simulation of surfactant-free water films, no bonded potential energies existed and just electrostatics and van der Waals interaction were reported. The decrease of potential energies in the broken films indicates that the electrostatics and van der Waals interactions between atoms become weaker throughout the simulation time, so film rupture occurred. As for the unbroken films, the stability was achieved probably because the electrostatics and van der Waals interactions between atoms remain constant and reach the equilibrium during the simulation time. As expected, the analysis demonstrates that at the molecular

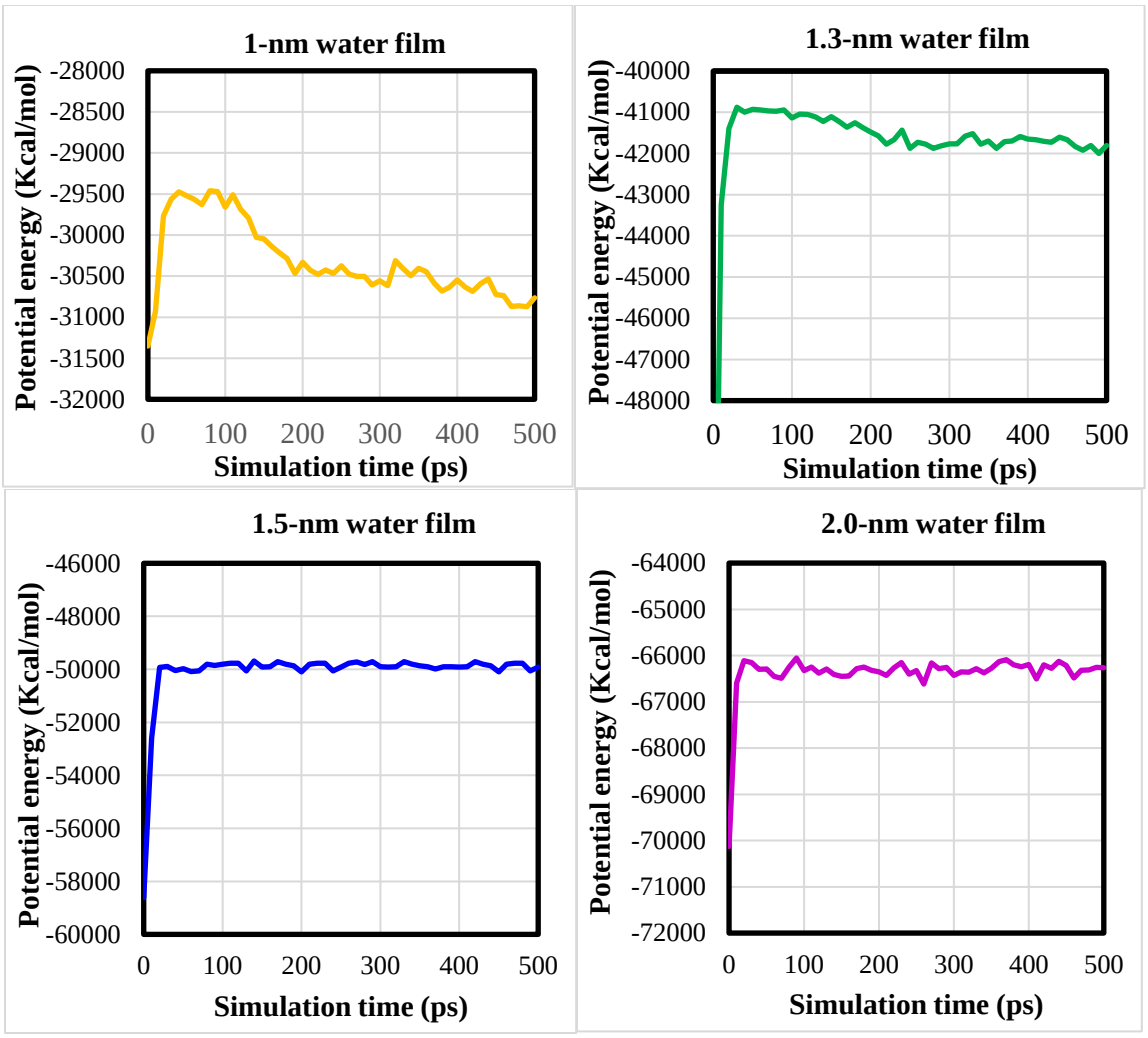

Figure 2.9 Potential energy of water films at different thicknesses.

level of understanding, the interactions between water molecules in a water film play the important role in film stability. This finding is in good agreement with the experimental research of film stability in regard to the disjoining pressure and interaction forces in the thin film. Karakashev et al. reported the significant effect of DLVO disjoining pressure in general and the double-layer interaction in particular to the film stability and film drainage (Karakashev et al., 2008). The theoretical studies reported in Chapter 3 will also demonstrate that the classical DLVO interactions including van der Waals interaction and double-layer repulsive interaction are of great significance in the control of film stability.

2.3.2.2. Molecular Porosity and Percolation Theory

As described in Section 2.2.2 with the conversion procedure to transform the MDS results of water trajectories in the water film to 3D images, image processing analysis can be done to provide more detailed information. Of particular interest in this section is the molecular porosity in a water film at specific thickness in order to further explain film instability. It is worth finding that although the watershed segmentation was implemented to purposely separate the molecular pores in the water film, analysis results with the 3D Object Counter reveal that only one object could be detected, which means that all the molecular pores were connected and impossible to define the individual molecular pore size. As a result, the volume of molecular pores in the water film during the simulation time was determined. Then the molecular porosity was computed from Equation(2-4). Figure 2.10 shows the molecular porosity of water films at different thicknesses as a function of simulation time. The results reveal that the porosity of unbroken films remained unchanged during the simulation time whereas the increase in porosity was observed for

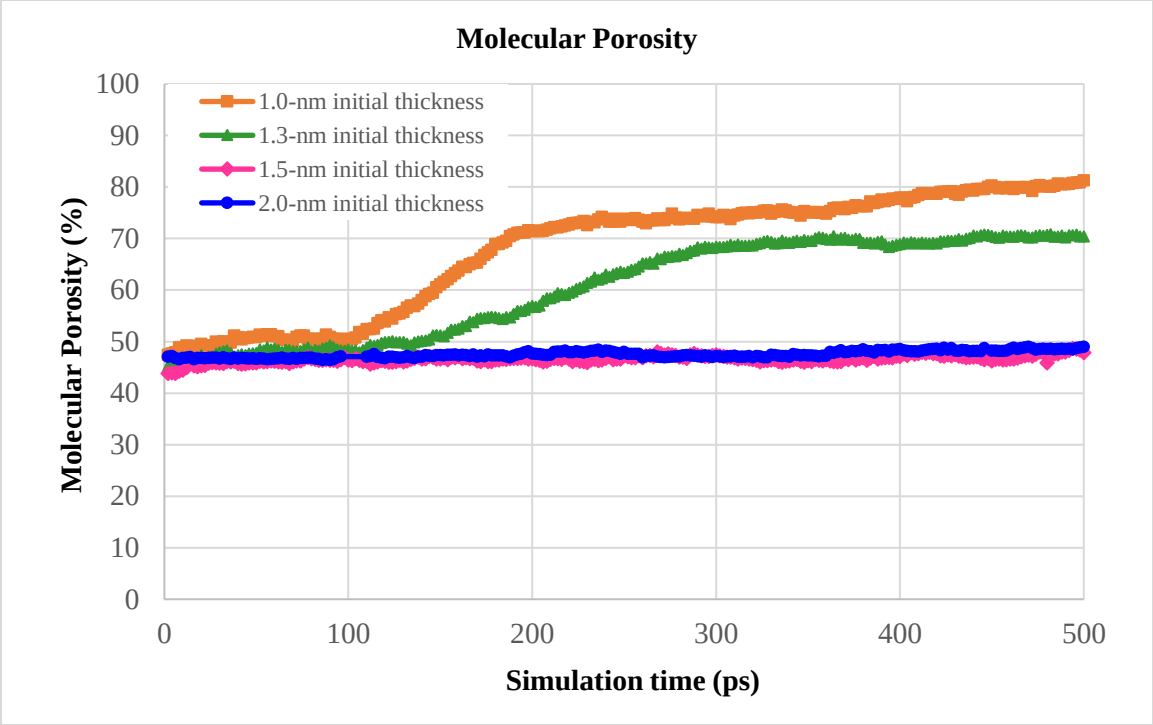

Figure 2.10 Molecular porosity of water films at different initial film thicknesses as a function of simulation time.

the broken films. Further from Figure 2.10 the existence of a transition state for the broken films can be observed. This transition state was found from 110 ps to 300 ps for the 1.3-nm water film, and it was from 100 ps to 180 ps for the 1-nm water film. As mentioned in Section 2.3.1, the MDS results revealed that the 1.3-nm water film started to be unstable after about 110 ps of simulation time. On the other hand, the molecular porosity of the 1.3-nm water film in Figure 2.10 gradually increased from about the same simulation time. A similar observation was noticed for the 1-nm water film, the molecular porosity dramatically increased after about 100 ps of simulation as agreed with the MDS water trajectories. In other words, the molecular porosity of the water film can be a significant parameter of the film instability at the molecular level. In this regard, the connectivity of molecular pore networks may control the film rupture process.

Table 2.4 provided the molecular porosity of different water films at some simulation time. It can be seen that the stable films maintain the molecular porosity of about 47 % $\pm$ 2%. The transition state can be defined from about 49 % $\pm$ 2 % to about 70 % $\pm$ 2 %. And the broken films have the molecular porosity up to 80% $\pm$ 2 % after 500 ps of simulation time. Therefore, the critical molecular porosity can be determined as about 49%, which means if the molecular porosity of a water film reaches 49% or above it, the film rupture can occur and the film instability is expected. These data of the molecular porosity in the water films together with the concept of the percolation theory can provide better understanding of film rupture process and film instability at the molecular level. In principle, concepts from the percolation theory should be appropriate to characterize the connectivity of preferred flow pathways (Jarvis et al., 2017; Renard and Allard, 2013). In this study, the flow pathways were considered as the pathways of molecular pores between

Table 2.4 Molecular porosity (percent) of water films at different thicknesses during 500 ps of simulation time.

Simulation time (ps)	1-nm	1.3-nm	1.5-nm	2-nm
10	48.60	46.32	44.44	46.78
50	50.81	47.83	45.84	46.60
100	50.50	48.48	46.46	47.20
120	53.91	49.89	46.19	47.20
150	61.07	51.24	46.60	47.39
180	68.94	54.74	46.42	47.46
200	71.42	56.92	46.70	47.96
220	72.70	59.49	46.59	48.15
250	73.60	63.33	47.22	47.21
280	73.71	67.04	46.98	47.03
300	74.14	68.42	47.42	47.08
320	75.03	68.65	46.49	47.34
350	75.05	69.51	46.33	47.97
380	76.27	69.13	46.89	48.38
400	77.89	68.94	47.09	48.21
420	78.67	69.03	47.66	48.18
450	80.30	70.52	46.27	48.52
480	80.14	70.69	47.35	48.46
500	81.29	70.42	47.83	48.63

water molecules and the percolation concepts can be used to describe the connectivity of molecular pore networks in water films. The molecular porosity is here represented for the critical threshold value of the occupancy probability. It is possibly expected that the molecular pores can percolate through the water film if the molecular porosity larger than the critical value of 49% as mentioned. Hence, the film coalescence occurs.

2.4 Summary

The surfactant-free water films at different thicknesses were investigated by MD simulations to identify the critical thickness at which the film rupture occurs, which was found to be 1.3 nm. This finding is in good agreement with the literature. It was observed from the trajectories of water molecules in the broken films that there was the existence of low-density areas and high-density areas before a small hole formed and grew resulting in film breakage. The broken film was further transformed to the droplet state due to the minimum potential energy achieved.

The potential energies of water films, which includes the van der Waals interaction and electrostatics interaction, at different thicknesses were analyzed by the compatible tool in Amber program. Results revealed that the potential energies of stable films remain unchanged during the simulation time whereas a decrease trend was found for broken films. The potential energies of broken films kept decreasing until the minimum value of the droplet state was obtained. This finding indicates that the interaction between water molecules in broken films was disturbed, so the film rupture occurred.

For the first time, the percolation analysis following MD simulation was investigated to examine the connectivity of the molecular pores in the water films. A

conversion procedure from MD trajectories of water molecules to 3D images was developed. The image processing software, ImageJ/ Fiji, was used to conduct further analysis of the molecular porosity and percolation concept for a better understanding of film rupture process. As for the stable films, it was found that the molecular porosity was fluctuated around the equilibrium value and kept constant during the simulation time. On the other hand, the molecular porosity in the broken films kept increasing after a short time of stability. A critical value of the molecular porosity was defined as 49 %, which means that the molecular pore network can possibly percolate through the water film if the molecular porosity exceeds this critical value, and hence, the film rupture occurs.

Although a gap between the theoretical simulation results and the experimental values of a water critical film thickness still exists, the study of a surfactant-free water film by MD simulations also significantly gains the fundamental understanding of the film rupture process at the molecular level. Also, the conversion procedure from MD trajectories to 3D images allows the application of image processing tool for further analysis. It is expected that the percolation theory of molecular pores in the water films can provide the important outlook for the scientific research of thin film stability, and hence, the future findings in this field can be achieved.

Due to the limitations in computational ability, the simulation of water-only films was investigated. However, it is expected that the results from this work provide a promising topic for future simulation research including the analysis of aqueous films in surfactant solutions.

CHAPTER 3

THEORETICAL CONSIDERATIONS OF SDS ADSORPTION EFFECT ON DISJOINING PRESSURE AND FILM DRAINAGE

3.1 Electrical Double Layer Component of Disjoining Pressure

3.1.1 Introduction

Thin liquid films between two bubbles of foams are of significant interest in a wide range of processes such as flotation, food processing, biological cell interaction and so on. The stability and properties of thin liquid films have played a decisive role in those processes and have been studied in recent decades. One of the most important properties of thin liquid film is the disjoining pressure, which is formed by the variation between the Gibbs free energy of the thin film and interfaces to counterbalance the external forces, i.e, the capillary force at the air-liquid interface. This has been investigated theoretically based on of classical DLVO theory which consists of two interaction types, the long-range repulsive electrical double layer (EDL) interaction and the short-range attractive van der Waals dispersion interaction (Lyklema and Mysels, 1965; Nguyen and Schulze, 2003).

The electrical double layer interaction is generated by the overlap of two diffuse

layers between the interfaces in the thin liquid foam film. Because of the nature of the Coulombic interaction, this long-range double layer interaction contributes significantly to the stability of the charged foam films. One normally discusses the electrical double layer interaction together with the Poisson-Boltzmann (PB) model, which describes the electrostatic potential around a surface in an ionic solution (Nguyen and Schulze, 2003). Due to the limitation of an analytical solution for the nonlinear PB equation, the linearized Debye - Huckel approximation was introduced to approximate the electrical double layer disjoining pressure. However, this approximation is only valid for a low electrostatic potential, less than 25 mV. To quantify more accurately the electrical double layer disjoining pressure, the full solution of a nonlinear second order Poisson-Boltzmann equation is required. The common charging mechanisms of either constant potential or constant charge have been applied to boundary conditions (Chan et al., 1980). The constant charge interaction can be applied when the system cannot regulate its charge during the interaction. This phenomenon seldom occurs in the bubble-bubble collision. The constant potential condition is applicable when two interfaces are separated by a moderate thickness, so the electrostatic potential remains constant with a change of film thickness. However, because of the small separation between thin films, neither constant potential nor constant charge is valid (Israelachvili, 1992). The surface properties including surface potential, and the surface charge should change with a change in film thickness and should regulate each other (Israelachvili, 1992; Nguyen and Schulze, 2003). As a result, the charge regulation mechanism has recently become the focus of considerable research , so the nature of the electrical double layer disjoining pressure in thin liquid foam films can be more fully understood.

Furthermore, in the presence of an ionic surfactant solution and a monovalent electrolyte, it has been shown that the adsorption of surfactant ions and counter-ions leads to an increase of surface charge density and to the generation of an electrical double layer. When the ions are adsorbed at the interfaces, the surface charge is generated by the accumulation of ions. The charged interfaces, therefore, can be characterized by surface potential, surface charge density, or the number of adsorbed ions (Trefalt et al., 2016). They can be modified significantly with different solution compositions. On the other hand, it has been found that the thermodynamics of surfactant adsorption get more complicated due to the presence of long-range electrical double layer interaction (Kralchevsky et al., 1999). The dependence of surface charge on surfactant adsorption requires that neither surface potential nor surface charge remain constant during the interaction of thin liquid foam films. The relationship between surfactant adsorption and electrical double layer interaction requires further quantitative study.

Recently, the disjoining pressure of thin liquid foam films has been of high interest experimentally and theoretically to many research groups (Andersson et al., 2010; Bergeron and Radke, 1992; Exerowa et al., 1987; Schelero and von Klitzing, 2015; Wang and Yoon, 2004). Disjoining pressures can be measured experimentally by a pressure balance method using the porous – plate technique first developed by Mysels (Mysels and Jones, 1966), and improved by Exerowa (Exerowa and Scheludko, 1971) as illustrated in Figure 3.1. The film is formed from a droplet in a hole 0.5 – 4 mm in diameter which is drilled in a porous glass disk of the film holder. The gas pressure in the cell is regulated and measured electronically by a pressure transducer. More details of the porous-plate technique designed by Mysels-Jones or the modified cell can be found in the literature

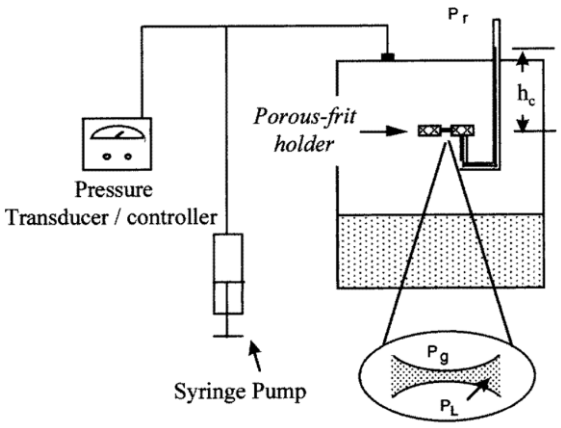

Figure 3.1 Schematic diagram of a typical thin-film balance to measure disjoining pressure isotherms. Reprinted from (Vance, 1999).

(Danov et al., 2016; Vance, 1999). The film thickness is determined by the interferometric method from the intensity of the monochromatic light reflected from the film (Exerowa et al., 1979; Sheludko, 1967). The disjoining pressure isotherm Π(h) is established. Theoretical studies of disjoining pressure have been investigated to validate the experimental data; however, the discrepancies still remain. A work from Exerowa reported direct measurements of disjoining pressure in common black films from ionic surfactants (Exerowa et al., 1987). The results showed significant deviations from theoretical predictions. Later, Mishra et al. studied the interaction free energy in foam films at different solution concentrations and also noticed the existence of systematic deviation between the measured disjoining pressure and the predicted values from DLVO theory (Mishra et al., 2005). Deviations were explained by assuming a small decrease of adsorption density during the formation of foam films.

The theoretical study of disjoining pressure, in particular, the electrical double layer interaction has been concerned commonly with either the constant potential or the constant

charge condition. Chan et al. explored the use of the fast-numerical approach to calculate the electrical double layer interactions using Fortran language, which is more efficient than the traditional elliptic functions (Carnie and Chan, 1993; Chan et al., 2006; Chan et al., 1980). Nguyen et al. developed approximate solutions of the Poisson – Boltzmann equation to predict the electrical double layer interaction force including the Debye – Huckel approximation and superposition approximation (Karakashev and Nguyen, 2007; Nguyen et al., 2000; Nguyen and Schulze, 2003). The theoretical study of electrical double layer interaction still remains of interest with regard to missing factors which may have some influence such as ion specificity (Hofmeister effect), dissolved gas, and ion correlation (Kolev et al., 2002; Ninham et al., 2017). Of special interest in this section is the theoretical effect of ionic adsorption on the electrical double layer interaction from thin liquid films. The goal is to achieve better understanding from which a general approach to predict the electrical double layer disjoining pressure in thin liquid films in the presence of ionic surfactants and monovalent electrolytes will be proposed.

3.1.2 Theoretical Modelling

3.1.2.1 Ionic Adsorption in Aqueous Films: A Charge Regulation Condition for Determining the Quantitative Electrical Double Layer Component of Disjoining Pressure

Surfactants have been of special interest in the past because of their significance in colloid science and interfaces such as wetting, lubrication, adhesion and so on. Changes in interfacial properties, including surface tension and surface charge density at air-liquid and solid-solid interfaces have been substantiated (Kolev et al., 2002; Kralchevsky et al., 1999).

In aqueous films, the adsorption of surfactant also significantly affects and modifies the dynamic properties of the interfaces. Ionic surfactants in the presence of a monovalent electrolyte, which is commonly composed of dissociated surfactant ions, counter-ions, and co-ions, potentially generate a diffuse electrical double layer from each surface in the thin liquid films. The thermodynamics of the adsorption of ionic surfactants is more complicated due to the dependence of the electrochemical potential of the ionic species on the electrostatic potential shown in the equation below.

$$\mu_i = \mu_i^{(0)} + kT \ln c_i + z_i e\psi \tag{3-1}$$

where e is the electron charge, ψ is the electrical surface potential, z_i is the valence of the ionic component i, c_i is its concentration.

In this study, we considered a thin plane – parallel symmetrical film of ionic surfactant solution with the presence of a monovalent electrolyte, as shown in Figure 3.2, to examine the effect of surfactant adsorption on disjoining pressure. A thin film example of sodium dodecyl sulfate (SDS) solution in the presence of sodium chloride (NaCl) has been investigated. We denote $c_{1\infty}$, $c_{2\infty}$, $c_{3\infty}$ as the bulk concentrations of DS^-, Na^+ and Cl^-, respectively in which the electroneutral requirement in the solution requires to $c_{2\infty} = c_{1\infty} + c_{3\infty}$. The activities of ions in this study were considered to be equivalent to the values of concentration.

The surfaces of the aqueous film are negatively charged by the migration of dodecyl sulfate ions (DS^-). Sodium ions, as counter-ions, can move further away from the interfaces to the center of the thin film. As a result, the surfaces of the thin film will become negatively charged and an electric field will appear. The diffuse double layer will then be formed by charged surfaces and surrounding ions. If we denote Γ_i as the number of adsorbed ions with

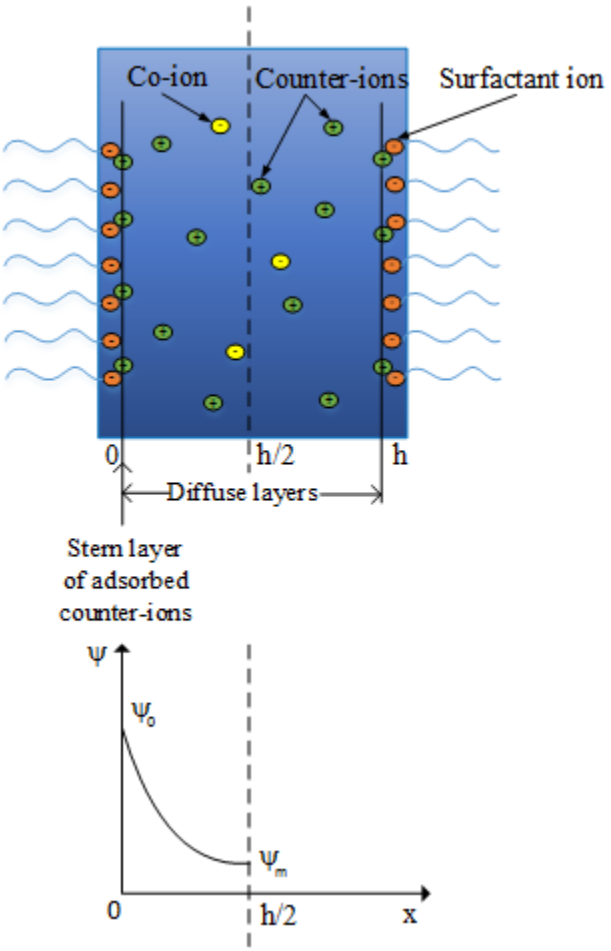

Figure 3.2 Illustration of a thin plane-parallel symmetrical film with thickness h in the presence of an ionic surfactant and monovalent electrolyte. The schematic plot at the bottom represents the electrostatic potential ψ as the function of the separation distance x, ψ_0 and ψ_m are the absolute values of ψ at the interfaces and at the mid-plane. Thickness of the Stern layer is negligible.

charge $z_i e$ per unit area, the corresponding surface charge density will be equal to $z_i e\Gamma_i$. So the total charge σ of the interfaces will be

$$\sigma = \sum z_i e \Gamma_i \tag{3-2}$$

The need for overall electroneutrality requires that the total charge of the counter-ions in the thin film be equal to the charge at the interfaces, which is implied by

$$\sigma = \int_0^{h/2} ze\rho dx = -\varepsilon\varepsilon_0 \int_0^{h/2} (d^2\psi / dx^2) dx = \varepsilon\varepsilon_0 (d\psi / dx)_{x=0} \tag{3-3}$$

where ρ is the counter-ion' density, ψ is the electrical surface potential, ε_0 is the permittivity of vacuum, and ε is the relative permittivity (the dielectric constant) of the solution.

The electric field $E = d\psi/dx$ at the interfaces can be obtained by the first derivation of the non-linear Poisson - Boltzmann equation

$$\varepsilon\varepsilon_0 \frac{d^2\psi}{dx^2} = -\rho = -e\sum z_i n_i(\infty) \exp\left\{-\frac{ez_i\psi}{k_B T}\right\} \tag{3-4}$$

The first integration of Equation (3-4) gives

$$(\frac{d\psi}{dx})^2 = 2\kappa^2[\exp(-\frac{ez_i\psi}{k_B T}) - \exp(-\frac{ez_i\psi_m}{k_B T})] \tag{3-5}$$

$$\text{with } \kappa^2 = \frac{e^2 \sum z_i^2 n_i(\infty)}{\varepsilon\varepsilon_0 k_B T} \tag{3-6}$$

where κ is the Debye constant, k_B is the Boltzmann's constant, T is the absolute temperature (in Kelvin), $n_i(\infty)$ is the number per unit volume of ions of type i with valence z_i in the bulk solution far from the interface, ψ_m is the electrostatic potential at the mid-plane position in this film.

The combination of Equation (3-2), Equation (3-3) and Equation (3-5) gives

$$2\kappa^2\varepsilon^2\varepsilon_0^2[\exp(-\frac{ez_i\psi_0}{k_BT})-\exp(-\frac{ez_i\psi_m}{k_BT})]=\sigma^2=e^2(\sum z_i\Gamma_i)^2 \tag{3-7}$$

Equation (3-7) shows the quantitative relationship between the surface potential and adsorption isotherm. Theoretically, it confirms that ionic adsorption modifies surface charge and surface potential, which regulates the electrical properties of the foam films. Further consideration was given to the application of specific adsorption isotherm models to the contribution of electrostatic potential in thin liquid foam films. The Langmuir adsorption isotherm is applied for the surfactant ions, described as (Kralchevsky et al., 1999):

$$\frac{\Gamma_1}{\Gamma_\infty}=\frac{Kc_{1s}}{1+Kc_{1s}} \tag{3-8}$$

And the Stern counter-ion adsorption isotherm is given by

$$\frac{\Gamma_2}{\Gamma_1}=\frac{K_2c_{2s}}{K_1+K_2c_{2s}} \tag{3-9}$$

where Γ_1 is the surfactant adsorption isotherm, Γ_2 is the counter-ion adsorption isotherm, Γ_∞ is the maximum possible value of Γ_1, K is the adsorption constant which is composed of the contribution of the surfactant adsorption constant and the counter-ion adsorption constant K_1 and K_2, respectively, as

$$K=K_1+K_2c_{2s} \tag{3-10}$$

The terms c_{1s} and c_{2s} represent the concentration of surfactant ions and counter-ions at the interfaces, respectively, which can be determined by the Boltzmann distribution.

$$c_{is}=c_{i\infty}\exp(-\frac{ez_i\psi_0}{k_BT}) \tag{3-11}$$

The negatively charged co-ions are expected not to bind to any ions at the interfaces

so the adsorption constant is negligible expressed as $\Gamma_3 = 0$.

Surface charge density now is given by

$$\sigma = e(z_1\Gamma_1 + z_2\Gamma_2) = \{\frac{z_1(K_1 + K_2c_{2s}) + z_2K_2c_{2s}}{K_1 + K_2c_{2s}}\}\{\frac{(K_1 + K_2c_{2s})c_{1s}}{1+(K_1 + K_2c_{2s})c_{1s}}\}e\Gamma_\infty \qquad (3\text{-}12)$$

Equation (3-7) and Equation (3-12) together with a definition of normalized electrical surface potential as $u = \psi e/k_BT$ become

$$\begin{aligned}&\sum 2\kappa^2\varepsilon^2\varepsilon_0^2\left[\exp\left(-z_iu_s\right) - \exp\left(-z_iu_m\right)\right] = \\ &\left(\frac{z_1(K_1 + K_2c_{2\infty}\exp(-z_2u_s)) + z_2K_2c_{2\infty}\exp(-z_2u_s)}{K_1 + K_2c_{2\infty}\exp(-z_2u_s)}\right)^2 \\ &\left(\frac{(K_1 + K_2c_{2\infty}\exp(-z_2u_s))c_{1\infty}\exp(-z_1u_s)}{1+(K_1 + K_2c_{2\infty}\exp(-z_2u_s))c_{1\infty}\exp(-z_1u_s)}\right)^2 e^2\Gamma^2{}_\infty\end{aligned} \qquad (3\text{-}13)$$

Equation (3-13) accounts for the charge regulation condition, which specifically shows the relation between surface potential and the adsorption isotherm of ions at the interfaces of aqueous films. Theoretically, when surfactant ions are adsorbed at the interfaces, the surface charge and surface potential gradually change because of a change in the number of surfactant ions. It is also noted that with regard to adsorption isotherms of ions, Equation (3-8) and Equation (3-9) are assumed to be thermodynamically compatible (Kralchevsky et al., 1999), which should satisfy the Euler condition given by

$$\frac{\partial G_1}{\partial \ln c_{2\infty}} = \frac{\partial G_2}{\partial \ln c_{1\infty}} \qquad (3\text{-}14)$$

3.1.2.2 General Theory of Electrical Double Layer Disjoining Pressure in Thin Liquid Films

The general theory of electrical double layer disjoining pressure was first developed in the late 1930s by Derjaguin and has been discussed in a number of published books and

articles (Israelachvili, 1992; Ivanov, 1988; Nguyen and Schulze, 2003; Vance, 1999). Surfaces normally are charged by the adsorption of ions from solutions. As discussed, the electrical double layer interaction is dependent on the charging mechanisms. The electrical double layer component of disjoining pressure is normally described with the Poisson – Boltzmann (PB) model (Nguyen and Schulze, 2003). In this study of a thin plane-parallel symmetrical thin film, the electrical double layer disjoining pressure $\Pi(h)$ generally can be calculated as (Nguyen and Schulze, 2003)

$$\Pi(h) = k_B T \sum n_i(\infty) \left\{ \exp\left[-\frac{e z_i \psi}{k_B T} \right] - 1 \right\} - \frac{\varepsilon \varepsilon_0}{2} \left\{ \frac{\mathrm{d}\psi}{\mathrm{d}x} \right\}^2 \tag{3-15}$$

In order to solve Equation (3-15), the full solution of the nonlinear PB equation as shown in Equation (3-16) is required.

$$\varepsilon \varepsilon_0 \frac{d^2\psi}{dx^2} = -e \sum z_i n_i(\infty) \exp\left\{ -\frac{e z_i \psi}{k_B T} \right\} \tag{3-16}$$

This model assumes that the solvent is a structure-less continuum; the ions are point charges; and the potential of mean force and the average electrostatic potential are the same (Nguyen and Schulze, 2003).

To further solve the nonlinear PB equation, a normalized electrical surface potential, and scaled distance are introduced as $u = \psi e / k_B T$, and $\xi = x\kappa$, respectively. The nonlinear PB equation becomes

$$\frac{\mathrm{d}^2 u}{\mathrm{d}\xi^2} = -\sum \beta_i z_i \exp(-z_i u) \tag{3-17}$$

$$\text{where } \beta_i = \frac{n_i(\infty)}{\sum n_i(\infty)(z_i)^2} \tag{3-18}$$

The first integration of PB equation for a film of ionic surfactant solution leads to

$$\left(\frac{\mathrm{d}u}{\mathrm{d}\xi}\right)^2 = 2\sum \beta_i \left[\exp(-z_i u) - \exp(-z_i u_m)\right] \tag{3-19}$$

where u_m is the normalized potential at the mid-plane film.

The electrical double layer disjoining pressure in Equation (3-15) is re-written by

$$p(h) = \frac{\Pi(h)}{k_B T \sum n_i(\infty)} = \sum \beta_i \left\{\exp\left[-z_i u\right] - 1\right\} - \frac{1}{2}\left\{\frac{du}{d\xi}\right\}^2 \tag{3-20}$$

which can be computed for a thin film with thickness h by applying the normalized potential at the mid-plane position. It is noted that no electric field exists at the mid-plane position. Hence, the normalized disjoining pressure of the electrical double layer in foam films leads to

$$p(h) = \sum \beta_i \left\{\exp\left[-z_i u_m\right] - 1\right\} \tag{3-21}$$

To completely solve Equation (3-21), the normalized mid-plane potential is required, which can be achieved by solving the nonlinear PB equation with two appropriate boundary conditions. The first condition can be found easily as no electric field at the mid-plane position in the thin film shown in Equation (3-22)

$$\left.\frac{du}{d\xi}\right|_{\kappa h/2} = 0 \tag{3-22}$$

The second condition has been found by Equation (3-13) as discussed in the previous section in regard to the ionic adsorption at the interfaces. Accordingly, Poisson – Boltzmann equation can be solved numerically by using a Matlab computational tool which will be discussed in the next section. The electrical double layer component of disjoining pressure, therefore, can be determined by Equation (3-21).

3.1.2.3 Numerical Computation Approach

In this study, the full solution of the nonlinear Poisson – Boltzmann equation has been solved numerically by the support of Matlab language. The most difficult parts are the boundary values of the normalized potential u_s at the interface, x = 0, and the normalized potential u_m at the mid-plane position, x = h/2. The solution is achieved by a collocation method to function the original conditions into a general nonlinear, two-point boundary condition. The solution results in a system of nonlinear algebraic equations on a uniform 1D mesh, which can be solved iteratively by linearization employing the linear equation solvers in Matlab. The computational approach also requires the initial guess of the surface potentials u_s and u_m, so the Debye – Huckel approximation theory of the PB equation was used to initialize the numerical solution.

A profile of the electrostatic potential as a function of separation distance is achieved by the solution of the nonlinear Poisson – Boltzmann equation. The normalized electrostatic potential at the mid-plane position is determined. Hence, the normalized electrical double layer disjoining pressures in the thin liquid foam films can be computed by Equation (3-21). The theoretical electrical double layer component of the disjoining pressure is validated by the appropriate experimental data at the same study conditions obtained from the literature.

3.1.3 Results and Discussion

In this study, a foam film of sodium dodecyl sulfate SDS in the monovalent electrolyte, NaCl, has been investigated. The adsorption constants and related parameters of the surfactant ion, DS^-, and counter-ion, Na^+, were obtained from literature (Kolev et

al., 2002; Kralchevsky et al., 1999): K_1 = 156 (m^3/mol), K_2 = 0.128 (m^6/mol^2), Γ_∞ = 4.42 x 10^{-6} (mol/L). Other parameters are in SI units. A foam film was studied at 298 K with the relative permittivity of the solution as 78.3. The experimental disjoining pressure isotherm was extracted from Exerowa publications (Exerowa et al., 1987). Figure 3.3 shows the best comparison fit between the experimental and theoretical disjoining pressure isotherm at the condition of 1 x 10^{-3} M SDS and 1 x 10^{-3} M NaCl. It has been agreed from several research works (Ivanov, 1988; Lyklema and Mysels, 1965; Ninham, 1999) that at low electrolyte concentration, the electrical double layer plays a very dominant role and the van der Waals is negligible. Following the classical Derjaguin-Landau-Verwey-Overbeek (DLVO) theory, the disjoining pressure of a thin film is given by the two components of the van der Waals interaction and the electrical double layer interaction.

$$\Pi = \Pi_{EDL} + \Pi_{vdW} \tag{3-23}$$

Therefore, the total disjoining pressure in a thin film at this condition is mainly controlled by the electrical double layer interaction. Hence, the present model possibly can be applied for the prediction of the disjoining pressure as a function of film thickness. The theoretical values showed very good agreement with the experimental data in the thickness range of 10 nm to 30 nm.

Figure 3.4 presents the theoretical values of surface potential at the interfaces which are derived from the present model. It can be seen that the absolute values of the surface potentials slightly decrease with an increase in film thickness. The surface potential is about 167.05 mV for a 10-nm film and decreases to 166.90 mV for a 30-nm film. Considering the nanometer values of thin films, this decrease contributes substantially the properties of the thin film. The observation proves that the constant surface potential model

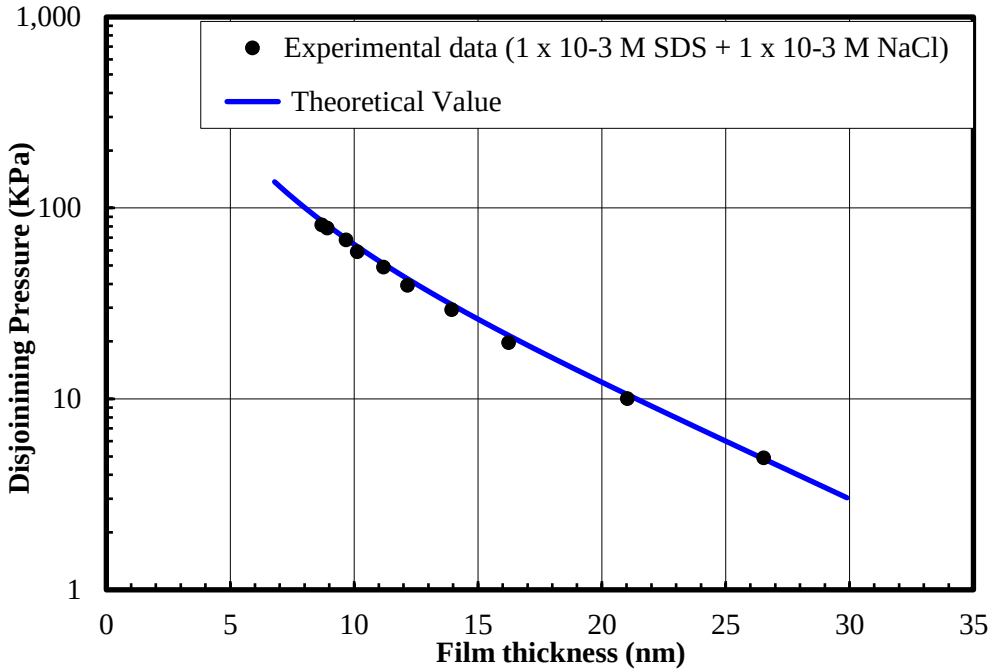

Figure 3.3 Comparison of experimental (•) and modeling (continous line) disjoining pressure for foam film from 1 x 10^{-3} M SDS solution and 1 x 10^{-3} M NaCl electrolyte added. Experimental data are extracted from the literature (Exerowa et al., 1987).

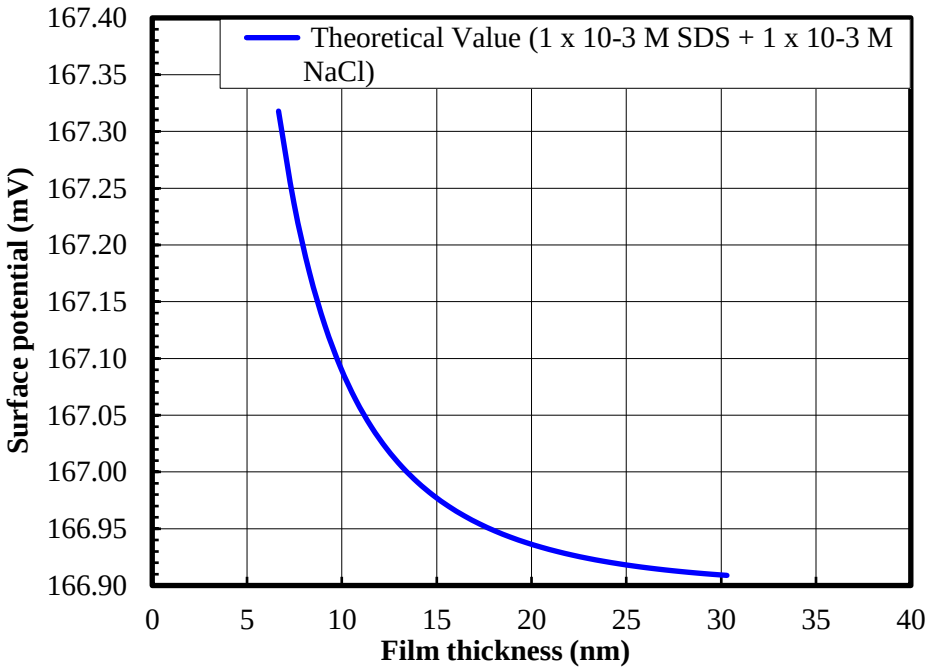

Figure 3.4 Theoretical absolute value of surface potential as a function of film thickness derived from the proposed model.

which has been applied in the theory of thin films for recent decades is no longer valid.

As discussed, our study proposes a full solution of the Poisson-Boltzmann model by the charge regulation mechanism, which computes the electrostatic potentials at each separation distance from the interface. Generally, the present model allows for computing the electrostatic potential profile in a specific solution condition as a function of separation distance from the surfaces of aqueous films. In the solution of 1×10^{-3} M sodium dodecyl sulfate and 1×10^{-3} M sodium chloride, the electrostatic potential profile for a 26-nm film thickness was calculated and is shown in Figure 3.5. It can be seen that the potential at the mid-plane position in the thin film is a comparable value at about 25.34 mV. This result clarifies that the potential at the mid-plane position is incorrectly considered to be zero value. Basically, electrostatic potentials gradually decrease with an increase of separation distance from the surfaces to the mid-plane position.

Figure 3.6 gives the modeling result of the electrical double layer disjoining pressure isotherm in the foam film of a 1×10^{-3} M surfactant SDS and 1×10^{-4} M NaCl compared with the experimental data. At a lower electrolyte concentration, a slight discrepancy was observed between the theoretical values and the experimental data. At the same surfactant concentration but lower sodium chloride concentration, the ionic strength was lower; the electrical double layer was not comparable with the previous case. The electrical disjoining pressure isotherm at this concentration accordingly plays a less dominant role. In the range of film thickness from 10 nm to 20 nm, the measured disjoining pressure was moderately higher than the theoretical value. From 20 nm to 30 nm of film thickness, the theoretical disjoining pressure isotherm agreed well with the experimental data. Several explanations can be proposed at this point. Within the thin liquid films 10 nm

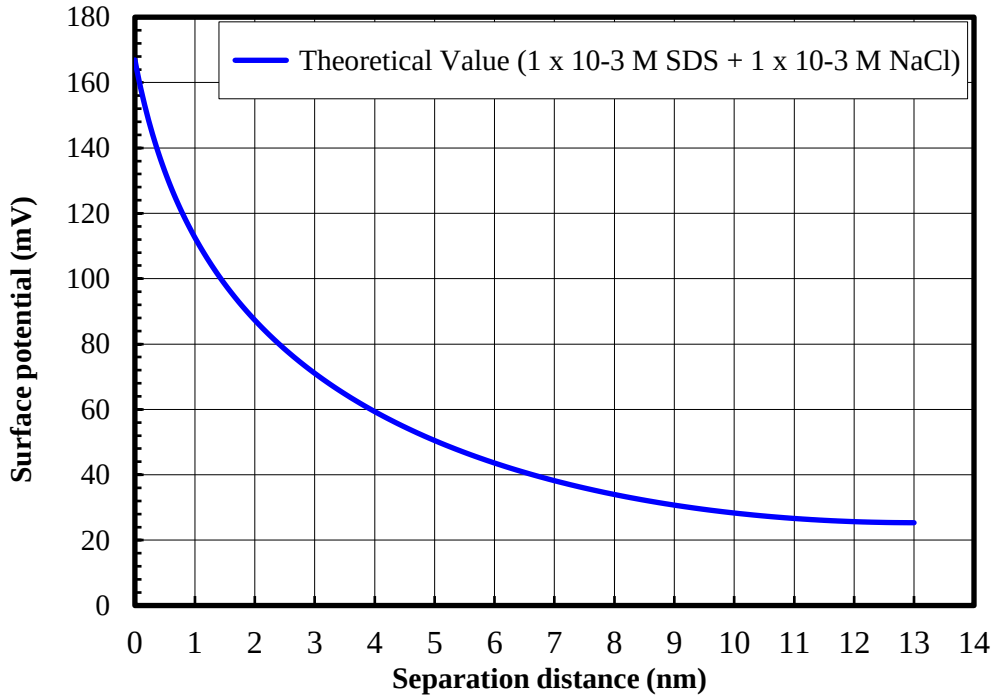

Figure 3.5 Theoretical absolute value of electrostatic potentials as a function of separation distance in a 26-nm film.

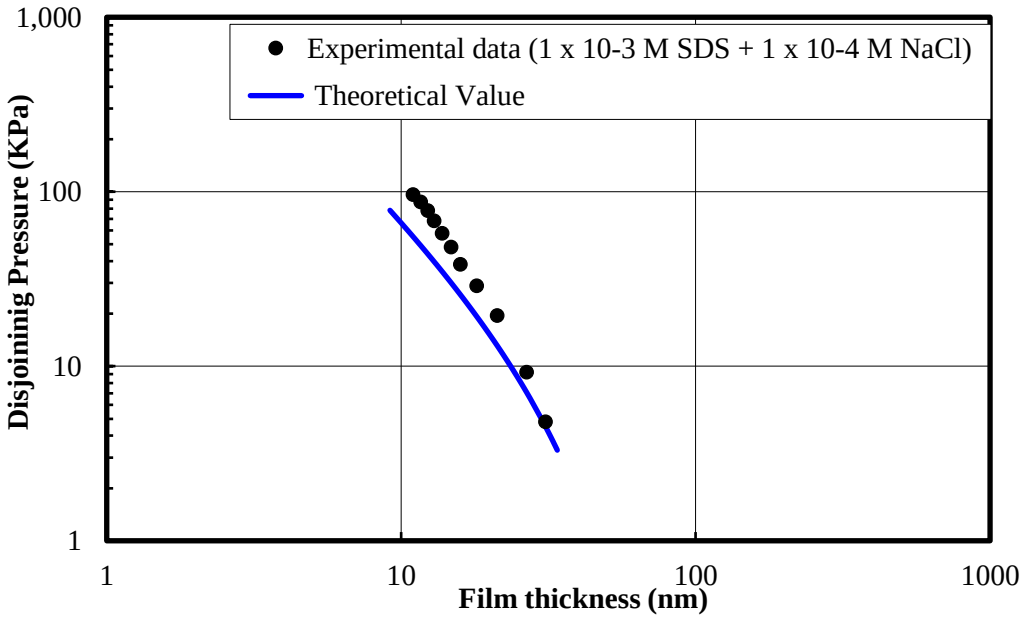

Figure 3.6 Comparison of experimental (•) and modeling (continuous line) of disjoining pressure for a foam film from 1 x 10^{-3} M SDS solution and 1 x 10^{-4} M NaCl electrolyte added. Experimental data are extracted from the literature (Exerowa et al., 1987).

to 20nm in thickness, the excess of experimental disjoining pressures initiates an additional repulsive interaction. It can originate from the adsorption of the surfactant group at the lower electrolyte concentration. With regard to the adsorption theory, the validity of the classical uniform monolayer adsorption model has been investigated and an adsorption model with the immersion of adsorbed molecules at the single interface has also been proposed (Shahir et al., 2016). Here we provide a similar hypothesis that at this low electrolyte concentration, within the film thickness from 10 nm and 20 nm, there still remain some surfactant ions immersed in the subinterface which may exert an additional repulsive interaction. The other possibility of additive repulsion in the experimental disjoining pressure isotherm can be the solvation force or hydration force. At the lower electrolyte concentration (1×10^{-4} M sodium chloride) compared to the previous study case, the repulsive hydration interaction in that short range of thin film, which is generated from the hydrogen bonding and dipole polarization among water molecules (Vance, 1999), may also contribute to the total disjoining pressure isotherm. In the range of film thickness from 20 nm to 30 nm, further separation distance is provided between the two interfaces, so the adsorption of surfactant ions onto the interfaces is uniform and the electrical double layer still exists and plays a dominant role. The electrical disjoining pressure isotherm, as a result, shows a very good fit between the experimental data and the theoretical values. Figure 3.7 gives another example from experimental works in the other research group (Mishra et al., 2005). Similarly, a good fit has been observed in the range of film thickness from 20 nm to 30 nm (the last two experimental points).

Figure 3.8 provides more comparisons between the theoretical values achieved from the present model and the experimental data from the literature (Danov et al., 2016;

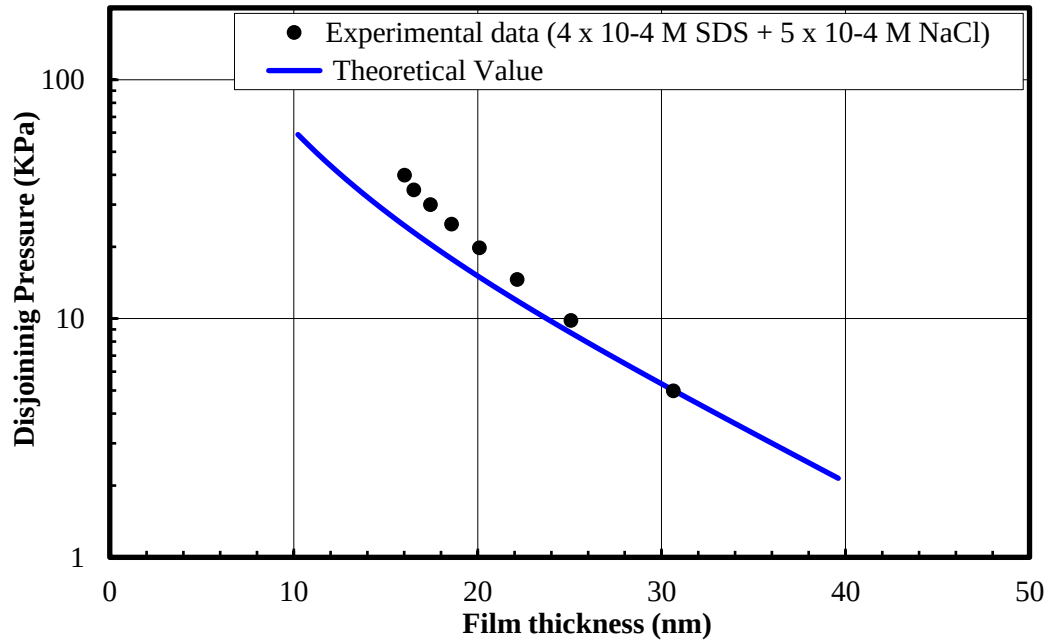

Figure 3.7 Comparison of experimental (•) and modeling (continuous line) of disjoining pressures for foam films. Experimental data are extracted from the literature (Mishra et al., 2005).

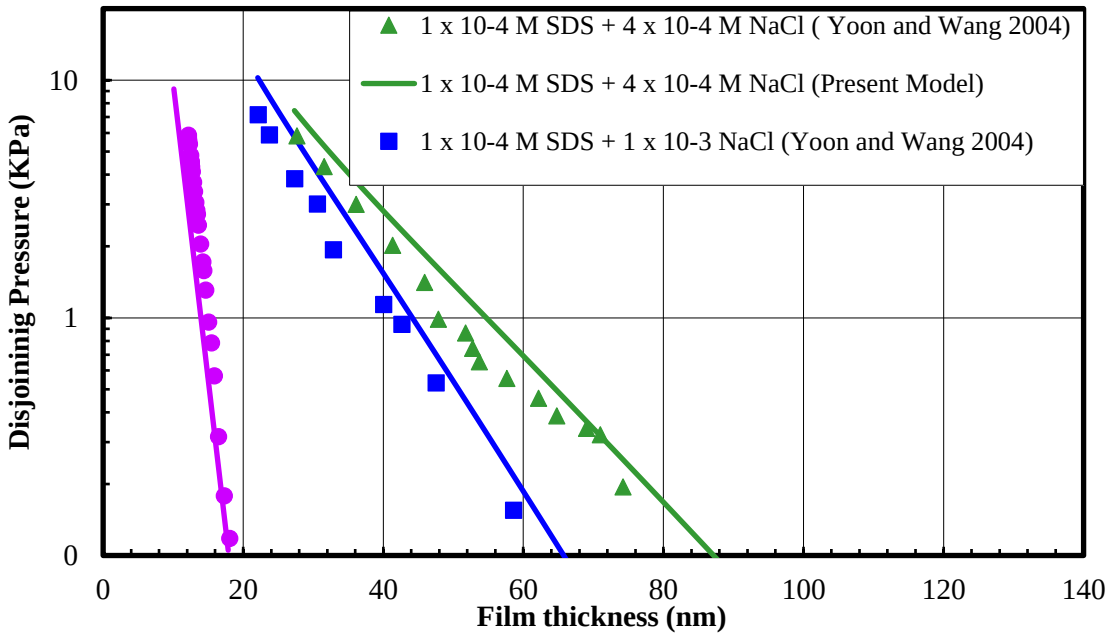

Figure 3.8 Comparison of experimental (circle points; square points and top triangular points) and modeling (continuous lines) of disjoining pressures for aqueous films. Experimental data are extracted from the literature (Danov et al., 2016; Mishra et al., 2005; Wang and Yoon, 2004).

Wang and Yoon, 2004). It can be seen that although a slight discrepancy still exists at low SDS concentration of 1 x 10^{-4} M and 4 x 10^{-4} M NaCl, in general, the present model gives a good prediction of the disjoining pressure as a function of the film thickness. Of special interest in Figure 3.8 is the good fit between the theoretical values and experimental data at the condition of 1 x 10^{-3} M SDS and 30 x 10^{-3} M NaCl. At higher electrolyte concentrations, eventually the electrical double layers are compressed, the thickness becomes thinner, and the film is more stable. The great agreement at this condition indicates that the present model, with the charge regulation condition as discussed, is an efficient tool to predict the electrical double layer disjoining pressure in a thin aqueous film.

3.1.4 Summary

In this section, a theoretical model was proposed to predict the electrical double layer component of disjoining pressure in a thin aqueous film based on the generalized theory of the nonlinear Poisson-Boltzmann model and the adsorption of ionic surfactants at the interfaces. The charge regulation mechanism was used as one of the boundary conditions for the full solution of nonlinear Poisson - Boltzmann equation. The Langmuir adsorption model was applied for the surfactant ions and the Stern adsorption model was used for the counter-ions in the study of ionic surfactants and a monovalent electrolyte. A numerical computation by a collocation method in Matlab was explored to quantitatively define the electrical double layer component of disjoining pressure in the thin film. The outcome of this work provides a reasonable prediction of the disjoining pressure in the aqueous films at the appropriate concentration, where the electrical double layer interaction

plays a critically dominant role compared to the van der Waals interaction in the classical DLVO theory.

3.2 Effect of Electrical Double Layer Disjoining Pressure in Film Drainage

3.2.1 Introduction

Foam films are of special interest in a number of significant fields including both natural and industrial applications. Foam can be either a desirable factor or an unexpected phenomenon in the industrial process. This leads to the important role of the study of foam stability and foam film thinning. Film thinning, therefore, has been investigated in the last several decades by many researchers. When the thickness of a thin film is in the range of hundreds of nanometers, two types of interactions should be considered. The first one, which is the thermodynamic interaction, consists of van der Waals, electric double layer, and other similar forces. A measurable parameter of this interaction, called disjoining pressure, was introduced by Derjaguin in the early 40s (Derjaguin, 1937) and until recently the components of this interaction have still been in debate, as discussed in the previous Section 3.1. The second consideration is known as the hydrodynamic interaction. When the thickness of a thin film becomes much smaller than its radius, the hydrodynamic interactions are strongly influenced by the deformation and tangential mobility of the interfaces (Ivanov, 1988). The interplay between these two interactions determines the formation of the thin liquid film. Hence, film thinning is of critical significance in determining the foam behavior.

Experimentally the drainage of aqueous films can be measured by the Scheludko

microinterferometry approach which was originally invented by Scheludko and later computerized by the support of programming software (Karakashev et al., 2008; Sheludko, 1967). The experimental set-up as described in Figure 3.9 consists of a Scheludko cell for the aqueous film formation, a metallurgical inverted microscope, a high-speed camera, and a computer for controlling and recording the video for further image analysis. Briefly, the aqueous film is formed in the film holder of a Scheludko cell and it gets thinner by withdrawing the liquid out with a gastight microsyringe. The radius of a thin film is required to be smaller than 100 μm so that the film surfaces are considered to be plane parallel. The film is illuminated by a monochromatic light with the wavelength of 546 nm. When the interference of the light occurs, a set of bright and dark fringes (Newton ring) is observed and recorded in the computer using the high-speed video camera system. The film thickness is calculated using the Scheludko interferometric equation as described from the published articles (Karakashev et al., 2008; Karakashev and Nguyen, 2007). The film thickness experimentally was reported as a function of the film lifetime in the literature.

With regard to the theoretical studies, Scheludko first proposed the thinning of a single microscopic foam film based on the Reynolds equation with several conditions, such as, the film surfaces are tangentially immobile and liquid flows between the plane-parallel film surfaces (Sheludko, 1967). This theory was confirmed by experiments from Manev et al. that it is only applicable to sufficiently small radii, below 0.05 mm (Manev et al., 1997b). Radoev, later on, pursued the other investigation on the mobility of film surfaces. In recent years, Karakashev and Nguyen have investigated the effect of surface shear viscosity and elasticity, and the surfactant diffusions, as well as the intermolecular forces on the film drainage (Karakashev et al., 2008; Karakashev and Nguyen, 2007). Generally,

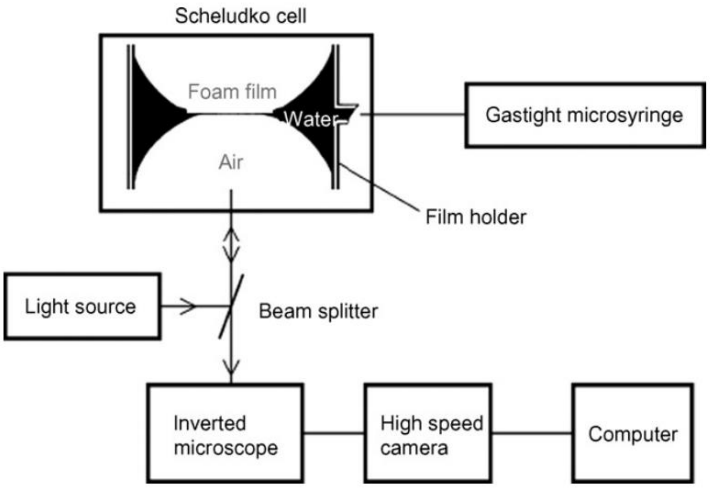

Figure 3.9 Experimental set-up for film thinning measurement. Reprinted from (Karakashev et al., 2008).

most of the studies have concentrated on surface rheology, interface shape, and intermolecular forces (Karakashev et al., 2008).

Although many research studies have been done regarding the theoretical development of film drainage kinetics, the validity of the reported models is still limited. In this section, a new model is proposed based on the prediction of electrical double layer disjoining pressure as discussed in the previous Section 3.1. It is generally accepted that disjoining pressure is one of the critical parameters in the kinetics of film drainage. In the previous section, a new model of electrical double layer disjoining pressure was developed based on the effect of surfactant adsorption and the charge regulation condition. This model will be applied in the study of film drainage kinetics. Hence, a new model of film drainage kinetic will be developed accordingly.

3.2.2 Theoretical Modelling of Film Drainage

In this section, the foam film drainage theory was studied for plane parallel immobile surfaces. Of particular interest is the effect of surface forces on the drainage kinetics of thin aqueous films. It was assumed that other effects including the Marangoni effect, surfactant surface diffusion, and surface viscosity can be neglected. In general, the kinetics of thin film drainage can be described by the Stefan-Reynolds equation as shown below (Nguyen and Schulze, 2003).

$$-\frac{dh}{dt} = \frac{2h^3}{3\mu R^2}(P_\sigma - \Pi) \tag{3-24}$$

where $-\frac{dh}{dt} = V_{\mathrm{Re}}$ is the drainage velocity from the Stefan-Reynolds lubrication theory, h is the film thickness, μ is the liquid viscosity in the film, R is the film radius, P_σ and Π are the capillary pressure and total disjoining pressure in the thin film, respectively.

The capillary pressure can be determined from Equation (3-25)

$$P_\sigma = \frac{2\gamma R_c}{R_c^2 - R^2} \tag{3-25}$$

where γ is the surface tension of the surfactant solution and R_c is the radius of the film holder in the Scheludko cell (R_c = 2 mm) as mentioned in Section 3.2.1. Figure 3.10 illustrates the identification of film holder radius R_c and film radius R in the experimental set-up of film drainage measurement.

Equation (3-24) shows the inverse correlation between the total disjoining pressure and the film drainage rate. It can be seen that the disjoining pressure is a critical parameter of the film drainage rate since the other parameters should not fluctuate in a wide range. Total disjoining pressure in thin liquid film, according to the DLVO theory, should be

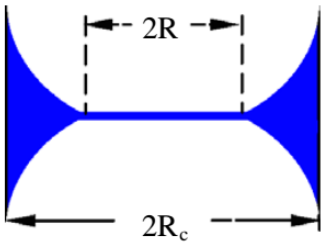

Figure 3.10 Illustration of film holder radius and film radius in the experiment of film drainage measurement. Reprinted from (Karakashev and Ivanova, 2010).

given by the summation of van der Waals interaction Π_{vdw} and electric double layer interaction Π_{edl} (Israelachvili, 1992; Mahanty and Ninham, 1977; Nguyen and Schulze, 2003; Sheludko, 1967)

$$\Pi = \Pi_{vdW} + \Pi_{edl} \tag{3-26}$$

The van der Waals interaction can be calculated by microscopic Hamaker approach or the macroscopic Lifshitz approach. In the application of foam film surfaces, van der Walls disjoining pressure as the function of film thickness is expressed in Equation (3-27) with the combination of two approaches (Karakashev and Nguyen, 2007; Nguyen and Schulze, 2003).

$$\Pi_{vdW} = -\frac{d}{dh}\{-\frac{A(h,\kappa)}{12\pi h^2}\} = \frac{A(h,\kappa)}{6\pi h^3} + \frac{1}{12\pi h^2}\frac{dA(h,\kappa)}{dh} \tag{3-27}$$

where $A(h,\kappa)$ is the Hamaker - Lifshitz function described as

$$A(h,\kappa) = (1+2\kappa h)e^{-2\kappa h}A_o + \frac{3\hbar\omega}{16\sqrt{2}}\frac{(1-n^2)^2}{(1+n^2)^{3/2}} \times [1+(\frac{h}{\lambda})^q]^{-1/q} \tag{3-28}$$

In Equation (3-28), κ is Debye constant; h is film thickness; $\hbar$ is Planck constant (divided by 2π); ω is the adsorption frequency in the UV region, about 2.068 x 10^{16} rad/s

for water; n^2 = 1.887 is the square of the characteristic refractive index of the aqueous film in the UV region (Nguyen, 2000); q = 1.185; λ is the characteristic wavelength, λ = 5.59 nm (Karakashev and Nguyen, 2007).

The zero-frequency term of the Hamaker – Lifshitz constant, A_o, is a function of the Boltzmann constant k_B, absolute temperature T, and dielectric constant of the film ε_0 as shown in Equation (3-29).

$$A_0 = \frac{3k_BT}{4}\sum_{j=1}^{\infty}\frac{1}{j^3}\left(\frac{1-\varepsilon_0}{1+\varepsilon_0}\right)^{2j} \tag{3-29}$$

The dielectric constant of the aqueous films is usually $\varepsilon_0 \cong 80$ and the infinity summation in Equation (3-29) are approximately equal to 1.444, giving A_0 = 1.083k_BT (Karakashev and Nguyen, 2007).

For the interaction of the electric double layer in thin liquid film, as studied in the previous Section 3.1, a model of electric double layer disjoining pressure based on the charge regulation condition was developed. Basically, the electric double layer disjoining pressure is described in Equation (3-30).

$$\Pi_{el} = k_BT\sum n_{i\infty}[\exp(-\frac{ez_i\psi}{k_BT})-1]-\frac{\varepsilon\varepsilon_0}{2}\{\frac{d\psi}{dx}\}^2 = k_BT\sum n_{i\infty}[\exp(-\frac{ez_i\psi_m}{k_BT})-1] \tag{3-30}$$

where k_B is Boltzmann's constant k_B = 1.38 x 10-23 (J/K); T is absolute temperature; $n_{i\infty}$ is the number of ions of type i per unit volume in the bulk solution; e is the charge on electron; z_i is the valence of ion i; and ψ_m is the potential at the mid-plane position of thin film. The value of ψ_m was obtained from the numerical computation based on the charge regulation condition as discussed in Section 3.1. Hence, the electrical double layer disjoining pressure was determined.

The integration of Equation (3-24) provides the relation of film thickness and the

drainage time as described by

$$t = \int_{h_0}^{h} -\frac{2\mu R^2}{3h^3(P_c - \Pi)} dh \tag{3-31}$$

It was assumed that the film radius remains unchanged during the film drainage. The necessary parameters such as surface tension, film radius, as well as concentrations of SDS and electrolyte NaCl were obtained from the experimental work in the literature (Karakashev et al., 2008; Tsekov et al., 2010; Wang and Yoon, 2005). The values of film radius were reported from the literature that they were controlled to be well below 100 μm in order to obtain the tangentially immobile thin films. A computational code was developed in Matlab language to solve Equation (3-31) including the computation of the electrical double layer disjoining pressure numerically and the van der Waals components. The computed film thickness as a function of film lifetime was compared with the experimental data at the same conditions.

3.2.3 Results and Discussion

Figure 3.11 and Figure 3.12 present the theoretical results of film drainage kinetics of SDS solutions, compared with the experimental data from Karakashev's work (Karakashev et al., 2008; Tsekov et al., 2010). It can be seen that the present model with the effect of surfactant adsorption has failed to predict the film drainage at the low concentrations of SDS solutions. At low concentration 5 x 10^{-5} M of the SDS solution, the theoretical drainage rate was slower than the experimental data and the predicted equilibrium thickness was larger than the experimental value. This big discrepancy indicates that the validity of the present model was not appropriate for the low concentration of surfactant solutions. Probably because at the low concentration, the

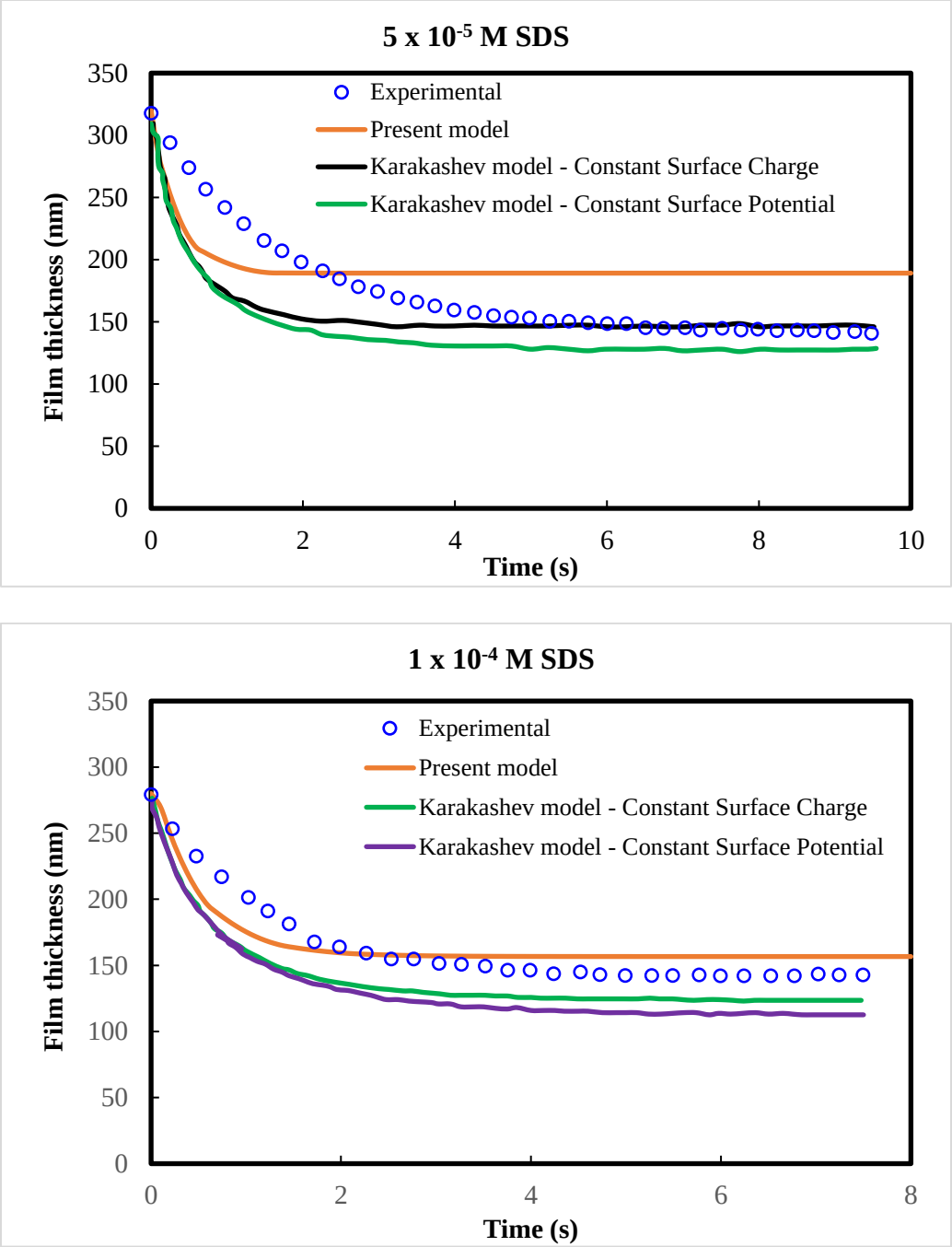

Figure 3.11 Kinetics of film drainage at 5 x 10^{-5} M and 1 x 10^{-4} M SDS solutions. The solid lines represent for theoretical results and the open circles represent experimental data. Experimental data were extracted from Karakashev's work (Karakashev et al., 2008).

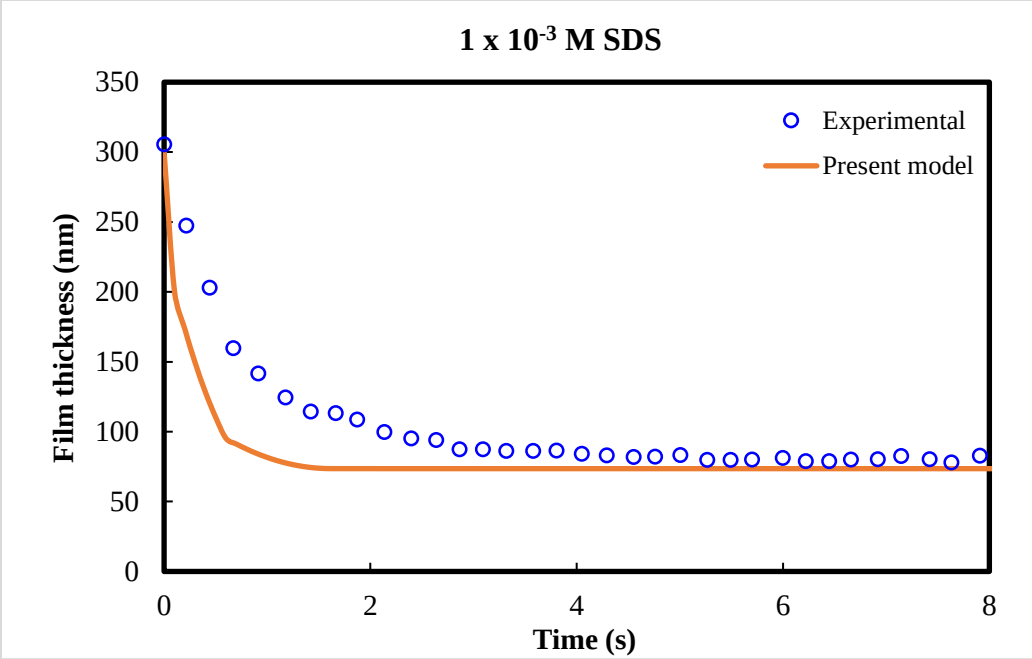

Figure 3.12 Kinetics of film drainage at 1 x 10^{-3} M SDS solution. The solid line represents for theoretical results and the open circles represent experimental data. Experimental data were extracted from Karakashev's work (Karakashev and Ivanova, 2010).

diffuse layer and the double layer are large, for example, $1/\kappa \approx 42.96$ nm for 5 x 10^{-5} M SDS solution, the electrical double layers do not actually overlap, and hence, the electrostatic interaction does not significantly affect the film drainage. The theoretical values from the present model are also compared with the results from Karakashev's models in Figure 3.11. It is noted that Karakashev et al. developed the models of film drainage kinetics based on the prediction of electrical double layer repulsion at either constant surface potential or constant surface charge conditions (Karakashev et al., 2008). As discussed in the previous Section 3.1, those predictions are possibly no longer valid due to the graduate change of surface potential and surface charge with the film thickness. The present model showed a better prediction at the concentration of 1 x 10^{-4} M SDS solution. This observation confirmed the accuracy of the present model at the appropriate condition

where the electrostatic interaction plays a significant role in the aqueous film.

At high concentration of 1 x 10^{-3} M, the theoretical equilibrium thickness in Figure 3.12 shows a very good agreement with the experimental value. However, the results also indicate that the present model predicts the faster drainage than the experimental data. The aqueous film reaches equilibrium thickness after about 3 seconds in the experimental measurement whereas it is predicted to be about 1.5 seconds. This can probably be explained by the neglection of Marangoni effect in the present mode, which potentially contributes to an increase of the drainage velocity (Karakashev and Ivanova, 2010).

In the presence of electrolyte NaCl, the theoretical results of film drainage at different concentrations show a good agreement with the experimental data from Tsekov's work as shown in Figure 3.13. The results reveal that with the added electrolyte of 0.02 M NaCl, the theoretical equilibrium thickness at either the low concentration of SDS solution (1 x 10^{-6} M) or rather high concentration of SDS solution (1 x 10^{-3} M) is predicted as accurately as the experimental values. Although the drainage velocity shows a bit offset between theoretical and experimental data, it can be reported that the present model provides very good agreement with the experimental data. These observations indicate that the added electrolyte, as well as the ionic strength, plays an important role in the accuracy of predicting the film drainage rate by the present model because the added electrolyte compresses the electrical double layer in the aqueous film, and hence, the double layers overlapped, and the electrostatic disjoining pressure significantly dominates in the surface forces. As a result, the electrostatic interaction mainly affects the film drainage kinetics. Hence, the present model with the charge regulation condition and the effect of surfactant adsorption provides a good theoretical prediction for the drainage rate of the thin film at

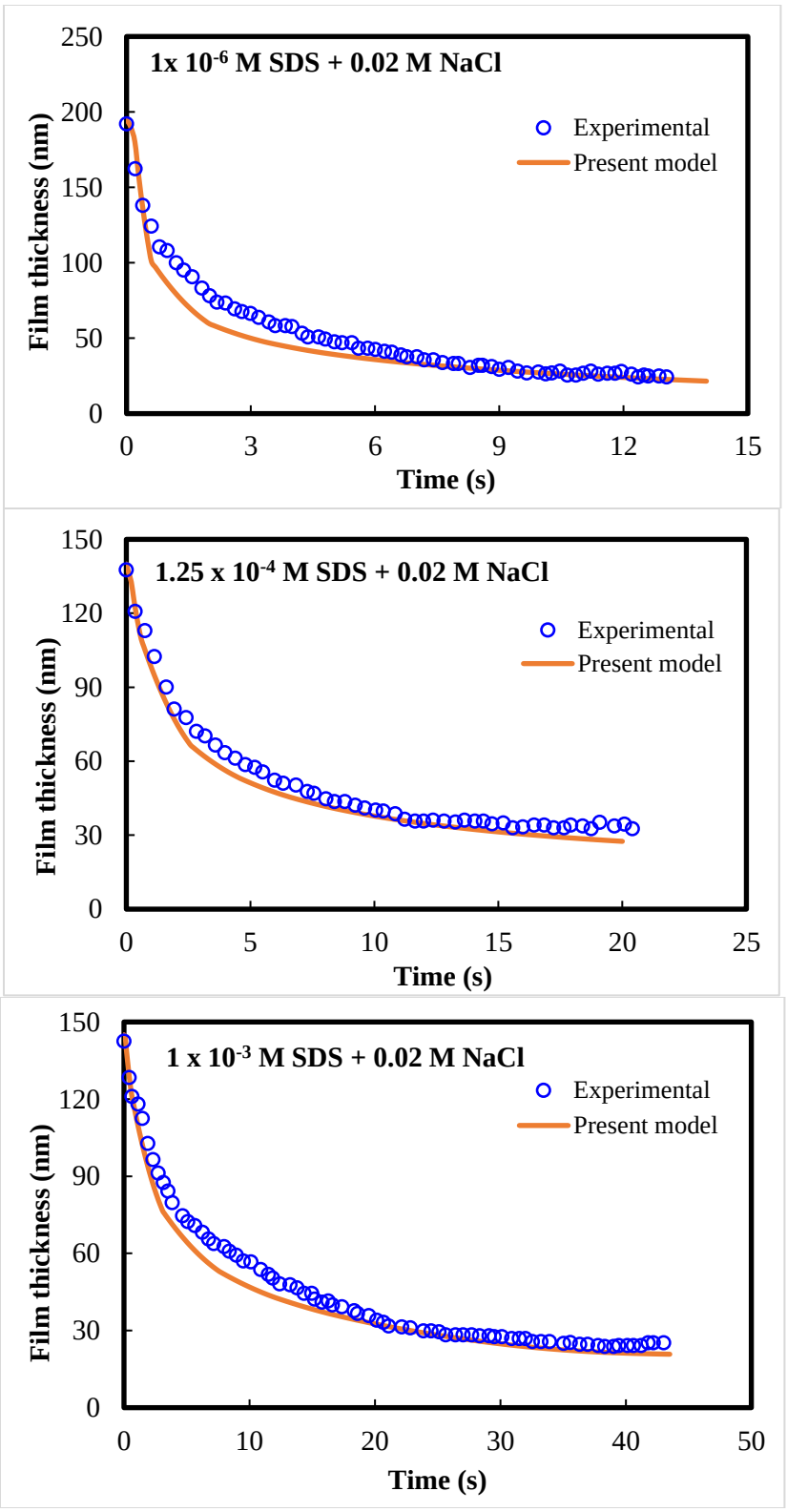

Figure 3.13 Kinetics of film drainage at different SDS concentration and 0.02 M NaCl. The solid line represents theoretical results and the open circles represent experimental data. Experimental data were extracted from Tsekov's work (Tsekov et al., 2010).

these conditions.

In addition, the experimental work reported by Yoon and Wang was also applied to validate the present model (Wang and Yoon, 2005). The kinetics of film thinning was also measured by a Scheludko cell in a similar experimental system with Karakashev's work.

Figure 3.14 presents the theoretical results of film drainage in comparison with the experimental data at the different concentrations of SDS and NaCl solutions. It can be seen that at the concentrations of 1 x 10^{-4} M SDS and 4 x 10^{-4} M NaCl, the theoretical film drainage agreed very well with the experimental data. It was also explained by Yoon and Wang that at this high SDS and NaCl concentration, the disjoining pressure is dominated by the electrostatic interaction and other interactions are negligible. Hence, the addition of surfactant and electrolyte at this condition effectively affects the film drainage rate. This observation confirms the accuracy of the present model at the appropriate condition where the electrostatic interaction plays a significant role in the aqueous film. Further the results of film drainage rate at different SDS concentrations and 0.3 M NaCl were reported. At this high concentration of electrolyte NaCl, it was reported that the electrical double layer force is significantly screened so that it can be negligible (Wang and Yoon, 2005). However, as discussed, the present model of film drainage consists of the numerical computation of electrostatic interaction with the charge regulation condition, and hence, the theoretical values given in the present model are taken into account by the electrostatic interactions even at the high ionic strength condition. At a very low concentration of SDS (5 x 10^{-7} M) and 0.3 M NaCl, a small discrepancy between the theoretical values and the experimental data was observed probably because the distribution of surfactant adsorption

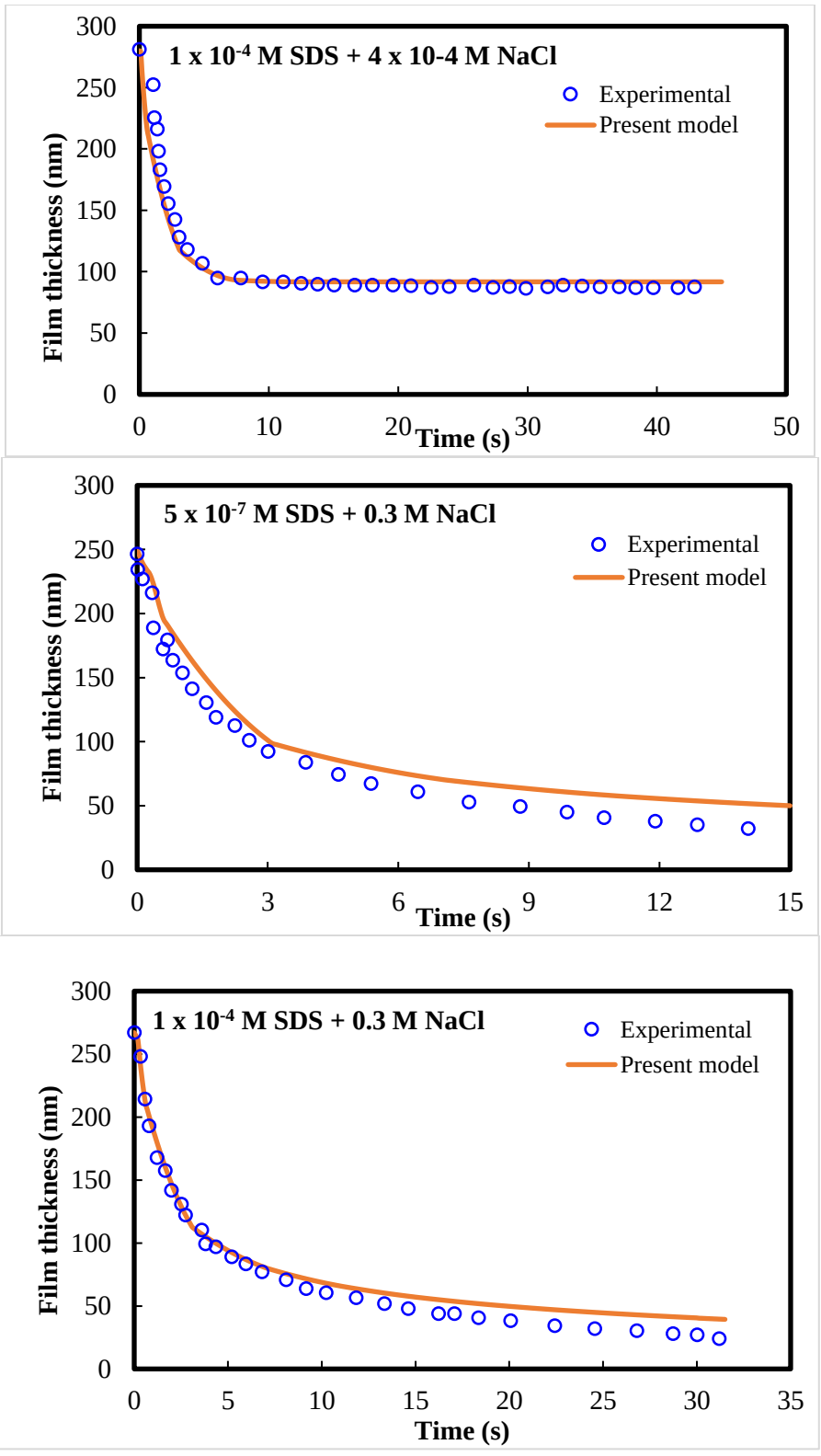

Figure 3.14 Kinetics of film drainage at different SDS and NaCl concentrations. The solid line represents theoretical results and the open circles represent experimental data. Experimental data were extracted from Yoon and Wang's work (Wang and Yoon, 2005).

at this condition is not uniform at the surfaces. The film drainage rate at a higher concentration of SDS solution (1×10^{-4} M) and 0.3 M NaCl shows a good agreement with the experimental data. Theoretical values predicted from the present model confirm the hypothesis that the surfactant adsorption provides a significant effect on the disjoining pressure as well as the film drainage kinetics.

3.2.4 Summary

In summary, a new model of film drainage kinetics was developed in this section based on the effect of classical DLVO interactions including van der Waals and electrical double layer interactions. The combination of Hamaker and Lifshitz approaches was used for the computation of van der Waals disjoining pressure. The model of electrical double layer disjoining pressure which was developed in the previous section was applied and taken into account in this study. It was shown that at the appropriate conditions where the electrical double layer plays a significant role, the theoretical results were in good agreement with the experimental data which were extracted from the literature of different research groups. The future research can be developed with the addition of the other effects including the Marangoni effect and/or the surface viscosity.

This chapter theoretically examined the effect of surfactant adsorption to the electrical double layer disjoining pressure as well as the film drainage rate. The studies indicated that the constant potential and/or the constant charge condition which was usually applied to compute the electrical double layer disjoining pressure are no longer valid in certain studied conditions. With the support of advanced computational tools, the charge regulation condition was able to solve, and hence, the electrical double layer disjoining

pressure was possibly computed. The theoretical film drainage rate accordingly was shown a good theoretical prediction by the present model. The studies in this chapter provided the significant contribution to the theoretical work of the disjoining pressure in aqueous films and the film drainage kinetics, which importantly gain a better understanding of the film stability.

CHAPTER 4

INTERFACIAL WATER FEATURES AS INFLUENCED BY ADSORBED SURFACTANTS

4.1 Introduction

The stability of foams has been considered as an important factor in many industrial applications such as mineral flotation, food processing, personal care products, and so on. Several parameters reported to influence foam stability are surface tension gradients, surface viscosity, critical packing parameters, and molecular interaction, as well as van der Waals and double layer forces. Of particular interest in recent decades is the behavior of surfactant adsorption and packing at air-water interfaces (Dominguez and Berkowitz, 2000; Li et al., 2017; Lu et al., 2000; Nakahara et al., 2005; Nguyen et al., 2014). The Gibbs adsorption isotherm equation, surface tension measurements, and surface potential measurements have been used primarily to quantify the adsorption of surfactants at the interfaces. On the other hand, a wide range of modern experimental techniques including fluorescence, resonance Raman scattering, neutron reflection, sum frequency generation (SFG) vibrational spectroscopy can be applied to study the structure and orientation of surfactants at interfaces. At the same time, due to the dramatic increase of computational resources, computer simulations allow us to obtain a better understanding of the structural

properties and behavior of surfactants at the molecular level. Recent development of technology has provided promising tools to gain more understanding on how surfactant adsorption occurs at the air-water interface and its effect on foam stability.

Anionic sodium dodecyl sulfate (SDS) and cationic dodecyl ammonium hydrochloride (DDA), well-known surfactants, have been widely used as detergents as well as collectors in the mineral flotation process. A number of research studies have been conducted on the adsorption behavior of SDS and DDA surfactants as well as the properties of surfactant solutions (Hore et al., 2005; Nakahara et al., 2005; Wang et al., 2009; Yoon and Yordan, 1986). Richmond and co-workers have provided important information about how the molecular structure of SDS and DDA alter the orientation of water molecules at the air-water interface by employing sum frequency vibrational spectroscopy experiments (Gragson et al., 1997b). Nguyen et al. studied different effects of single and binary surfactant systems of SDS and DDA on their adsorption, packing and water structures at the air-water interface (Nguyen et al., 2014). With respect to MD simulations, Berkowitz and co-workers explored a molecular picture of SDS surfactant molecules at the water-vapor and water-carbon tetrachloride interfaces. The molecular structure of the SDS surfactant was reported for the head group and hydrocarbon chain locations, dihedral distribution and head group-water radial distribution function (Schweighofer et al., 1997).

Although a number of experimental and theoretical reports confirm the interaction between surfactant and water molecules at interfaces, very limited research on the fundamental understanding of interfacial water at the air-water interface has been found. Not much attention has been given to the mechanism of how interfacial water structures affect foam stability. In this chapter, results on structure and properties of interfacial water

molecules are reported for sum frequency generation (SFG) vibrational spectroscopy experiments and molecular dynamics simulation (MDS) analysis with the following organization. At first, SFG experimental results are reported at the air-water interfaces for the SDS and DDA solutions at varying concentrations and neutral pH. This is followed by MDS analysis of the interfacial water structures at the air-water interfaces for the SDS and DDA solutions. Then, the pH effect on the interfacial water structures of both the SDS and DDA solutions is reported. The pH effect is of interest because alkaline conditions are common in mineral flotation processes. Finally, a hypothesis on how interfacial water structures affect foam stability is proposed and confirmed by foam stability and foam weight experiments.

4.2 Materials and Methods

4.2.1 Materials

Sodium dodecyl sulfate (SDS) with purity higher than 99% was purchased from Sigma-Aldrich. Dodecyl Ammonium Hydrochloride (DDA) was received from ACROS Organics (99%). Potassium hydroxide (KOH) was purchased from Mallinckodt (98%) and used as received. Purified deionized water with the resistivity of 18.2 mΩ.cm was obtained from a Milli-Q system and used to prepare the surfactant solutions in all experiments.

In SFG air-water interface experiments, the surfactant solutions of appropriate concentrations and pH conditions were contained in a 25-ml glass cell. To clean the glass cell properly, the appropriate cleaning method was conducted with acetone, methanol, washing with deionized water, and then drying with high-purity nitrogen gas.

4.2.2 Sum Frequency Generation (SFG) Vibrational Spectroscopy

Widely known as a second-order nonlinear vibrational spectroscopy technique with the great capabilities for interfacial studies, SFG has been used efficiently to study the molecular features at the solid-liquid, liquid-liquid, solid-air and liquid-air interfaces. Two incident beams in SFG, one with fixed visible frequency and the other beam tunable in the infrared region, are focused to overlap at the surface or interface of interest to emit a photon whose frequency is their sum ($\omega_{SFG} = \omega_{vis} + \omega_{IR}$) as shown in Figure 4.1.

An EKSPLA, Ltd. sum frequency generation spectrometer was used in all SFG experiments. The laser system was described in the previous study from our group (Nickolov et al., 2004). The incident angles of the visible and IR beams were set as 60^o and 66^o at the air-water interface, respectively. The angle of the reflected SFG beam was taken at 65^o. The spectra were collected in ssp polarization conditions (s-polarized sum-frequency, s-polarized visible, and p-polarized infrared) and were normalized to the visible and IR energies. Each data point was collected at 4 cm^{-1} increments and is the average of 30 laser shots.

The SFG measurements of surfactant solutions at the air-water interfaces were

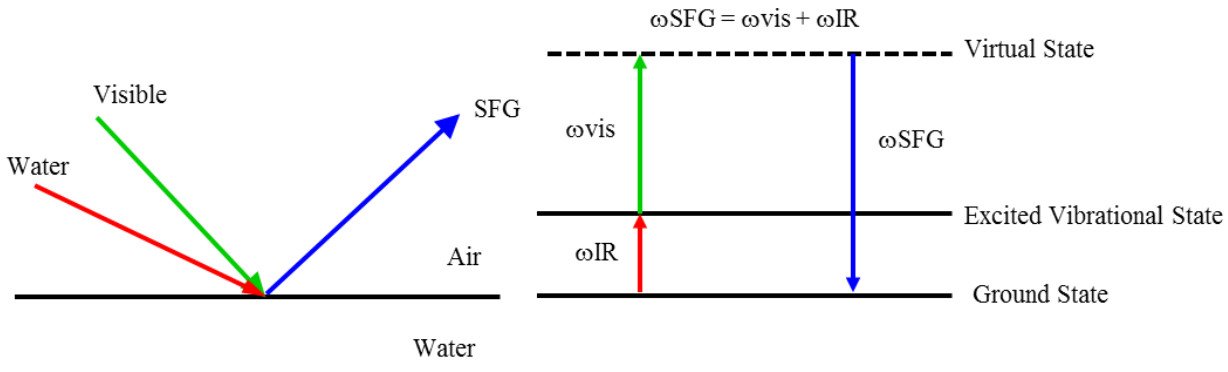

Figure 4.1 Sum frequency generation at air-water interface.

conducted at room temperature (~23 ^{o}C) to minimize evaporation. The experiments were designed to obtain the interfacial water structure in the region of 3000-3600 cm^{-1}, as well as the hydrocarbon nonpolar groups of adsorbed SDS and DDA at the solution surface in the range of 2800-3000 cm^{-1}.

4.2.3 Molecular Dynamics Simulation

The Amber 14 program was used for the MDS study of SDS and DDA at the air-water interface for both neutral and high pH conditions. The simulation system for the air-water interface consisted of 4,322 water molecules in a primary water box of 4.0 x 4.0 x 8.0 nm. Basically, four simulation systems were examined as listed in Table 4.1.

The simulations were employed in the periodic boundary condition with the box size as 4.0 x 4.0 x 20.0 nm to provide vacuum space between the two water slabs. A snapshot of the initial simulation states for high coverage of SDS and DDA solutions is shown in Figure 4.2.

In all simulation studies, the SPC/E water model (Berendsen et al., 1987) was used and the water molecules were kept internally rigid by using the SHAKE algorithm. The SDS and DDA molecules were constructed by Gaussview and followed by structural optimization in Gaussian before organization at the air-water interfaces. The general Amber force fields (GAFF) (Wang et al., 2004) were applied for the SDS and DDA molecules. Some intermolecular potential parameters are presented in Table 4.2.

The air-water interface system was simulated in the NVT ensemble where the number of particles (N), the simulation box volume (V) and the temperature (T) were kept constant. The temperature was kept at 298.0 K using the Anderson thermostat. The energy

Table 4.1 List of simulation studies.

Type	Number of surfactant molecules	Number of KOH molecules	Number of water molecules
Neutral condition	25 SDS	0	4,322
Neutral condition	25 DDA	0	4,322
Alkaline condition	25 SDS	5	4,322
Alkaline condition	25 DDA	5	4,322

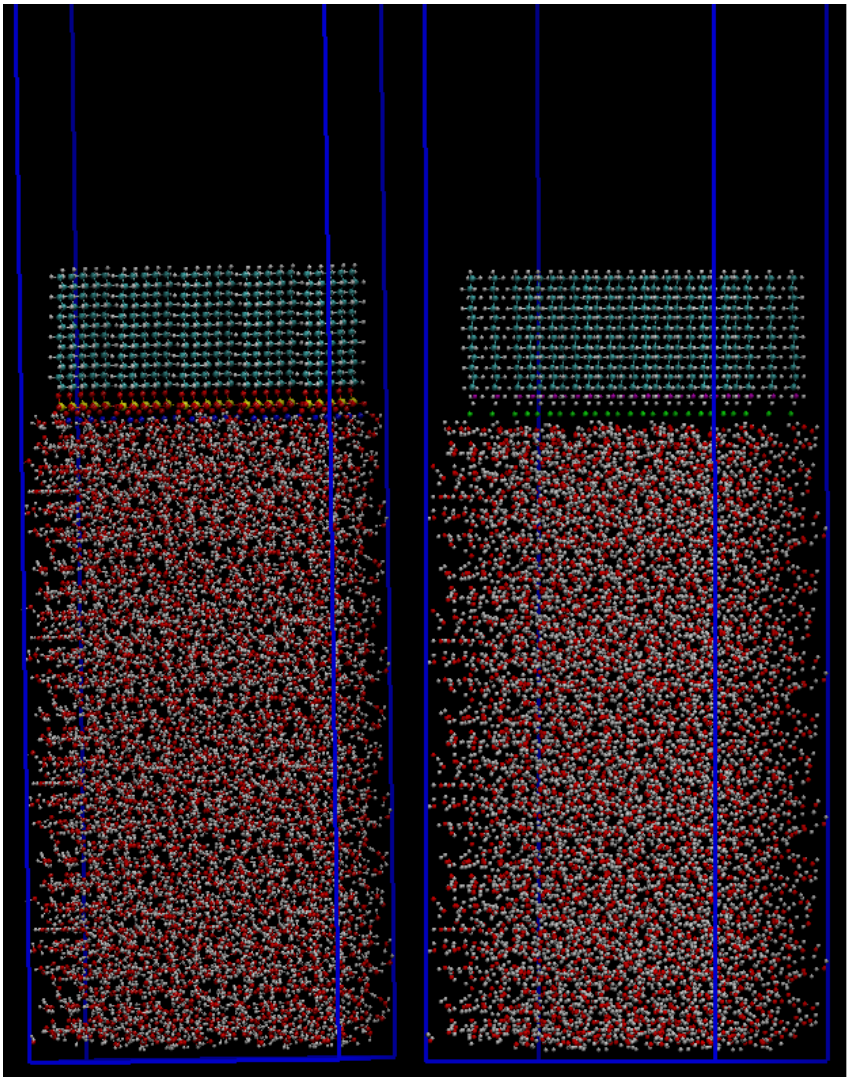

Figure 4.2. Snapshot of initial simulation state at the air-water interface a) SDS molecules b) DDA molecules. The color code for atoms is as follows: red, O; white, H; cyan, C; yellow, S; blue, Na; purple, N; green, Cl.

Table 4.2. Intermolecular potential parameters for SDS, DDA and SPC/E water molecules.

	Atom type	σ (Å)	ε (kcal/mol)	Q
SDS	c3	3.816	0.1094	-0.1805
	hc	2.974	0.0157	0.0423
	os	3.3674	0.1700	-0.4807
	s6	2.0000	0.2500	-0.0326
	o	3.3224	0.2100	-0.2162
	Na^+	2.54	0.1000	0.6344
DDA	c3	3.816	0.1094	-0.2752
	hc	2.974	0.0157	0.0603
	n4	3.6480	0.1700	-0.7652
	hn	1.2000	0.0157	0.3530
	Cl^-	3.8960	0.2650	-1.0173
SPC/E	OW	3.5534	0.1553	-0.8476
	HW	0.0000	0.0000	0.4238

of the system was initially minimized and equilibrated for 500 ps before the simulation. Simulations were carried out with a 2-fs time step for a total time of 1.0 ns. The van der Waals and electrostatic interactions were cut off at 9 Å, and the long-range electrostatic interactions were calculated using Particle Mesh Ewald (PME), a method available in the Amber program.

To analyze the MDS results of interfacial water molecules, water number density profiles, hydrogen bonding, water dipole orientation, and water residence time were computed from the trajectory coordinators of the water molecules. Fortran 90 language was used for coding the programs of interfacial water analysis. The information about interfacial water molecules at the air-water interface in the presence of anionic SDS and

DDA cationic surfactants provided a better understanding of molecular features and behavior of interfacial water molecules.

4.2.4 Foam Stability and Foam Weight Tests

Foam stability and foam weight tests were implemented for SDS and DDA solutions at the same concentration and pH conditions as used in SFG measurements. Foam stability measurements were carried out with a 125-ml column cell (2 x 22 cm) having a fine capillary (10 μm), porous glass frit for bubble generation. For each experiment, the solution was foamed by slowly injecting air (80 ml/min) into 20 ml of surfactant solution contained in the column cell. The time for foam collapse to a particular column height was recorded and the foam stability curve was constructed. Foam weight measurements were conducted by collecting foams of each surfactant solution in approximately 30 seconds and measuring the weight. Foams were formed by injecting air (80 ml/min) into 30 ml of surfactant solution contained in the same column cell.

4.3 Results and Discussion

4.3.1 SFG Analysis of Interfacial Water

The adsorption features of anionic sodium dodecyl sulfate (SDS) and cationic dodecyl ammonium chloride (DDA) surfactants at the air-water interface were studied at different bulk concentrations below the critical micelle concentration (CMC). Four solution concentrations of anionic SDS surfactant including $2x10^{-4}$M; $5x10^{-4}$ M; $1x10^{-3}$ M and $5x10^{-3}$ M were investigated and the concentrations of $5x10^{-4}$ M; $1x10^{-3}$ M; $5x10^{-3}$ M and $1x10^{-2}$ M were studied for the cationic DDA surfactant. The SFG spectra collected at

the air-water interface at neutral pH are shown in Figure 4.3 and Figure 4.4 for SDS and DDA solutions, respectively. Of particular interest in this dissertation research is the interfacial water structure with respect to three typical characteristic peaks for O-H vibrational modes including 3,200 cm^{-1}, 3,450 cm^{-1} and 3,700 cm^{-1} as reported in previous SFG studies (Nguyen et al., 2015; Wang et al., 2009; Ye et al., 2001). Our SFG results of interfacial water structure show two significant peaks at 3,200 cm^{-1} and 3,450 cm^{-1} for both anionic SDS and cationic DDA solutions. A strong enhancement of O-H vibrational signals is noticed in Figure 4.3 with an increase in SDS concentration. Particularly, the 3,200 cm^{-1} peak, which represents the O-H stretching of strongly hydrogen bonded water molecules, dominates in comparison with the 3,450 cm^{-1} peak of asymmetrically bonded water molecules. It is evident that the interfacial water molecules strongly interact with the sulfate head groups at the air-water interface for the anionic SDS solution. In addition, for the more concentrated SDS solution, a strong enhancement of O-H vibration in the region of 3,000-3,600 cm^{-1} is found and suggests that interfacial water molecules become highly-ordered at the surface.

Quite the opposite was found for SFG spectra of the DDA solution. In contrast to the SDS results, SFG spectra of O-H vibrational peaks in the water region (3,000 – 3,600 cm^{-1}) decrease with an increase in the concentration of the cationic DDA surfactant. Further, it can be seen in Figure 4.4 that the peaks of the C-H vibrations for the hydrocarbon chain of the DDA molecules are very sharp and strong compared to the spectra for the O-H vibrations of the interfacial water molecules. These results indicate that the interaction between interfacial water molecules and cationic ammonium head groups is not as strong as in the case of the anionic SDS surfactant. As a result, the interfacial water network does

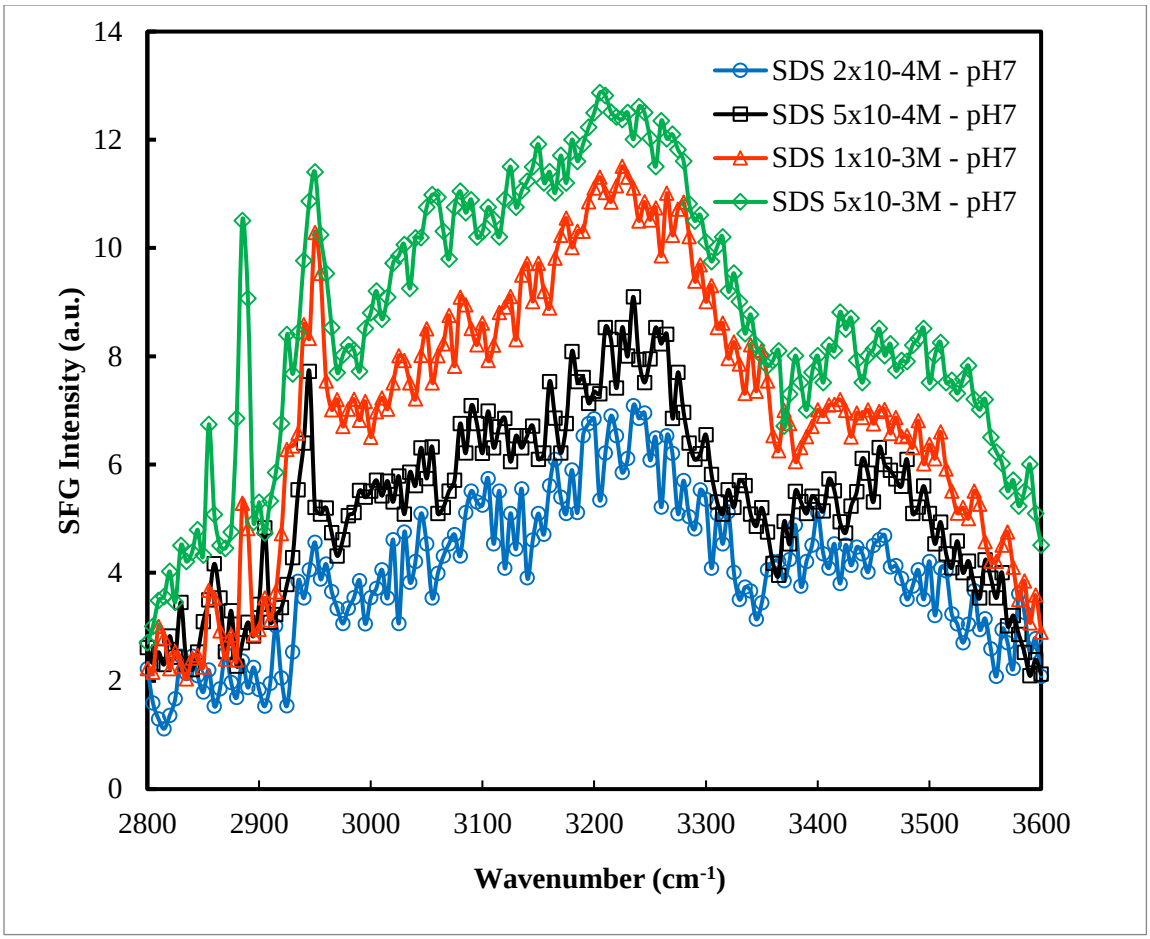

Figure 4.3 SFG spectra under SSP polarization conditions of the air/water interface of SDS solutions.

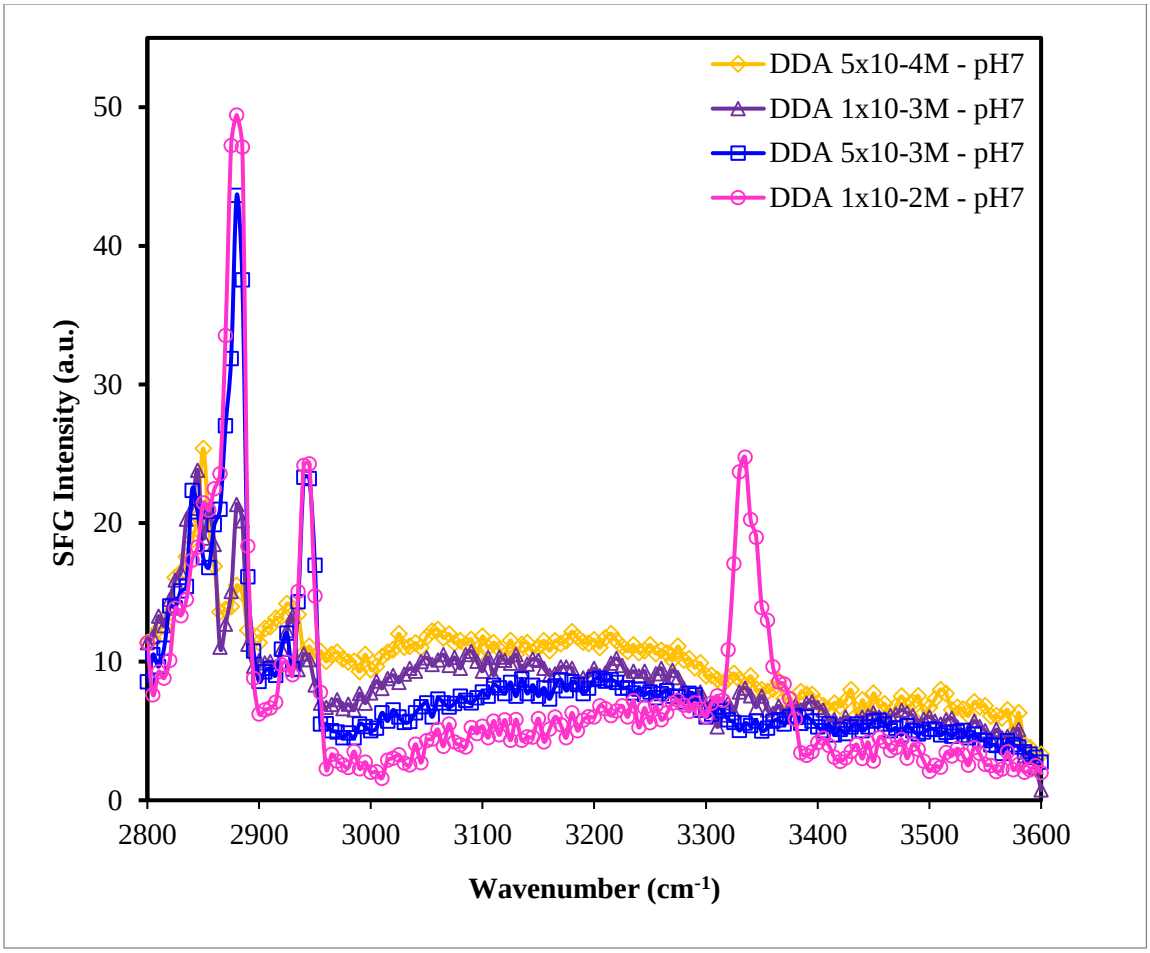

Figure 4.4 SFG spectra under SSP polarization conditions of the air/water interface of DDA solutions.

not play a significant role at the interface of the DDA surfactant solution. A similar observation has been found in the study of a charged surfactant at the air-water interface (Gragson and Richmond, 1998). Furthermore, at the highest DDA concentration studied ($1x10^{-2}$ M), very sharp and high-intensity peaks of CH_3- symmetric stretching and CH_3-Fermi resonance at 2,880 cm^{-1} and 2,940 cm^{-1}, respectively, together with an N-H symmetric stretching peak of 3,300 cm^{-1} were observed, but with very weak interfacial water signals. This confirms that the surfactant molecules form a strong and dense packing structure at the surface and interfacial water molecules are not easily accommodated at the interfaces.

In order to elucidate the interfacial phenomena for SDS and DDA, the head group size of anionic SDS and cationic DDA molecules should be considered. The SDS and DDA molecules were evaluated using Gaussview 09 software. The geometry optimization was executed and followed by a single-point energy calculation using the DFT method in the Gaussian simulation program. Figure 4.5 illustrates the optimized SDS and DDA molecules. The bond distance between the sulfur atom and oxygen atoms in the SDS molecule and the bond distance between the nitrogen atom and hydrogen atoms in the DDA molecule were calculated and are listed in Table 4.3. Results show that the bond distances of elemental atoms in the SDS group are significantly greater than for the DDA group. In other words, the anionic SDS head group is of a larger size than the cationic DDA head group. Therefore, at the air-water interface, the sulfate group provides more available

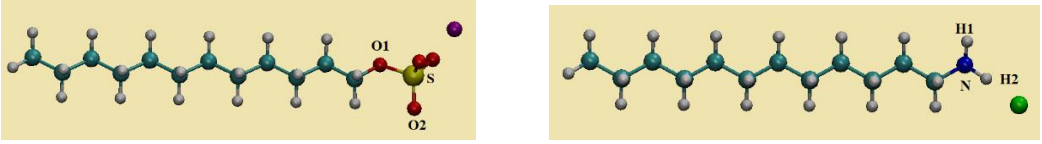

Figure 4.5 SDS and DDA molecule optimized by Gaussian simulation.

Table 4.3 Bond distances between atoms in SDS and DDA head groups.

	Bonding distance (Å)
S – O1	1.461
S – O2	1.582
N – H1	1.006
N – H2	1.085

spaces for the interfacial water molecules, and together with the charging effect, the interaction between the sulfate group and interfacial water molecules is strongly enhanced.

In addition, it is considered that the molecular packing of surfactant molecules at the air-water interface should impact the population of interfacial water molecules. It was reported that the molecular areas of anionic SDS and cationic DDA at CMC concentrations (8 mM for SDS and 14 mM for DDA) are 45 $Å^2$ and 35 $Å^2$, respectively (Gragson et al., 1997a; Gragson et al., 1997b; Lu et al., 1993), which means that for the same conditions, the number of cationic DDA molecules at the interface are more densely packed than the anionic SDS molecules. Figure 4.6 illustrates the molecular packing of SDS molecules and DDA molecules at the air-water interface. Regardless of the orientation of the hydrocarbon chain for either SDS or DDA, the hypothesis is proposed here that due to the denser molecular packing of the DDA molecules, fewer water molecules are present at the interface. Therefore, SFG signals of O-H stretches decrease with an increase of DDA bulk concentration. The proposed explanation is also supported by the extremely sharp and strong intensity of CH_3- symmetric stretching and CH_3- Fermi resonance peaks at the high concentration of DDA concentrations shown in Figure 4.4. Also, MDS snapshots of the

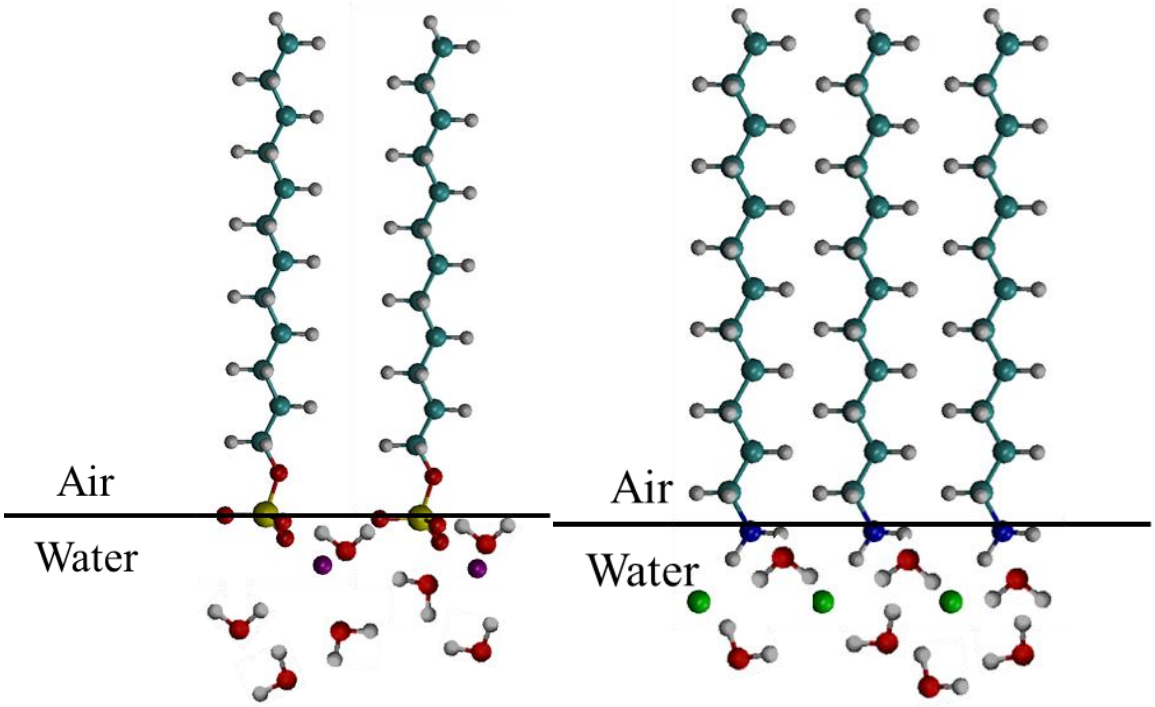

Figure 4.6 Illustration of molecular packing of SDS molecules and DDA molecules at the air-water interface. The code for atoms is as follows: white, H; cyan, C; red, O; yellow, S; purple, Na; blue, N; green, Cl.

SDS and DDA interfacial surfactant molecules after 1 ns of simulation time, presented in Figure 4.7, are in good agreement with the hypothesis. It can be seen that SDS molecules at the surface occupy a greater surface area per molecule whereas DDA molecules occupy less surface area. On further consideration, the average distance between two neighboring SDS head groups was computed and compared with the average distance between two neighboring DDA head groups. It was found that the spacing was 5.944 Å for SDS and 4.775 Å for the DDA molecules. These observations provide additional support to confirm the hypothesis of denser packing characteristics for the DDA surfactant molecules at the air-water interface.

SFG measurements of anionic SDS and cationic DDA surfactants at the air-water

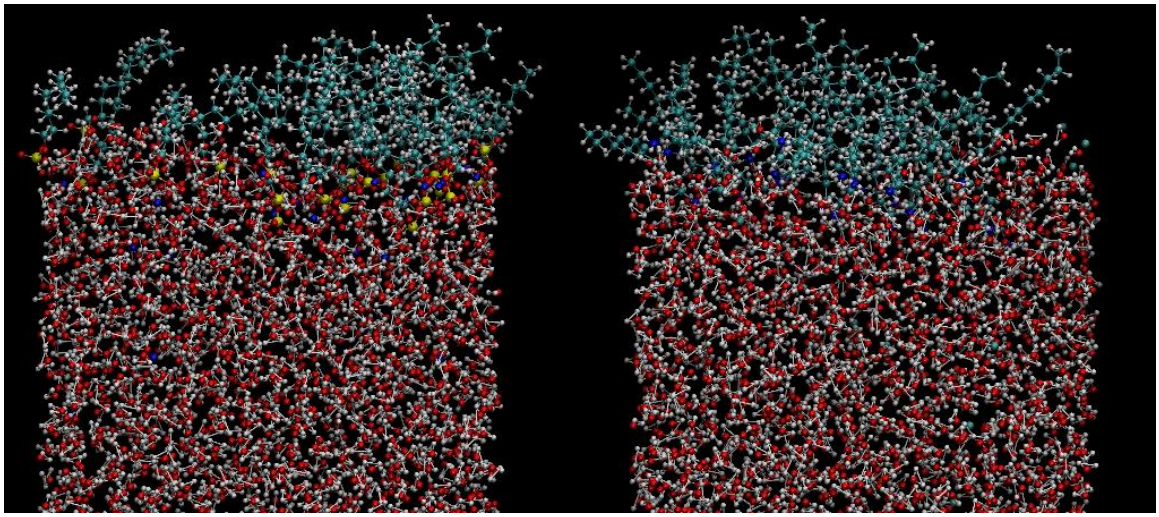

Figure 4.7 MDS snapshots of interfacial SDS and DDA molecules after 1ns of simulation time; on the left is the organization of SDS molecules and on the right is the organization of DDA molecules.

interface at neutral pH provide the fundamental understanding of interfacial water structure and the interaction between interfacial water molecules and surfactant head groups at the interface.

4.3.2 MDS Analysis of Interfacial Water Structures at Air-Water Interfaces

To gain a better understanding of the behavior of interfacial water structure at the air-water interface for anionic SDS and cationic DDA surfactant solutions, Molecular Dynamics Simulations (MDS) was employed. Results in the following sections indicate that the interfacial water structure agrees well with the SFG experimental results as discussed in the previous section, 4.3.1. It is noted that in the analysis of the MDS results presented as plots of interfacial water characteristics versus distance in the following sections, the position of the air-water interface, shown as 0 value on the x axis, was defined

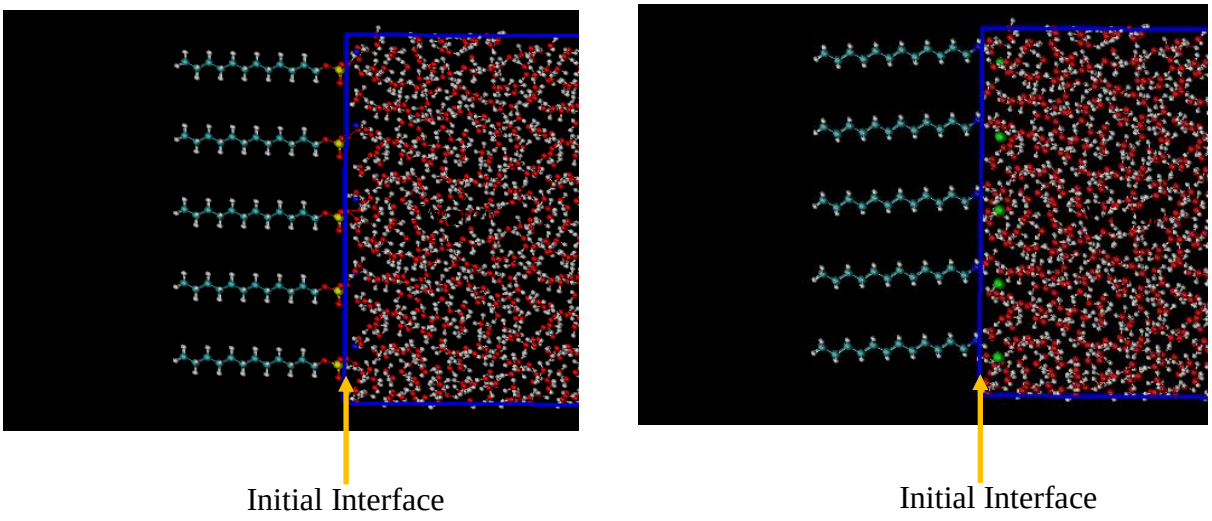

Figure 4.8 Initial arrangement of surfactant molecules at the air-water interfaces and the definition of the position of the air-water interface; on the left is the organization of SDS molecules and on the right is the organization of DDA molecules.

by the initial uniform location of surfactant head groups. Figure 4.8 shows the organization of surfactant molecules at the air-water interface at the beginning of simulation and the definition of the position of the air-water interface.

4.3.2.1 Relative Number Density Profile

The number density profiles of interfacial water molecules at the air-water interface provide a quantitative distribution analysis obtained from the trajectory of water coordinates. It is noted in this study that the position of a single water molecule is defined as the position of the center of mass for that water molecule. The number of water molecules in each bin of 0.5 A^o was counted and normalized by the number of water molecules in the bulk phase. Figure 4.9 presents the density distribution of water molecules at the interfaces with high coverage SDS and DDA surfactants. The density profiles are very similar to the reported studies of surfactants at interfaces (Bandyopadhyay

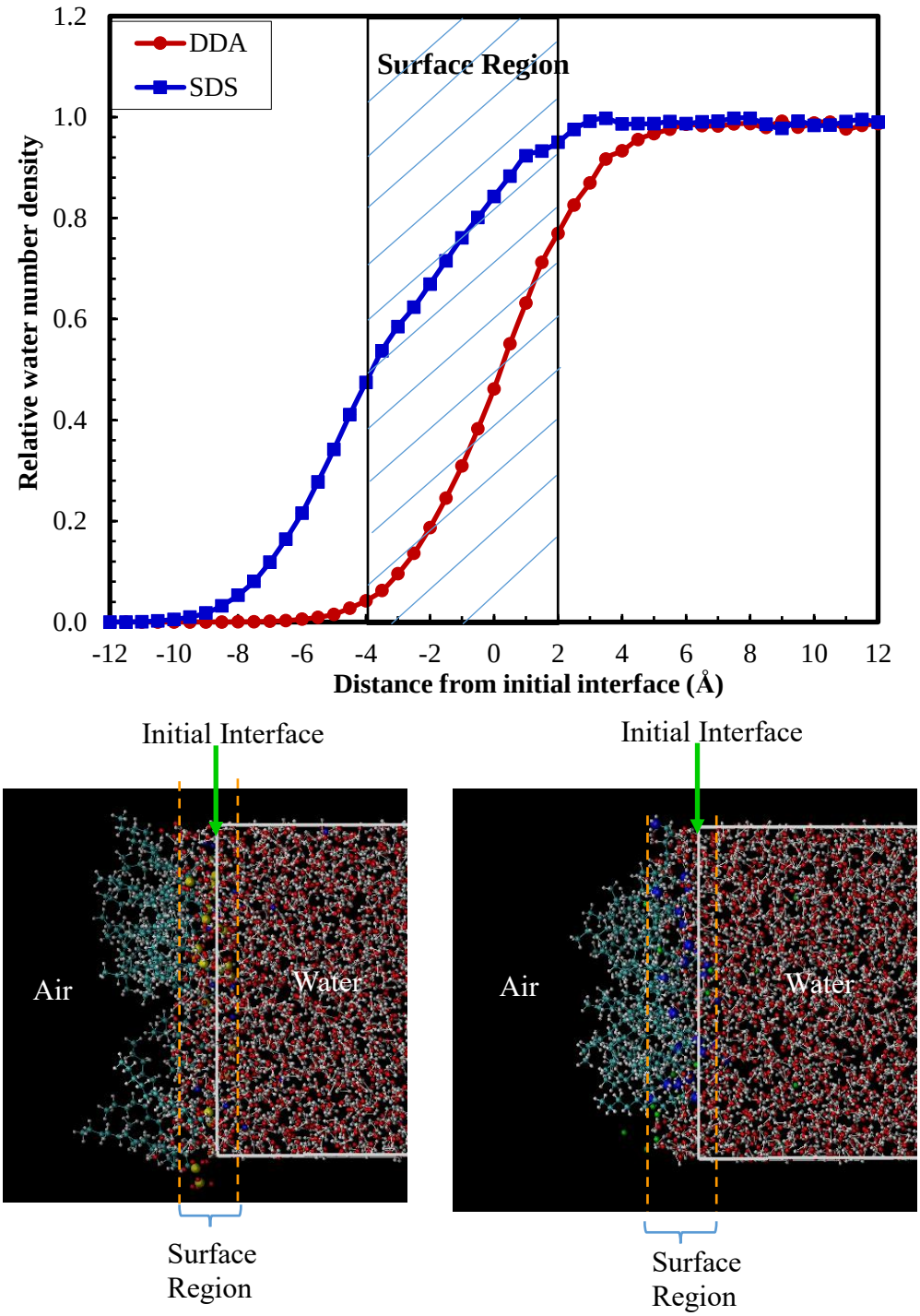

Figure 4.9 Top figure: Relative water number density profiles of anionic SDS and cationic DDA surfactant solutions; on the x axis, positive value is distance toward the water phase and negative value is distance toward the air phase. Bottom figure: on the left is the MDS snapshot of SDS molecules and on the right is the MDS snapshot of DDA molecules at the air-water interface. Initial interface is the same in both cases. See Figure 4.8.

and Chanda, 2003; Dominguez and Berkowitz, 2000; Schweighofer et al., 1997). Simulation results in this research indicate that the interfacial water molecules are more crowded at the interface for the SDS solution in comparison with the DDA solution. As for the SDS solution, the interfacial water density was about 84% of the bulk water density while it was only 46 % in the case of DDA solution. The bulk water density was retrieved at 2 Å from the initial interface of the SDS solution and 6 A^{o} from the initial interface of the DDA solution. The results imply that the atomic structure of surfactant molecules affects the distribution of interfacial water molecules, probably by the establishment of a hydrogen bond network between interfacial water-surfactant head groups at the interface and between interfacial water-water in the aqueous phase.

In addition, it is worth pointing out from Figure 4.9 that water molecules penetrate within the surfactant head groups. Interfacial water molecules have a more prominent distribution around the anionic sulfate group than around the cationic ammonium group. Only a few water molecules coordinate with the ammonium group whereas there are more water molecules accommodated by the sulfate group. The results show that more water molecules are expected at the SDS surface than at the DDA surface. Hence, the SFG experimental results shown in Figure 4.3 and Figure 4.4 are supported from MDS.

4.3.2.2 Hydrogen Bonding Network

Other significant information provided from the simulation results is the hydrogen bonding, including the hydrogen bonding between two water molecules, and the hydrogen bonding between oxygen in the sulfate group and the water molecules. Two water molecules for the SPC/E water model are defined as being hydrogen bonded if the distance

between two oxygen atoms is less than 3.5 Å and the O…O-H angle is less than 30^{o} (Luzar and Chandler, 1996). The number of hydrogen bonds per water molecule is determined by dividing the total number of hydrogen bonds in each water layer by its corresponding water number.

Figure 4.10 presents the average number of hydrogen bonds per water molecule as a function of the distance from the air-water interface. The simulation results show that the average number of hydrogen bonds per water molecule in the bulk phase is about 3.42 Å, in good agreement with simulation results reported for the SPC/E model of bulk water (Marti et al., 1996; Nieto-Draghi et al., 2003). Generally, water molecules at interfaces and in the air phase are less hydrogen bonded than water molecules in the bulk phase. Figure 4.10 also shows that the water molecules penetrated within the sulfate group are more strongly hydrogen bonded than the water molecules around the ammonium group. Also, at the air-water interface, there are 3.20 hydrogen bonds per water molecule for the SDS solution, whereas there are just 2.83 hydrogen bonds per water molecule for the DDA solution. Results in Figure 4.10 support the hypothesis mentioned in Section 4.3.1 that the interfacial water network at the surface of the SDS solution is more strongly connected than for the DDA solution. This observation suggests that the interfacial structure is dependent not only on the surfactant properties but also on the structural properties of interfacial water at the interface. Hence, as expected, water-water hydrogen bonds are in large part responsible for determining interfacial water structure.

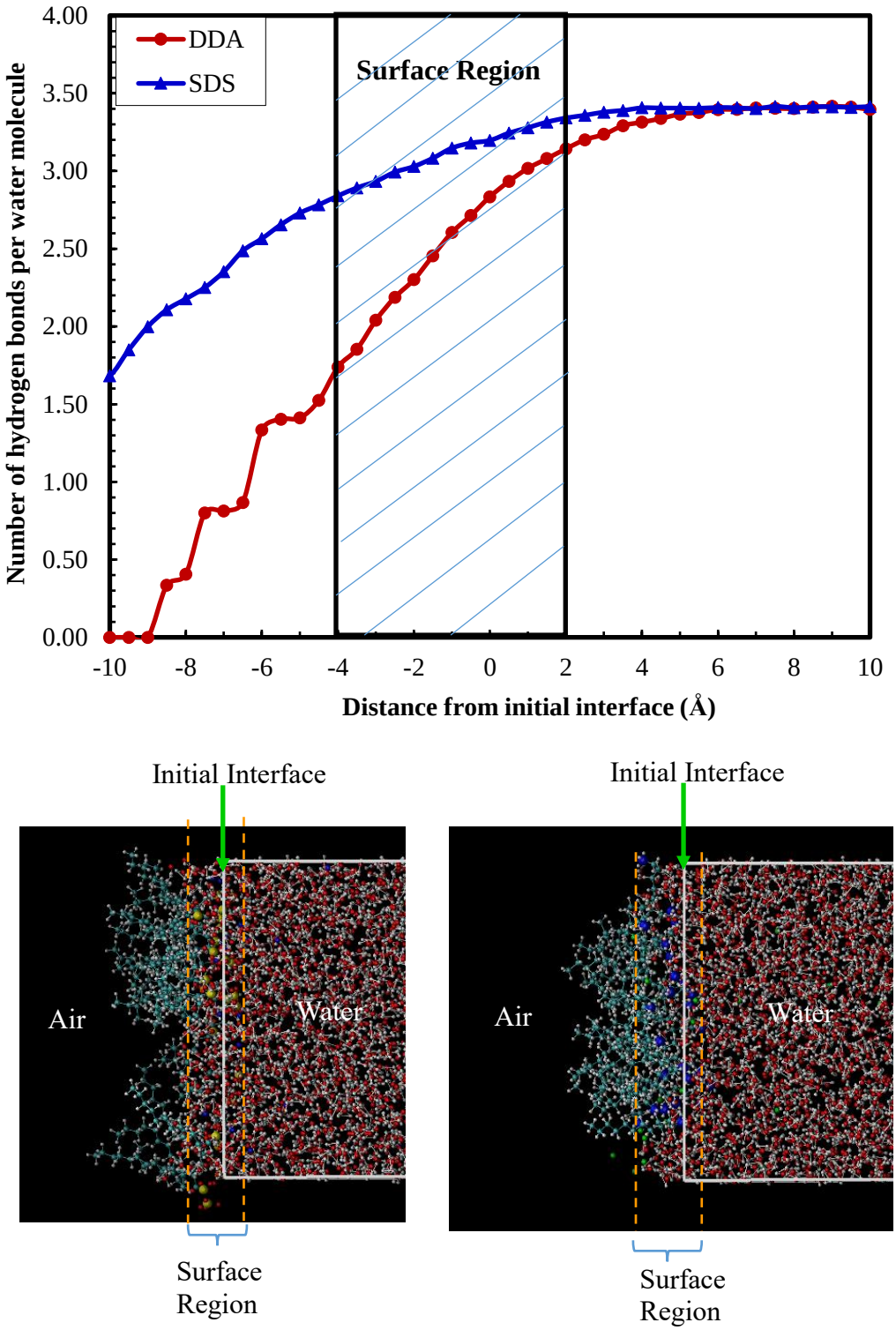

Figure 4.10 Top figure: Number of hydrogen bonds per water molecule of SDS and DDA solutions; on the x axis, positive value is distance toward the water phase and negative value is distance toward the air phase. Bottom figure: on the left is the MDS snapshot of SDS molecules and on the right is the MDS snapshot of DDA molecules at the air-water interface. Initial interface is the same in both cases. See Figure 4.8.

4.3.2.3 Water Dipole Orientation at the Interface

In this study, water dipole orientation is defined by the angle alpha between the water dipole moment (oriented from negative to positive) and the surface normal. To compute the density distribution for water dipoles, the simulation box size was divided into 0.5 Å bins parallel to the interface. In each bin, the angle α of water molecules was measured, and the number density distribution for different degrees was determined. It is noted that the range of angle α is from 0^o to 180^o. Results of water dipole orientation analysis of interfacial water molecules are shown in Figure 4.11. The results indicate that at the air-water interface for the SDS solution, the average water dipole is pointing approximately 16^o away from the surface normal. Figure 4.12 illustrates the orientation of water molecules with a 16-degree orientation, which demonstrates the highly-ordered behavior of water molecules occurring at the interface. As for the DDA solution, the water dipole distribution randomly distributed from the range of 0^o and 180^o. This observation, which is consistent with our results of relative density profiles and hydrogen bonding analysis, demonstrates the reliability of the SFG experimental results which suggest the interfacial "ice-like" water structure at the interface for the SDS solution when compared to the DDA solution.

4.3.2.4 Water Residence Time

Analysis of water residence time of interfacial water molecules can also be analyzed from MDS results and such analysis reveals the dynamic characteristics of interfacial water. The water residence time, τ, is defined as the time that a water molecule spends in each water layer along the surface (Chowdhuri and Chandra, 2001; Koneshan et

$$\tau = \int_0^\infty \{R(t)dt \tag{4-1}$$

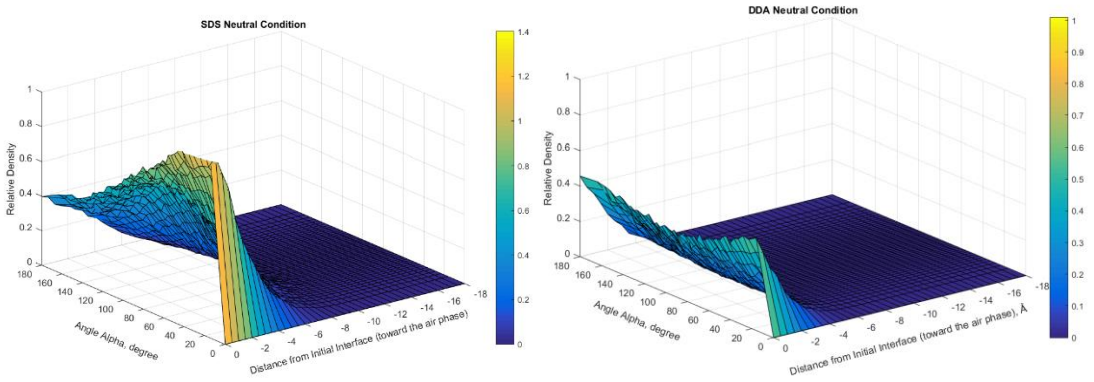

Figure 4.11 Water dipole moment relative density distribution along the interface (toward the air phase) at the air-water interface of the SDS solution (left figure) and the DDA solution (right figure).

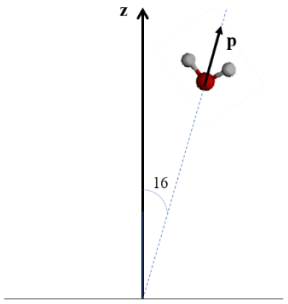

Figure 4.12 Illustration for the average water dipole orientation from the surface normal for the SDS solution surface.

al., 1998) and can be calculated using the residence time correlation functions defined by Equation (4-1).

$$R(t) = \frac{1}{N_h} \sum_{i=1}^{N_h} [\theta_i(0)\theta_i(t)] \tag{4-2}$$

It is noted the term $\theta_i(t)$ is the Heaviside unit step function, which has the value of 1 if a water molecule, *i*, is in the hydration shell of the reference water molecule at time *t*, and is zero otherwise. The term N_h is the apparent dynamic hydration number. Average residence times of interfacial water molecules for SDS and DDA solutions are shown in Figure 4.13. It is of interest to observe that interfacial water molecules of surfactant solutions remain at the surface longer than water molecules in the bulk. Further interfacial water molecules of the SDS solution stay longer around the surface than molecules of the DDA solution, which is consistent with previous results. This observation possibly can be explained by the interaction of interfacial water molecules and charged head groups.

4.3.3 The Effect of pH Condition on the Interfacial Water Structures at the Air-Water Interface

In this section, the effect of pH on the interfacial water structures at the air-water interface for SDS and DDA solutions was investigated. SFG measurements and MDS simulations were conducted using a similar approach as mentioned in previous sections, 4.3.1 and 4.3.2. In all SFG experiments, the concentrations of SDS and DDA solutions remain unchanged, and pH 9 was prepared by adding potassium hydroxide to the solution. As for the MDS study, five potassium hydroxide molecules were added into the solution of 25 surfactant molecules and 4,322 water molecules as mentioned in Section 4.2.3.

Figure 4.14 and Figure 4.15 show SFG experimental results of interfacial water

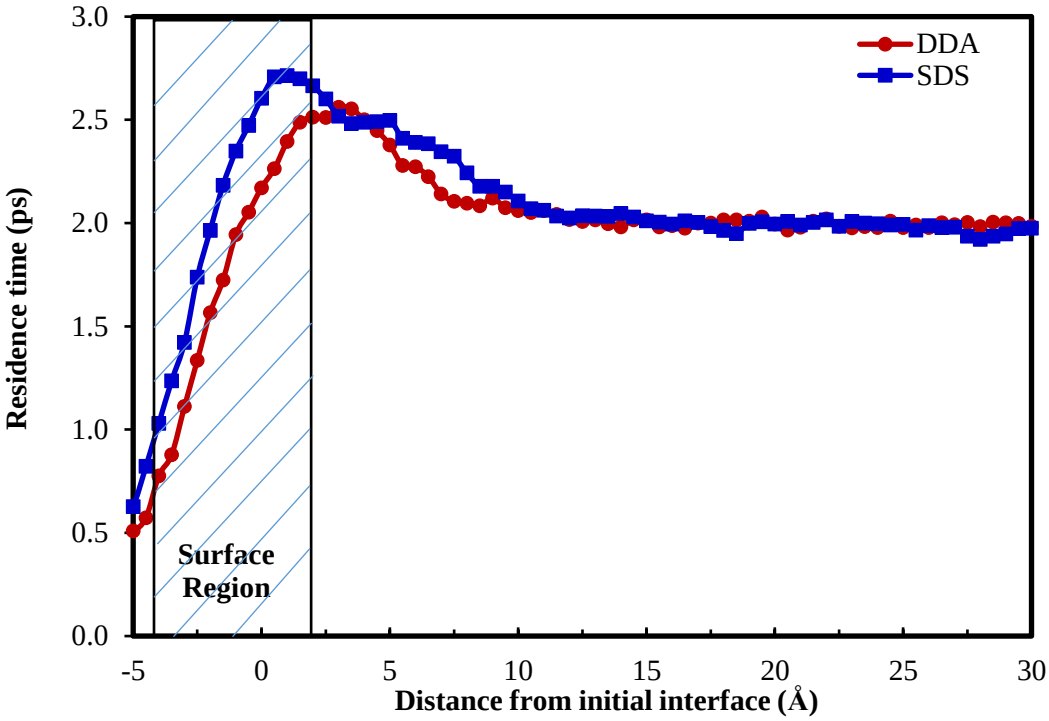

Figure 4.13 Average residence time of water molecules at the surfaces of SDS and DDA solutions. On the x axis, positive value is distance toward the water phase and negative value is distance toward the air phase. Initial interface is the same in both cases. See Figure 4.8.

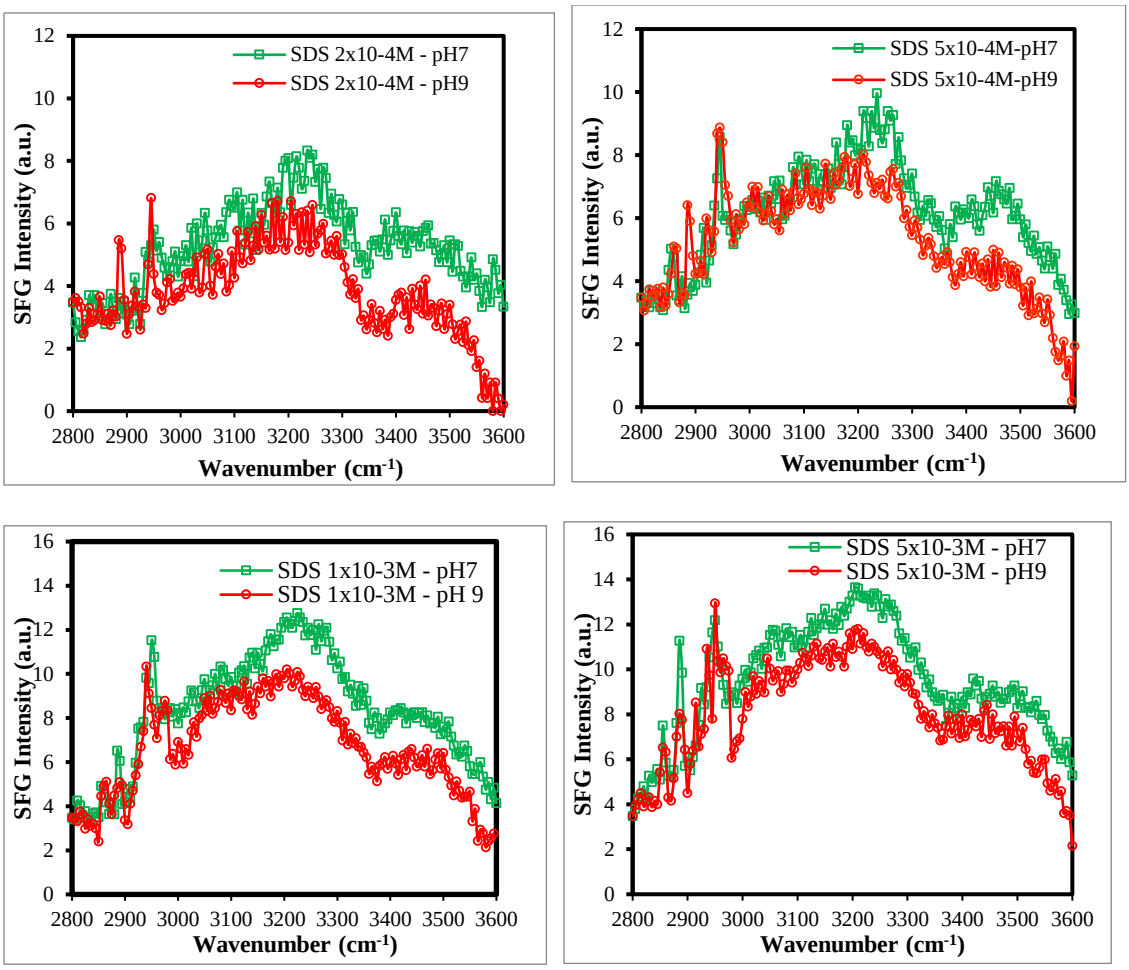

Figure 4.14 SFG signals of interfacial water structure at the air-water interface of the SDS solution.

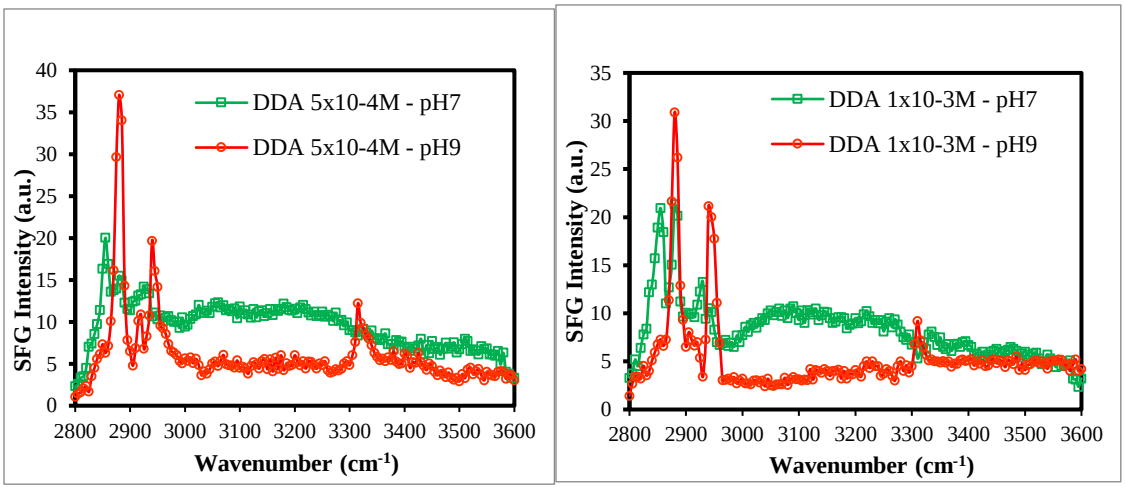

Figure 4.15 SFG signals of interfacial water structures at the air-water interface of DDA molecules.

structures at the air-water interfaces of SDS and DDA solutions. Due to the precipitation which occurs for DDA solutions at high concentration and high pH, SFG measurements are reported for DDA solutions at only 5 x 10^{-4} M and 1 x 10^{-3} M. Basically, it can be observed that increasing pH reduces the O-H vibrational modes of interfacial water structures at the air-water interface of both SDS and DDA solutions. Further, the ordering of interfacial hydrocarbon chains for both SDS and DDA solutions is stronger at pH 9 when compared with the neutral pH. It is of particular interest here that at pH 9, the interfacial water structures still present at the interface of the SDS solution with lower SFG intensity, whereas it disappears at the interface of the DDA solution. The phenomenon of interfacial water structure at higher pH values possibly can be explained by the hydrogen bond network of the hydroxide group and water molecules in the solution. By analyzing the neutron-diffraction data for potassium hydroxide solutions, Imberti et al. reported that the presence of potassium and hydroxide ions in the solution seriously affects the hydrogen bond network (Imberti et al., 2005). Particularly, the hydration shell of hydroxide ions is characterized by four strong noncoplanar hydrogen bonds between hydroxide oxygen and water hydrogens. This important finding supports the SFG experimental data that, due to the strong interaction between hydroxide ions and water molecules in the solution at high pH values, fewer water molecules associate at the air-water interface and the interfacial water structure becomes less ordered.

As for the interfacial water structures at the air-water interface for the DDA solution at pH 9, a very weak SFG signal, or even no SFG signal, was observed in the O-H vibrational region of 3,000 – 3,600 cm^{-1}. A sharp strong peak at about 3,315 cm^{-1} represents the N-H vibrational stretch. However, this analysis is still debated in the literature (Nguyen

et al., 2014; Wang et al., 2009). SFG spectra indicate a strong effect of pH on the interfacial water network at the interface of the DDA solution. The effect of pH on zeta potentials of microbubbles generated using DDA solution was investigated by Yoon and Yordan, and it was reported that the positive zeta potentials begin to decrease at pH values above approximately 8 (Yoon and Yordan, 1986). In other words, the counter-ions in the DDA solution tend to concentrate near the interface when the pH value is above pH 8. At pH 9, the counter-ions in the DDA solution possibly consist of chloride ions and hydroxide ions. As a result, the stronger interaction between dodecyl ammonium head groups and counter-ions has brought the highly-ordered hydrocarbon chain of the DDA surfactant at the interface as observed in Figure 4.15. Besides, the well-known weak electrolyte and positively charged surfactant, dodecyl ammonium chloride, has been studied extensively. Laskowski reported that its CMC point decreases from 1.2×10^{-2} M at pH 5 to 3×10^{-4} M at pH 9 (Laskowski, 1999). The pH diagram for a DDA solution is reprinted in Figure 4.16. It can be seen that for the conditions studied, the DDA solution at pH 9 reaches above the CMC concentration. Hence, the disappearance of interfacial water structures at the interface possibly can be explained by the highly-ordered and fully-packed DDA molecules at the interface, so no space for interfacial water molecules is available.

To provide more evidence for the behavior of interfacial water molecules at the interface of SDS and DDA solutions, MD simulation was conducted for the same system with the addition of 5 potassium hydroxide molecules. Simulation analysis results of number density profiles, hydrogen bonding networks, and water dipole orientations are presented as the following. The computational approaches of all simulation analysis are referred to Section 1.3.2.

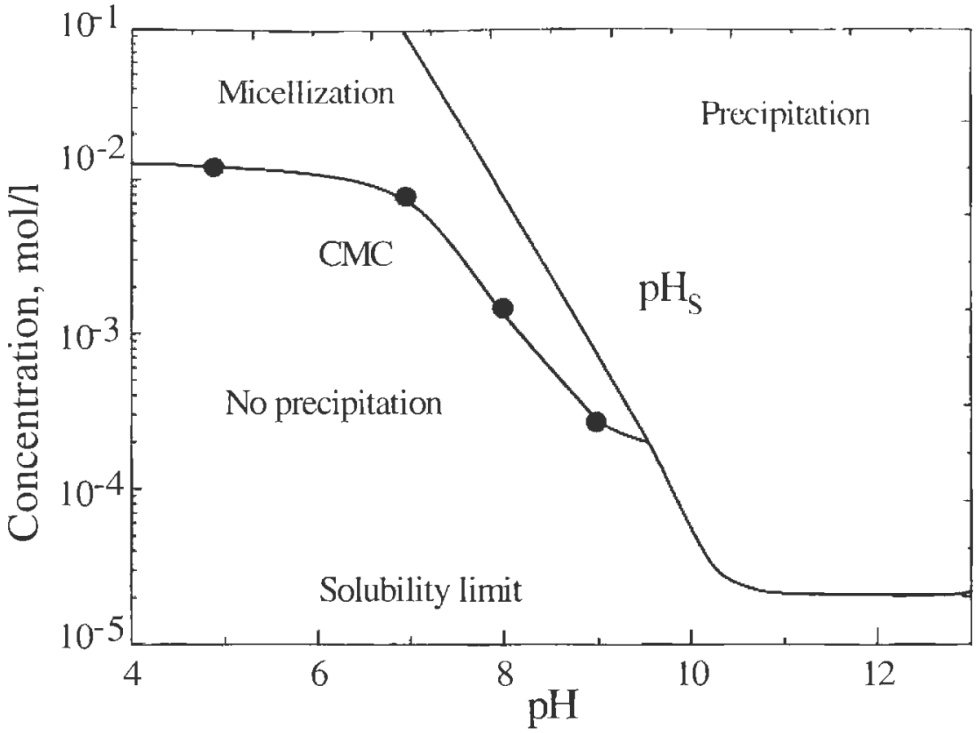

Figure 4.16 pH diagram of DDA solution (Laskowski, 1999).

Figure 4.17 shows the relative number density profiles of interfacial water molecules at the interfaces of SDS and DDA solutions in both neutral and alkaline conditions. It is worth noting here that in an alkaline condition, a reduced number of water molecules are found at the interface for both the SDS and DDA solutions. This observation is consistent with the SFG signal of O-H vibrational modes in the region of 3,000-3,600 cm^{-1}. More particularly, for the DDA solutions, a big discrepancy is observed in the water phase, whereas just a slight difference occurs at the interfaces of SDS solutions. At neutral pH, the water density reaches the bulk phase density at about 6 Å from the initial interface. However, it is up to 10 Å away from the initial interface in the alkaline condition.

Figure 4.18 presents the number of hydrogen bonds per water molecule at the air-water interface of SDS and DDA surfactants in both neutral and alkaline conditions. The

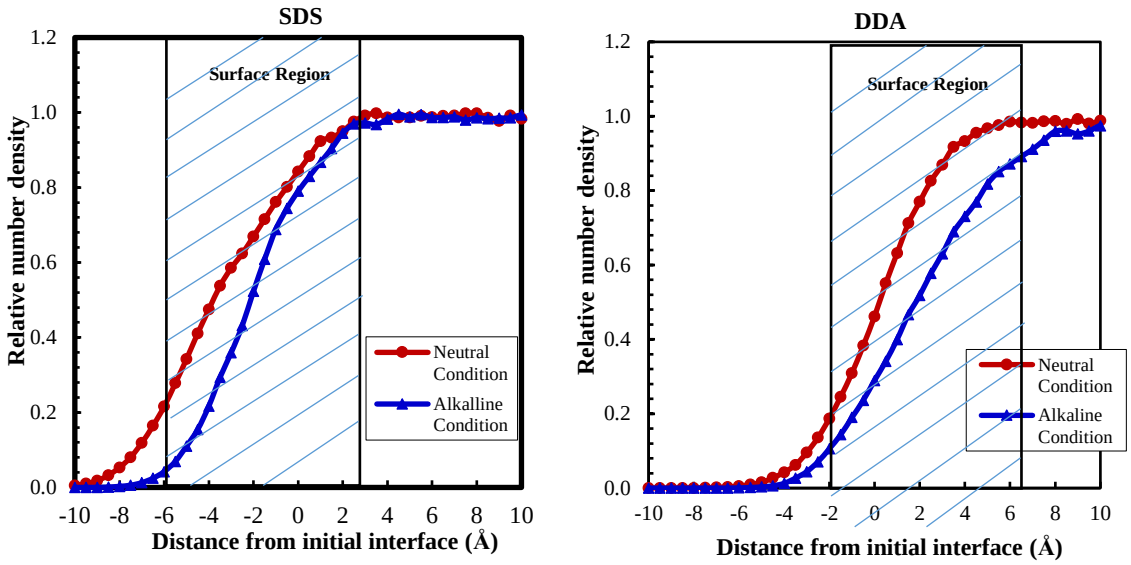

Figure 4.17 Relative water number density profiles of SDS and DDA solutions in both neutral and alkaline conditions. On the x axis, positive value is distance toward the water phase and negative value is distance toward the air phase. Initial interface is the same in both cases. See Figure 4.8.

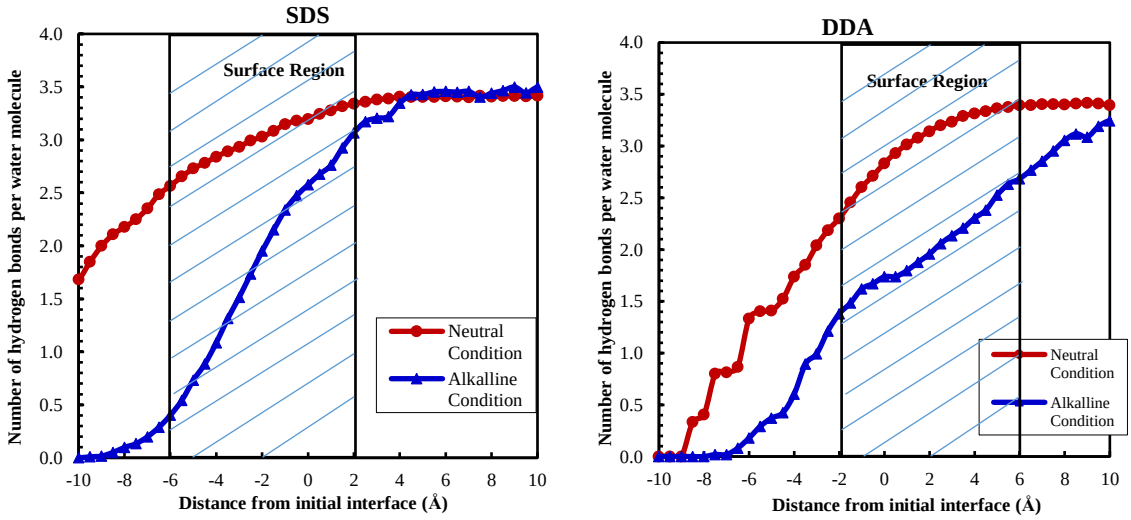

Figure 4.18 Number of hydrogen bonds per water molecule at the air-water interface of the SDS and DDA surfactants in both neutral and alkaline conditions. On the x axis, positive value is distance toward the water phase, negative value is distance toward the air phase. Initial interface is the same in both cases. See Figure 4.8.

results indicate that interfacial water molecules at the alkaline condition for both SDS and DDA solutions are less hydrogen bonded than at the neutral condition, which is consistent with the density profiles discussed. Also, for the DDA solution, there are an average of 2.83 hydrogen bonds per water molecule at the initial interface for the neutral condition, whereas there are just 1.73 hydrogen bonds per water molecule for the alkaline condition. This observation confirms the disappearance of interfacial water molecules in the SFG signal of O-H stretches, as discussed previously. Also, the water molecules underneath the interface reveal weak hydrogen bonds compared to the neutral condition.

The water dipole orientations at the air-water interface of the SDS and DDA solutions for both neutral and alkaline conditions are shown in Figure 4.19. Results reveal a slight difference at the interface for the SDS solution. However, as for the DDA solution, a big discrepancy is found between the neutral condition and alkaline condition due to the very low density of water molecules at the interface for the alkaline condition.

4.3.4 Foam Stability and Foam Weight Test

In this section, the important role of the water network to the foam stability is proposed and discussed based on foam stability and foam weight experiments. Foam stability and foam weight experiments were done for both SDS and DDA solutions at different concentrations and two pH values, 7 and 9, as studied for SFG measurements in the previous sections. Figure 4.20 and Figure 4.21 show the results from foam stability experiments, while foam weight experimental results are presented in Figure 4.22. The results indicate that for the SDS solutions, foams are less stable at pH 7 compared with pH 9, whereas the foams are more stable at pH 7 than at pH 9 in the DDA solutions. A similar

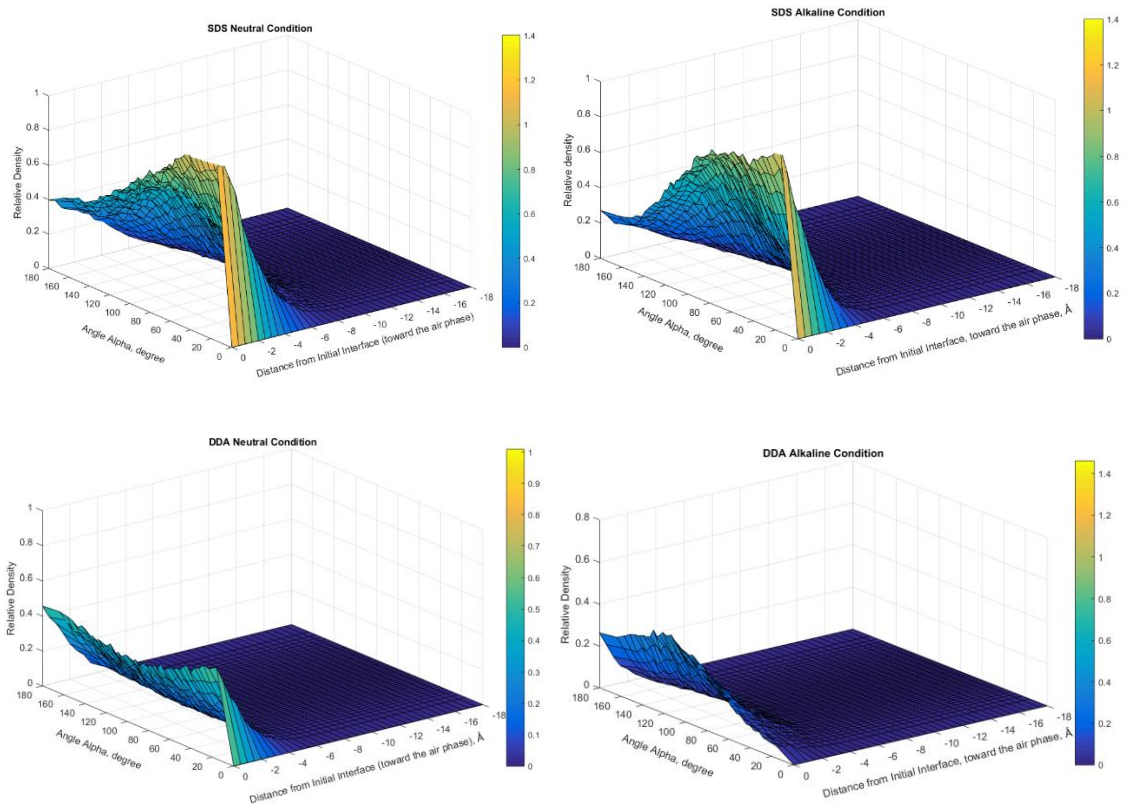

Figure 4.19 Water dipole moment relative density distribution along the interface (toward the air phase) at the air-water interface for SDS solutions and DDA solutions.

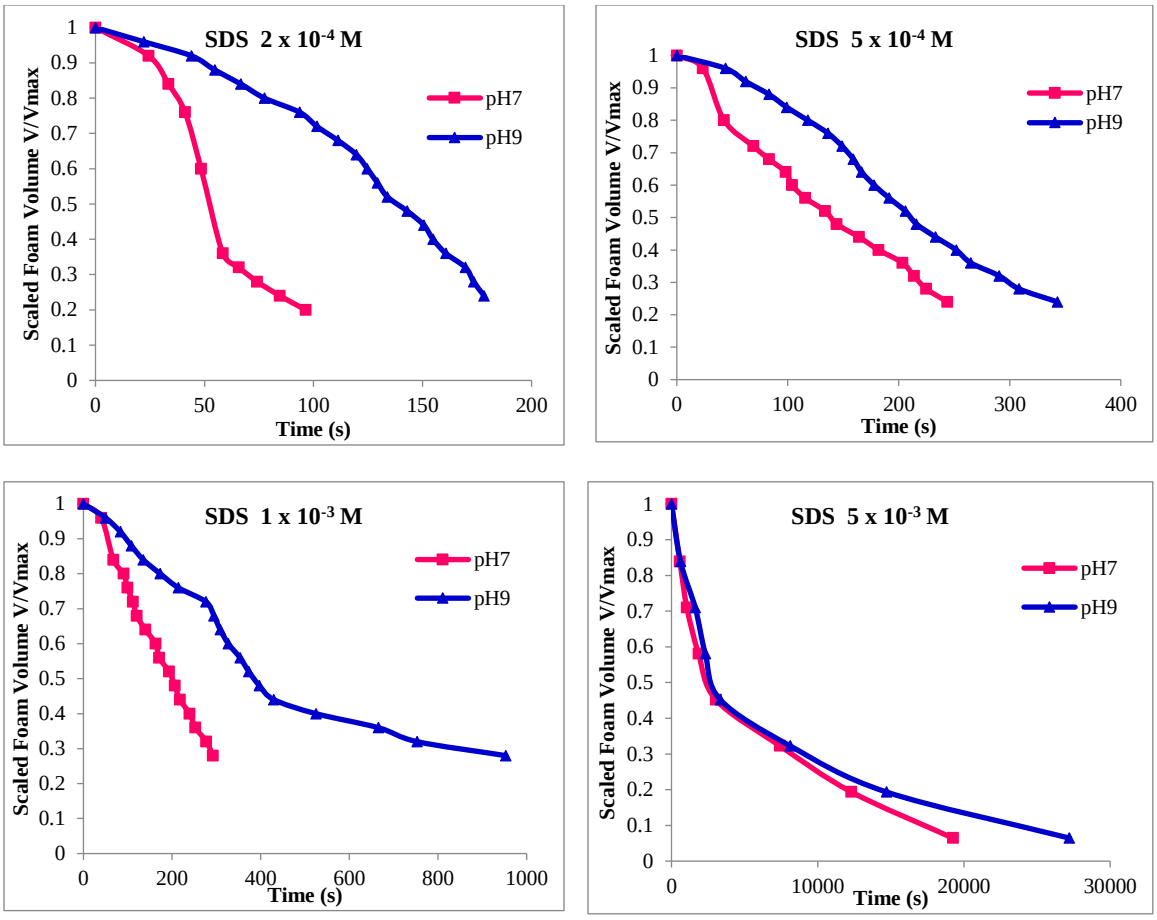

Figure 4.20 Foam stability tests for SDS solutions at different concentrations and pH values.

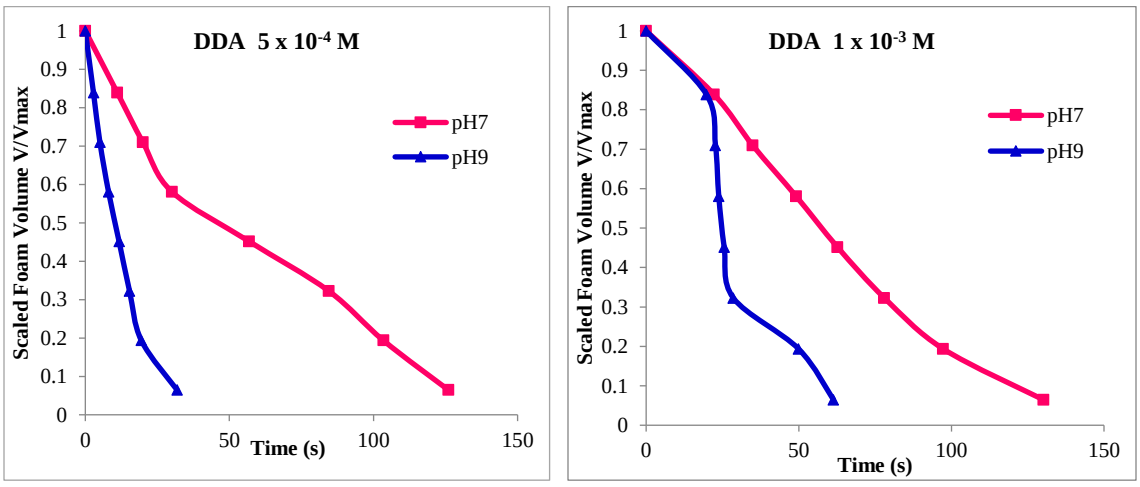

Figure 4.21 Foam stability tests for DDA solutions at different concentrations and pH values.

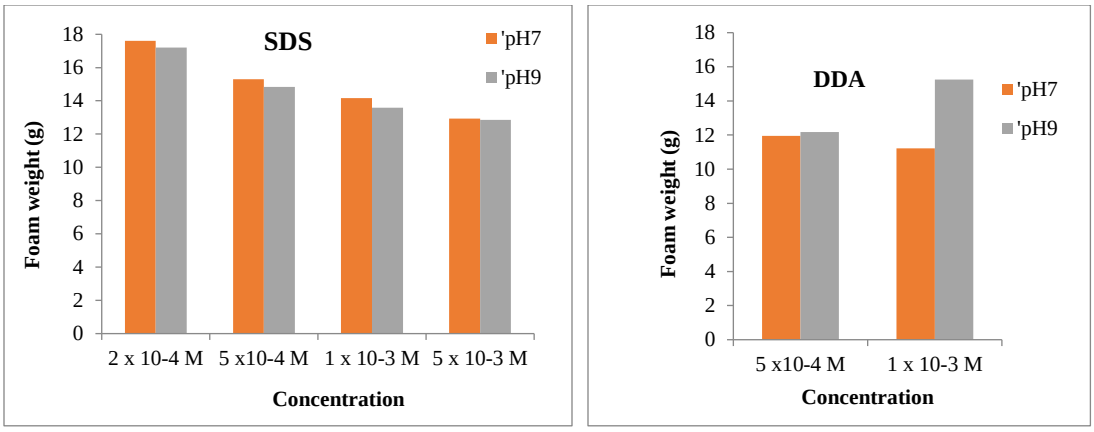

Figure 4.22 Foam weight experiments for both SDS and DDA solutions at different concentrations and pH values.

observation is noted from the results of foam weight experiments. The foams are heavier at pH 7 than at pH 9 for the SDS solutions and it is the opposite trend for the DDA solutions. In other words, in SDS solutions foams carry less water at pH 9 than at pH 7, and the foams are more stable.

It is strongly believed that besides the adsorption of surfactant at the interface, the water network should play a significant role in the foam stability. It is worth noting that the control of foam stability is governed by three different phenomena: foam drainage, foam coarsening, and film rupture. In the thin film between two bubbles, the interaction between the surfactant head groups and interfacial water molecules at the interface and the interaction between interfacial water-water molecules should control the foam drainage and stabilize the thin film, so film rupture can be avoided. As reported in Section 4.3.1, for the SDS solutions at neutral pH, SFG signals of O-H vibrational modes showed a strong peak at 3,200 cm^{-1} representing the “ice-like” water structure. As for the DDA solutions, the interfacial water molecules do not reveal a highly-ordered structure as compared with the SDS solution. In the foam stability experiment, an example of results at the same

concentration of 5.0 x 10^{-4} M and neutral pH are shown in Figure 4.23. It is evident that foams are made more stable by SDS than by DDA. Based on the SFG experimental results and MDS analysis as reported, the behavior of foams in these conditions can possibly be explained by the impact of the water network on the foam. Since the interfacial water molecules are highly ordered at the interface and strongly interact with not only surfactant head groups but also the water molecules in the thin film, it is difficult for the drainage to occur. Hence, the foam stability will be enhanced.

In addition it is found that the experimental data and the hypothesis discussed above are supported by the single film thickness measurements of the SDS and DDA solutions (Aksoy, 1997). Table 4.4 shows the equilibrium film thickness of the SDS and DDA solutions at the same conditions. It can be seen that the film of the SDS solution is more stable than the film of the DDA solution by the thinner thickness values reported. In other words, SDS provides for better film stability than DDA. This observation agrees well with the foam stability experimental data, and these results can be explained by the stronger water network for SDS, as discussed previously.

As observed in Figure 4.20 for the SDS solutions, foams have better stability at pH 9 than at pH 7. SFG experimental results and MDS analysis, as mentioned in Section 4.3.3, revealed that interfacial water structures at the interface for pH 9 are not highly ordered nor strongly hydrogen bonded compared with SDS solution at pH 7. A possible explanation for this result is the strong interaction of the hydroxide group with the water molecules by the four hydrogen bonds between the hydroxide oxygen and the water hydrogens, as discussed in Section 4.3.3. In order words, both the interaction between the interfacial waters and the surfactant head groups and the interaction between the interfacial waters

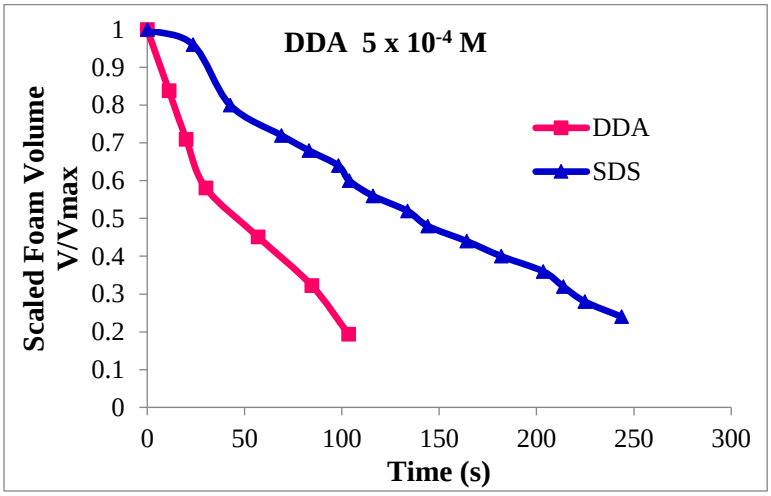

Figure 4.23 Foam stability at 5.0 x 10^{-4} M for SDS and DDA solutions at neutral pH.

Table 4.4 Results of equilibrium film thickness measurements stabilized by SDS and DDA solutions at pH 5.7-6.0, data from (Aksoy, 1997).

Surfactant concentration	Equilibrium film thickness of SDS solution	Equilibrium film thickness of DDA solution
1 x 10^{-5} M	158.5 nm	169.2 nm
5 x 10^{-5} M	152.6 nm	162 nm
1 x 10^{-4} M	125.1nm	141.5 nm

and the water molecules in a thin film should provide the same significant contribution to film stability. The water networks in aqueous films at pH 7 and pH 9 for the SDS solutions are proposed in Figure 4.24. The stronger water network significantly contributes to the more stable foam films, so the foam stability at pH 9 is much better than at pH 7.

As for DDA solutions at pH 9, the dramatic decrease in foam stability was presented in Figure 4.21. This experimental data on foam stability are in good agreement with the single film thickness measurement reported in the literature (Yoon and Aksoy, 1999). Figure 4.25 shows the equilibrium film thickness as a function of pH for the DDA solutions, which reveals that the film thickness of DDA solutions basically increases with an increase of pH values. In other words, the thin film has better stability at a lower pH value. This significant finding supports the experimental data of foam stability for the DDA solution at pH values of 7 and 9. The lower stability of foams at the high pH value is probably due to the decrease of interfacial water molecules at the air-water interface as shown in the SFG experimental results and in the MDS analysis as discussed in Section 4.3.3. The weak water network of interfacial water-surfactant head groups and interfacial water-water molecules in the thin film at pH 9 will cause foam drainage to occur, the thin film will rupture and foams will collapse.

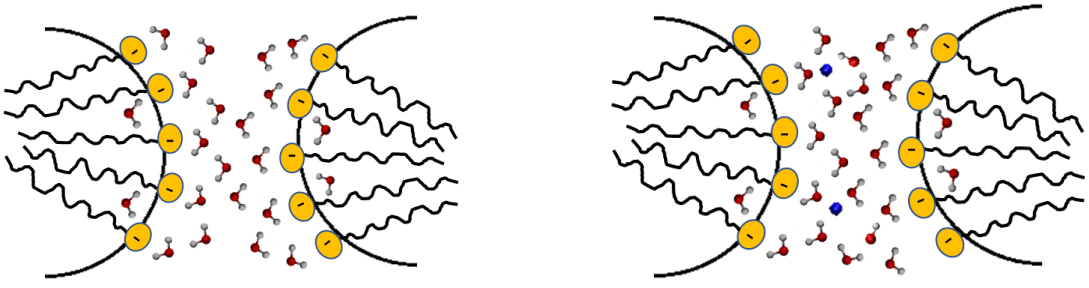

Figure 4.24 Illustration of water network in the thin film of SDS solutions: pH 7 (left sketch) and pH 9 (right sketch). The code for atoms is as follows: red, O; white, H; yellow, sulfate head group; blue, potassium.

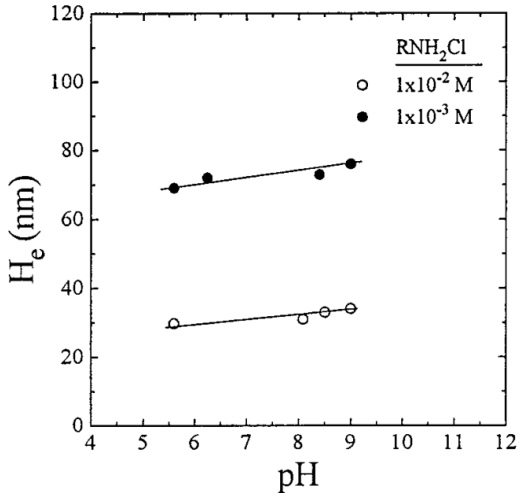

Figure 4.25 Equilibrium film thickness as a function of pH in 1 x 10^{-2} M and 1 x 10^{-3} M DDA solutions (reprinted) (Yoon and Aksoy, 1999).

4.4 Summary

The features of interfacial water molecules for anionic SDS and cationic DDA surfactant solutions were investigated at the air-water interface at neutral pH. SFG experimental results revealed that interfacial water molecules strongly interacted with the anionic sulfate group at the interface whereas the interaction between the cationic ammonium group with interfacial water molecules was not as strong as with the sulfate group. More highly-ordered water molecules were accommodated at the surface of the SDS solution than at the surface of the DDA solution. This observation was confirmed by the analysis of MDS results, including water number density profile, hydrogen bonding network, water dipole orientation and water residence time.

The effect of pH on the interfacial water structures at the air-water interface for SDS and DDA solutions was studied. SFG measurements and MDS simulations at the same concentrations of SDS and DDA at neutral pH and pH 9 were compared. The results indicate that interfacial water structures at the interfaces were disturbed at high pH for both

the SDS and DDA solutions. MDS analysis results demonstrated and supported SFG measurements of the O-H vibrational mode in the range of 3,000-3,600 cm^{-1} of interfacial water structures. Interfacial water molecules at pH 9 were less strongly-ordered and had weaker interactions with surfactant headgroups than at neutral pH.

Foam stability and foam weight experiments were examined at the same concentrations of SDS and DDA both at neutral pH and pH 9. Experimental results demonstrated that interfacial water structures and the water network in the thin film play a significant role in foam stability. At the same SDS concentration, foams were more stable at pH 9 than at pH 7. The opposite trend was observed for the DDA solutions; the higher pH dramatically decreased the foam stability. The hypothesis of interaction between interfacial water -surfactant head groups and interfacial water-water molecules in the thin film for both SDS and DDA solutions at neutral pH and at pH 9 was proposed to describe the behavior of foam stability. It was found that a strongly-connected water network structure prevents foam drainage, and hence, the foam stability will be enhanced.

This research demonstrates that the combination of SFG measurement with MDS simulations provides an excellent analysis to gain a better understanding of interfacial water features at the air–water interface. Results provide valuable fundamental information on how interfacial water structures affect foam stability at the molecular level of understanding. The effect of pH on the foam stability has also been considered by the examination of interfacial water structures at the interface, and it should be useful in the development of surfactant chemicals. It is expected that the results from this study will provide significant insight into the wide range of surfactant applications, especially in the area of flotation technology.

CHAPTER 5

SUMMARY, CONCLUSIONS AND FUTURE RECOMMENDATIONS

5.1 Summary and Conclusions

The major objectives of this dissertation were to investigate the stability of thin aqueous films by examination of fundamental features using molecular dynamics simulation (MDS), modelling using surface charge regulation theory, and sum frequency generation vibration spectroscopy to characterize interfacial water features. The major accomplishments and contributions are summarized as follows.

5.1.1 Film Structure During Rupture Process

New insights of film structure during the rupture process were investigated by MDS. The critical thickness of surfactant-free water films at nanometer scale were determined to be 1.3 nm by using Amber simulation software which results are similar to those results reported in the literature. It was observed from the trajectories of water molecules that the broken film was further transformed to the droplet state due to the minimum potential energy achieved.

The potential energies of water films were analyzed by the compatible tool of the

Amber simulation program, which includes the van der Waals interaction and the electrostatics interaction. As for stable films, potential energies were shown to fluctuate around an equilibrium value, while for broken films they kept decreasing until reaching the minimum value of the droplet state. The results indicate that the interactions between water molecules in broken films were disturbed, and hence, the film was ruptured.

By image processing analysis following MD simulations, a new approach was developed, which had not yet been reported. The percolation analysis was investigated to examine the connectivity of the molecular pores in the water films. The molecular porosity was calculated by image processing software, ImageJ/ Fiji. The results revealed that in stable films, the molecular porosity remained unchanged during the simulation time while in broken films, it kept increasing after a short time of stability. A critical value of molecular porosity was found as 49%. The percolation concept was proposed such that connectivity of the molecular pore network in the water film occurs when the molecular porosity exceeds this critical value, 49%, at which point film rupture occurs.

It is expected the contribution from this work will provide further insight on the rupture process and the film stability. Due to limitations in computational ability, simulation of water-only films was investigated. The results provide a promising topic for future research including analysis of aqueous films in surfactant solutions.

5.1.2 Effect of SDS Adsorption on Disjoining Pressure and Drainage Kinetics of Aqueous Films

A theoretical model was developed to predict the electrical double layer component of disjoining pressure in a thin aqueous film, based on the adsorption of SDS surfactants

and surface charge regulation analysis. The Langmuir adsorption model was applied for dodecyl sulfate ions and the Stern adsorption model was used for sodium ions (as counter-ions). A numerical computational approach was written by using Matlab tool. The theoretical values of electrical double layer disjoining pressure agreed well with the experimental data under appropriate conditions where the electrical double layer interaction plays a dominate role in the thinning of aqueous films.

A new model of film drainage kinetics was developed based on the effect of classical DLVO interactions including van der Waals and electrostatics interactions. The model of electrical double layer disjoining pressure developed previously was taken into account in this computational concept. A combination of Hamaker and Lifshitz approaches was used to calculate the van der Waals disjoining pressure. The newly-developed model of the theoretical film drainage rate based on the effect of classical DLVO interactions provided a good theoretical prediction without any fitting parameter and agreed well with the experimental data from the literature.

The theoretical studies of electrical double layer disjoining pressure and drainage kinetics in aqueous films contributed to more accurate quantitative models, which provide a better understanding of film stability.

5.1.3 Interfacial Water Features at the Air-Water Interface

The features of water molecules for anionic SDS and cationic DDA solutions were examined at the air-water interfaces by SFG experiments and MD simulations. SFG spectra of interfacial water molecules indicated that the water molecules strongly interact with the anionic sulfate group whereas their interaction with the cationic ammonium group was not

as strong as with the sulfate group. More highly-ordered water molecules were accommodated at the surface of the SDS solutions than at the surface of DDA solutions. This observation was confirmed by the analysis of MDS results for interfacial water molecules, including relative number density profile, hydrogen bonding network, water dipole orientation and water residence time.

SFG experiments and MD simulations at the same conditions for SDS and DDA solutions at neutral pH and pH 9 were examined and compared. The results revealed that interfacial water molecules at the interfaces were not strongly-ordered at pH 9 for both SDS and DDA solutions in comparison with neutral pH.

Foam stability and foam weight experiments were conducted at the same conditions used for the SFG experiments, both SDS and DDA solutions at pH 7 and pH 9. Experimental results demonstrated that the features of interfacial water and the water network in aqueous films crucially affect the foam stability. At the same SDS concentration, the foam stability is increased at pH 9 when compared to results at pH 7. For DDA solutions, foams at pH 7 are less stable than at pH 9. The explanation of interactions of interfacial waters-surfactant head groups and interfacial waters-water molecules in aqueous films was proposed to account for the variation in foam stability. In other words, the strongly-connected water network prevents film drainage, and hence, the foam stability will be enhanced.

These findings have provided valuable fundamental information on how interfacial water molecules contribute to foam stability at the molecular level of understanding. The study of pH effect on the foam stability is expected to be useful in the development of surfactant chemicals, and impact many technologies such as froth flotation.

5.2 Recommendations for Future Research

Regarding future research, the following areas can be considered.

(1). MDS study of film stability by percolation theory in the presence of surfactants. Due to the limitation of computational power, this procedure still constrains the study of aqueous film stability in surfactant solutions. It is expected that this limitation can be solved as the technology development is growing very fast. Besides, the high-advanced technique of image processing can be developed to compute the individual molecular pore size in thin aqueous films, which has still not been successful yet in this dissertation.

(2). Study of the disjoining pressures in thin aqueous films can be reviewed. The models developed in this dissertation are dependent on the accuracy of the Langmuir adsorption model. However, recently several publications have discussed the validity of the uniform adsorption models to solve the questions whether the surfactant molecules are adsorbed uniformly at the interfaces or they should be partly submerged in the solutions (Shahir et al., 2016). Due to the surface potential contribution, the disjoining pressures calculation for thin aqueous films becomes more complicated. A new theory of disjoining pressure can be developed in that direction.

(3). The examination of SFG measurements and MD simulations for nonionic surfactants can be investigated using the approach developed in this dissertation. Many frothers used in the flotation process are nonionic alcohols, for example the short chain alcohol methyl isobutyl carbinol (MIBC). The fundamental understanding of interfacial water features at the air-water interfaces of nonionic surfactant solutions will enhance our knowledge on how interfacial water molecules oriented and connected with the frother

molecules, which will provide a foundation for the development of improved flotation reagents.

REFERENCES

Abràmoff, M.D., Magalhães, P.J., Ram, S.J., 2004. Image Processing with ImageJ. Biophotonics International 11, 36-42.

Aksoy, B.S., 1997. Hydrophobic Forces in Free Thin Films of Water in the Presence and Absence of Surfactants. PhD Thesis. Virginia Polytechnic Institute and State University.

Andersson, G., Carey, E., Stubenrauch, C., 2010. Disjoining Pressure Study of Formamide Foam Films Stabilized by Surfactants. Langmuir 26, 7752-7760.

Argyris, D., Cole, D.R., Striolo, A., 2009. Dynamic Behavior of Interfacial Water at the Silica Surface. The Journal of Physical Chemistry C 113, 19591-19600.

Argyris, D., Ho, T., Cole, D.R., Striolo, A., 2011. Molecular Dynamics Studies of Interfacial Water at the Alumina Surface. The Journal of Physical Chemistry C 115, 2038-2046.

Bain, C.D., 1995. Sum-frequency Vibrational Spectroscopy of the Solid/Liquid Interface. Journal of the Chemical Society, Faraday Transactions 91, 1281-1296.

Bandyopadhyay, S., Chanda, J., 2003. Monolayer of Monododecyl Diethylene Glycol Surfactants Adsorbed at the Air/Water Interface: A Molecular Dynamics Study. Langmuir 19, 10443-10448.

Bélorgey, O., Benattar, J., 1991. Structural Properties of Soap Black Films Investigated by X-ray Reflectivity. Physical Review Letters 66, 313.

Berendsen, H., Grigera, J., Straatsma, T., 1987. The Missing Term in Effective Pair Potentials. Journal of Physical Chemistry 91, 6269-6271.

Bergeron, V., Radke, C.J., 1992. Equilibrium Measurements of Oscillatory Disjoining Pressures in Aqueous Foam Films. Langmuir 8, 3020-3026.

Bhatt, D., Newman, J., Radke, C.J., 2002. Molecular Simulation of Disjoining-Pressure Isotherms for Free Liquid, Lennard-Jones Thin Films. The Journal of Physical Chemistry B 106, 6529-6537.

Bhatt, D., Newman, J., Radke, C.J., 2003. Molecular Simulation of Disjoining-Pressure Isotherms for Free Aqueous Thin Films. The Journal of Physical Chemistry B 107, 13076-13083.

Bondi, A., 1964. van der Waals Volumes and Radii. The Journal of Physical Chemistry 68, 441-451.

Bresme, F., Faraudo, J., 2004. Computer Simulation Studies of Newton Black Films. Langmuir 20, 5127-5137.

Carnie, S.L., Chan, D.Y.C., 1993. Interaction Free Energy between Plates with Charge Regulation: A Linearized Model. Journal of Colloid and Interface Science 161, 260-264.

Chan, D.Y.C., Healy, T.W., Supasiti, T., Usui, S., 2006. Electrical Double Layer Interactions Between Dissimilar Oxide Surfaces with Charge Regulation and Stern–Grahame Layers. Journal of Colloid Interface Science 296, 150-158.

Chan, D.Y.C., Pashley, R.M., White, L.R., 1980. A Simple Algorithm for The Calculation of The Electrostatic Repulsion Between Identical Charged Surfaces in Electrolyte. Journal of Colloid and Interface Science 77, 283-285.

Chen, X., Hua, W., Huang, Z., Allen, H.C., 2010. Interfacial Water Structure Associated with Phospholipid Membranes Studied by Phase-Sensitive Vibrational Sum Frequency Generation Spectroscopy. Journal of the American Chemical Society 132, 11336-11342.

Chowdhuri, S., Chandra, A., 2001. Molecular Dynamics Simulations of Aqueous NaCl and KCl Solutions: Effects of Ion Concentration on the Single-Particle, Pair, and Collective Dynamical Properties of Ions and Water Molecules. The Journal of Chemical Physics 115, 3732-3741.

Cosima, S., Regine von, K., 2003. Disjoining Pressure in Thin Liquid Foam and Emulsion Films—New Concepts and Perspectives. Journal of Physics: Condensed Matter 15, R1197.

Danov, K.D., Basheva, E.S., Kralchevsky, P.A., 2016. Effect of Ionic Correlations on the Surface Forces in Thin Liquid Films: Influence of Multivalent Coions and Extended Theory. Materials 9, 145.

Derjaguin, B., 1937. The Theory of Interaction Between Particles in the Presence of Electrical Double Layers and Aggregative Stability of Lyophobic Colloids and Disperse Systems. Izv. Akad. Nauk SSSR, Ser. Khim, 1153-1164.

Derjaguin, B., 1941. Theory of the Stability of Strongly Charged Lyophobic Sols and the Adhesion of Strongly Charged Particles in Solutions of Electrolytes. Acta Physicochim. USSR 14, 633-662.

Derjaguin, B., 1989. Theory of Stability of Colloids and Thin Films, translated by RK

Johnson Consultants Bureau. New York.

Derjaguin, B.V., Churaev, N.V., 1978. On the Question of Determining the Concept of Disjoining Pressure and Its Role in the Equilibrium and Flow of Thin Films. Journal of Colloid and Interface Science 66, 389-398.

Dominguez, H., Berkowitz, M.L., 2000. Computer Simulations of Sodium Dodecyl Sulfate at Liquid/Liquid and Liquid/Vapor Interfaces. The Journal of Physical Chemistry B 104, 5302-5308.

Du, H., Miller, J., 2007. A Molecular Dynamics Simulation Study of Water Structure and Adsorption States at Talc Surfaces. International Journal of Mineral Processing 84, 172-184.

Du, Q., Superfine, R., Freysz, E., Shen, Y., 1993. Vibrational Spectroscopy of Water at the Vapor/Water Interface. Physical Review Letters 70, 2313.

Exerowa, D., Kolarov, T., Khristov, K., 1987. Direct Measurement of Disjoining Pressure in Black Foam Films. I. Films from an Ionic Surfactant. Colloids and Surfaces 22, 161-169.

Exerowa, D., Nikolov, A., Zacharieva, M., 1981. Common Black and Newton Film Formation. Journal of Colloid and Interface Science 81, 419-429.

Exerowa, D., Scheludko, A., 1971. Porous Plate Method for Studying Microscopic Foam and Emulsion Films. Comptes Rendus De l'Academie Bulgare Des Sciences 24, 47-50.

Exerowa, D., Zacharieva, M., Cohen, R., Platikanov, D., 1979. Dependence of the Equilibrium Thickness and Double Layer Potential of Foam Films on the Surfactant Concentration. Colloid and Polymer Science 257, 1089-1098.

Fan, Y., Chen, X., Yang, L., Cremer, P.S., Gao, Y.Q., 2009. On the Structure of Water at the Aqueous/Air Interface. The Journal of Physical Chemistry B 113, 11672-11679.

Frank, F., 1972. Water: A Comprehensive Treatise (The Physics and Physical Chemistry of Water vol 1). New York: Plenum.

Fuerstenau, M.C., Han, K.N., 2003. Principles of Mineral Processing. SME.

Fuerstenau, M.C., Jameson, G.J., Yoon, R.-H., 2007. Froth Flotation: A Century of Innovation. SME.

Gamba, Z., Hautman, J., Shelley, J.C., Klein, M.L., 1992. Molecular Dynamics Investigation of a Newtonian Black Film. Langmuir 8, 3155-3160.

Gragson, D., McCarty, B., Richmond, G., 1997a. Ordering of Interfacial Water Molecules

at the Charged Air/Water Interface Observed by Vibrational Sum Frequency Generation. Journal of the American Chemical Society 119, 6144-6152.

Gragson, D., Richmond, G., 1998. Investigations of the Structure and Hydrogen Bonding of Water Molecules at Liquid Surfaces by Vibrational Sum Frequency Spectroscopy. ACS Publications.

Gragson, D.E., McCarty, B.M., Richmond, G.L., 1996. Surfactant/Water Interactions at the Air/Water Interface Probed by Vibrational Sum Frequency Generation. The Journal of Physical Chemistry 100, 14272-14275.

Gragson, D.E., McCarty, B.M., Richmond, G.L., 1997b. Ordering of Interfacial Water Molecules at the Charged Air/Water Interface Observed by Vibrational Sum Frequency Generation. Journal of the American Chemical Society 119, 6144-6152.

Hore, D.K., Beaman, D.K., Richmond, G.L., 2005. Surfactant Headgroup Orientation at the Air/Water Interface. Journal of the American Chemical Society 127, 9356-9357.

Imberti, S., Botti, A., Bruni, F., Cappa, G., Ricci, M., Soper, A., 2005. Ions in Water: The Microscopic Structure of Concentrated Hydroxide Solutions. The Journal of Chemical Physics 122, 194509.

Israelachvili, J., 1992. Intermolecular and Surface Forces. London: Academic Press.

Israelachvili, J.N., Wennerstroem, H., 1992. Entropic Forces between Amphiphilic Surfaces in Liquids. The Journal of Physical Chemistry 96, 520-531.

Ivanov, I., 1988. Thin Liquid Films. CRC Press.

Jang, S.S., Goddard, W.A., 2006. Structures and Properties of Newton Black Films Characterized Using Molecular Dynamics Simulations. The Journal of Physical Chemistry B 110, 7992-8001.

Jarvis, N., Larsbo, M., Koestel, J., 2017. Connectivity and Percolation of Structural Pore Networks in a Cultivated Silt Loam Soil Quantified by X-ray Tomography. Geoderma 287, 71-79.

Jin, J., Miller, J.D., Dang, L.X., 2014. Molecular Dynamics Simulation and Analysis of Interfacial Water at Selected Sulfide Mineral Surfaces under Anaerobic Conditions. International Journal of Mineral Processing 128, 55-67.

Johnson, C.M., Tyrode, E., 2005. Study of the Adsorption of Sodium Dodecyl Sulfate (SDS) at the Air/Water Interface: Targeting the Sulfate Headgroup Using Vibrational Sum Frequency Spectroscopy. Physical Chemistry Chemical Physics 7, 2635-2640.

Karakashev, S.I., Ivanova, D.S., 2010. Thin Liquid Film Drainage: Ionic vs. Non-ionic

Surfactants. Journal of Colloid and Interface Science 343, 584-593.

Karakashev, S.I., Ivanova, D.S., Angarska, Z.K., Manev, E.D., Tsekov, R., Radoev, B., Slavchov, R., Nguyen, A.V., 2010. Comparative Validation of the Analytical Models for the Marangoni Effect on Foam Film Drainage. Colloids and Surfaces A: Physicochemical and Engineering Aspects 365, 122-136.

Karakashev, S.I., Manev, E.D., Nguyen, A.V., 2008. Effect of Double-layer Repulsion on Foam Film Drainage. Colloid Surface A 319, 34-42.

Karakashev, S.I., Nguyen, A.V., 2007. Effect of Sodium Dodecyl Sulphate and Dodecanol Mixtures on Foam Film Drainage: Examining Influence of Surface Rheology and Intermolecular Forces. Colloid Surface A 293, 229-240.

Knock, M.M., Bell, G.R., Hill, E.K., Turner, H.J., Bain, C.D., 2003. Sum-frequency Spectroscopy of Surfactant Monolayers at the Oil− Water Interface. The Journal of Physical Chemistry B 107, 10801-10814.

Kolev, V.L., Danov, K.D., Kralchevsky, P.A., Broze, G., Mehreteab, A., 2002. Comparison of the van der Waals and Frumkin Adsorption Isotherms for Sodium Dodecyl Sulfate at Various Salt Concentrations. Langmuir 18, 9106-9109.

Koneshan, S., Rasaiah, J.C., Lynden-Bell, R.M., Lee, S.H., 1998. Solvent Structure, Dynamics, and Ion Mobility in Aqueous Solutions at 25 °C. The Journal of Physical Chemistry B 102, 4193-4204.

Kralchevsky, P.A., Danov, K.D., Basheva, E.S., 2011. Hydration Force due to the Reduced Screening of the Electrostatic Repulsion in Few-nanometer-thick Films. Current Opinions of Colloid Interface 16, 517-524.

Kralchevsky, P.A., Danov, K.D., Broze, G., Mehreteab, A., 1999. Thermodynamics of Ionic Surfactant Adsorption with Account for the Counterion Binding: Effect of Salts of Various Valency. Langmuir 15, 2351-2365.

Laskowski, J.S., 1999. Weak Electrolyte Collectors. Advances in Flotation Technology, 58-82.

Li, E., Wang, X., Du, Z., Miller, J.D., Cheng, F., 2017. Specific Anion Effects on Adsorption and Packing of Octadecylamine Hydrochloride Molecules at the Air/Water Interface. Colloids and Surfaces A: Physicochemical and Engineering Aspects 522, 544-551.

Lu, J.R., Marrocco, A., Su, T.J., Thomas, R.K., Penfold, J., 1993. Adsorption of Dodecyl Sulfate Surfactants with Monovalent Metal Counterions at the Air-Water Interface Studied by Neutron Reflection and Surface Tension. Journal of Colloid Interface Science 158, 303-316.

Lu, J.R., Thomas, R.K., Penfold, J., 2000. Surfactant Layers at the Air/Water Interface: Structure and Composition. Advances in Colloid Interface 84, 143-304.

Luzar, A., Chandler, D., 1996. Hydrogen-bond Kinetics in Liquid Water. Nature 379, 55.

Lyklema, J., Mysels, K.J., 1965. A Study of Double Layer Repulsion and van der Waals Attraction in Soap Films. Journal of the American Chemical Society 87, 2539-2546.

Mahanty, J., Ninham, B., 1977. Colloid Science: Dispersion Forces. London: Academic Press.

Mahoney, M.W., Jorgensen, W.L., 2000. A Five-site Model for Liquid Water and the Reproduction of the Density Anomaly by Rigid, Nonpolarizable Potential Functions. The Journal of Chemical Physics 112, 8910-8922.

Manev, E., Tsekov, R., Radoev, B., 1997a. Effect of Thickness Non-homogeneity on the Kinetic Behaviour of Microscopic Foam Film. Journal Of Dispersion Science and Technology 18, 769-788.

Manev, E., Tsekov, R., Radoev, B., 1997b. Effect of Thickness Non-homogeneity on the Kinetic Behaviour of Microscopic Foam Film. Journal of Dispersion Science and Technology 18, 769-788.

Manev, E.D., Nguyen, A.V., 2005. Effects of Surfactant Adsorption and Surface Forces on Thinning and Rupture of Foam Liquid Films. International Journal of Mineral Processing 77, 1-45.

Marti, J., Padro, J., Guardia, E., 1996. Molecular Dynamics Simulation of Liquid Water Along the Coexistence Curve: Hydrogen Bonds and Vibrational Spectra. The Journal of Chemical Physics 105, 639-649.

Miller, J., Lin, C., 2009. High Resolution X-ray Micro CT (HRXMT)–Advances in 3D Particle Characterization for Mineral Processing Operations. Recent Advances in Mineral Processing Plant Design, 48.

Mishra, N.C., Muruganathan, R.M., Müller, H.J., Krustev, R., 2005. The Dependence of the Interactions in Foam Films on Surfactant Concentration. Colloids and Surfaces A: Physicochemical and Engineering Aspects 256, 77-83.

Mysels, K.J., 1959. Soap Films: Studies of Their Thinning and a Bibliography. Pergamon Press.

Mysels, K.J., Jones, M.N., 1966. Direct Measurement of the Variation of Double-layer Repulsion with Distance. Discussions of the Faraday Society 42, 42-50.

Nakahara, H., Shibata, O., Moroi, Y., 2005. Examination of Surface Adsorption of Sodium

Chloride and Sodium Dodecyl Sulfate by Surface Potential Measurement at the Air/Solution Interface. Langmuir 21, 9020-9022.

Nguyen, A.V., 2000. Improved Approximation of Water Dielectric Permittivity for Calculation of Hamaker Constants. Journal of Colloid and Interface Science 229, 648-651.

Nguyen, A.V., Evans, G.M., Jameson, G.J., 2000. Simple Approximate Expressions for Electrical Double-layer Interaction at Constant Moderate Potentials. Journal of Colloid and Interface Science 230, 205-209.

Nguyen, A.V., Schulze, H.J., 2003. Colloidal Science of Flotation. CRC Press.

Nguyen, K.T., Nguyen, A.V., Evans, G.M., 2015. Interfacial Water Structure at Surfactant Concentrations Below and Above the Critical Micelle Concentration as Revealed by Sum Frequency Generation Vibrational Spectroscopy. Journal of Physical Chemistry C 119, 15477-15481.

Nguyen, K.T., Nguyen, T.D., Nguyen, A.V., 2014. Strong Cooperative Effect of Oppositely Charged Surfactant Mixtures on Their Adsorption and Packing at the Air-Water Interface and Interfacial Water Structure. Langmuir 30, 7047-7051.

Nickolov, Z.S., Wang, X., Miller, J.D., 2004. Liquid/air Interfacial Structure of Alcohol–Octyl Hydroxamic Acid Mixtures: A Study by Sum-frequency Spectroscopy. Spectrochimica Acta Part A: Molecular and Biomolecular Spectroscopy 60, 2711-2717.

Nieto-Draghi, C., Bonet Ávalos, J., Rousseau, B., 2003. Transport Properties of Dimethyl Sulfoxide Aqueous Solutions. The Journal of Chemical Physics 119, 4782-4789.

Nihonyanagi, S., Yamaguchi, S., Tahara, T., 2014. Counterion Effect on Interfacial Water at Charged Interfaces and Its Relevance to the Hofmeister Series. Journal of the American Chemical Society 136, 6155-6158.

Ninham, B.W., 1999. On Progress in Forces Since the DLVO Theory. Advances in Colloid Interface 83, 1-17.

Ninham, B.W., Pashley, R.M., Nostro, P.L., 2017. Surface forces: Changing Concepts and Complexity with Dissolved Gas, Bubbles, Salt and Heat. Current Opinion in Colloid Interface 27, 25-32.

Overbeek, J.T.G., Verwey, E., 1948. Theory of the Stability of Lyophobic Colloids: The Interaction of Sol Particles Having an Electric Double Layer. Elsevier, Amsterdam.

Parekh, B., Miller, J., 1999. Advances in Flotation Technology. SME.

Peng, T., Peng, K., Li, Q., 2015. Methodology for Disjoining Pressure of Free Water Nanofilms. The Journal of Physical Chemistry C 119, 14273-14280.

Peng, T.F., Nguyen, A.V., Peng, H., Dang, L.X., 2012. Quantitative Analysis of Aqueous Nanofilm Rupture by Molecular Dynamic Simulation. Journal of Physical Chemistry B 116, 1035-1042.

Radke, C.J., 2015. Film and Membrane-model Thermodynamics of Free Thin Liquid Films. Journal of Colloid and Interface Science 449, 462-479.

Radoev, B., Dimitrov, D., Ivanov, I., 1974. Hydrodynamics of Thin Liquid Films Effect of the Surfactant on the Rate of Thinning. Colloid & Polymer Science 252, 50-55.

Rao, C., 1972. Theory of Hydrogen Bonding in Water, The Physics and Physical Chemistry of Water. Springer, pp. 93-114.

Renard, P., Allard, D., 2013. Connectivity Metrics for Subsurface Flow and Transport. Advances in Water Resources 51, 168-196.

Schelero, N., von Klitzing, R., 2015. Ion Specific Effects in Foam Films. Current Opinion of Colloid Interface 20, 124-129.

Scheludko, A., Exerowa, D., 1959. Über den elektrostatischen Druck in Schaumfilmen aus wässerigen Elektrolytlösungen. Colloid & Polymer Science 165, 148-151.

Schweighofer, K.J., Essmann, U., Berkowitz, M., 1997. Simulation of Sodium Dodecyl Sulfate at the Water−Vapor and Water−Carbon Tetrachloride Interfaces at Low Surface Coverage. The Journal of Physical Chemistry B 101, 3793-3799.

Shahir, A.A., Nguyen, A.V., Karakashev, S.I., 2016. A Quantification of Immersion of the Adsorbed Ionic Surfactants at Liquid|fluid Interfaces. Colloids and Surfaces A: Physicochemical and Engineering Aspects 509, 279-292.

Sheludko, A., 1967. Thin Liquid Films. Advances in Colloid Interface 1, 391-464.

Shen, Y., 1989. Optical Second Harmonic Generation at Interfaces. Annual Review of Physical Chemistry 40, 327-350.

Striolo, A., 2011. From Interfacial Water to Macroscopic Observables: A Review. Adsorption Science & Technology 29, 211-258.

Tarek, M., Tobias, D.J., Klein, M.L., 1995. Molecular Dynamics Simulation of Tetradecyltrimethylammonium Bromide Monolayers at the Air/Water Interface. The Journal of Physical Chemistry 99, 1393-1402.

Tchaliovska, S., Manev, E., Radoev, B., Eriksson, J.C., Claesson, P.M., 1994. Interactions in Equilibrium Free Films of Aqueous Dodecylammonium Chloride Solutions. Journal of Colloid and InterfaceScience 168, 190-197.

Trefalt, G., Behrens, S.H., Borkovec, M., 2016. Charge Regulation in the Electrical Double Layer: Ion Adsorption and Surface Interactions. Langmuir 32, 380-400.

Tsekov, R., Evstatieva, E., 2004. A Fractal Classification of the Drainage Dynamics in Thin Liquid Films. Trends in Colloid and Interface Science XVII, 93-96.

Tsekov, R., Ivanova, D.S., Slavchov, R., Radoev, B., Manev, E.D., Nguyen, A.V., Karakashev, S.I., 2010. Streaming Potential Effect on the Drainage of Thin Liquid Films Stabilized by Ionic Surfactants. Langmuir 26, 4703-4708.

Tsekov, R., Schulze, H.J., 1997. Hydrophobic Forces in Thin Liquid Films: Adsorption Contribution. Langmuir 13, 5674-5677.

Vance, B., 1999. Forces and Structure in Thin Liquid Soap Films. Journal of Physics: Condensed Matter 11, R215.

Walrafen, G., 1972. Raman and Infrared Spectral Investigations of Water Structure, The Physics and Physical Chemistry of Water. Springer, pp. 151-214.

Wang, J., Chen, C., Buck, S.M., Chen, Z., 2001. Molecular Chemical Structure on Poly(methyl methacrylate) (PMMA) Surface Studied by Sum Frequency Generation (SFG) Vibrational Spectroscopy. The Journal of Physical Chemistry B 105, 12118-12125.

Wang, J., Wolf, R.M., Caldwell, J.W., Kollman, P.A., Case, D.A., 2004. Development and Testing of a General Amber Force Field. Journal of Computational Chemistry 25, 1157-1174.

Wang, L., Yoon, R.-H., 2004. Hydrophobic Forces in the Foam Films Stabilized by Sodium Dodecyl Sulfate: Effect of Electrolyte. Langmuir 20, 11457-11464.

Wang, L., Yoon, R.-H., 2005. Hydrophobic Forces in Thin Aqueous Films and Their Role in Film Thinning. Colloids and Surfaces A: Physicochemical and Engineering Aspects 263, 267-274.

Wang, L., Yoon, R.-H., 2008. Effects of Surface Forces and Film Elasticity on Foam Stability. International Journal of Mineral Processing 85, 101-110.

Wang, X., Liu, J., Du, H., Miller, J., 2009. States of Adsorbed Dodecyl Amine and Water at a Silica Surface as Revealed by Vibrational Spectroscopy. Langmuir 26, 3407-3414.

Wang, X., Yin, X., Nalaskowski, J., Du, H., Miller, J.D., 2014. Molecular Features of Water Films Created with Bubbles at Silica Surfaces. Surface Innovations 3, 20-26.

Weng, J.-G., Park, S., Lukes, J.R., Tien, C.-L., 2000. Molecular Dynamics Investigation of Thickness Effect on Liquid Films. The Journal of Chemical Physics 113, 5917-5923.

Yaminsky, V., 1994. Thermodynamic Analysis of Solute Effects on Surface Forces. Adhesion between Silicates in Solutions of Cationic Surfactants. Langmuir 10, 2710-2717.

Yang, W., Wu, R., Kong, B., Zhang, X., Yang, X., 2009. Molecular Dynamics Simulations of Film Rupture in Water/Surfactant Systems. The Journal of Physical Chemistry B 113, 8332-8338.

Ye, S., Nihonyanagi, S., Uosaki, K., 2001. Sum Frequency Generation (SFG) Study of the pH-dependent Water Structure on a Fused Quartz Surface Modified by an Octadecyltrichlorosilane (OTS) Monolayer. Physical Chemistry Chemical Physics 3, 3463-3469.

Yeh, Y.L., Zhang, C., Held, H., Mebel, A., Wei, X., Lin, S., Shen, Y., 2001. Structure of the Acetone Liquid/Vapor Interface. The Journal of Chemical Physics 114, 1837-1843.

Yoon, R.-H., Aksoy, B.S., 1999. Hydrophobic Forces in Thin Water Films Stabilized by Dodecylammonium Chloride. Journal of Colloid and Interface Science 211, 1-10.

Yoon, R.-H., Yordan, J.L., 1986. Zeta-potential Measurements on Microbubbles Generated Using Various Surfactants. Journal of Colloid and Interface Science 113, 430-438.

Zhuang, X., Miranda, P., Kim, D., Shen, Y., 1999. Mapping Molecular Orientation and Conformation at Interfaces by Surface Nonlinear Optics. Physical Review B 59, 12632.